Titre: Title:	Modeling of Intraoperative Patient Positioning to Facilitate and Improve Corrective Spine Surgeries
Auteur: Author:	Guillaume Imbleau-Chagnon
Date:	2022
Type:	Mémoire ou thèse / Dissertation or Thesis
Référence: Citation:	Imbleau-Chagnon, G. (2022). Modeling of Intraoperative Patient Positioning to Facilitate and Improve Corrective Spine Surgeries [Mémoire de maîtrise, Polytechnique Montréal]. PolyPublie. https://publications.polymtl.ca/10492/

POLYTECHNIQUE MONTRÉAL

affiliée à l'Université de Montréal

Modeling of Intraoperative Patient Positioning to Facilitate and Improve Corrective Spine Surgeries

GUILLAUME IMBLEAU-CHAGNON

Institut de génie biomédical

Mémoire présenté en vue de l'obtention du diplôme de *Maîtrise ès sciences appliquées*

Génie biomédical

Août 2022

POLYTECHNIQUE MONTRÉAL

affiliée à l'Université de Montréal

Ce mémoire intitulé :

Modeling of Intraoperative Patient Positioning to Facilitate and Improve Corrective Spine Surgeries

présenté par Guillaume IMBLEAU-CHAGNON

en vue de l'obtention du diplôme de *Maîtrise ès sciences appliquées*

a été dûment accepté par le jury d'examen constitué de :

Abolfazl MOHEBBI, président
Carl-Éric AUBIN, membre et directeur de recherche
Olumide ARUWAJOYE, membre

DEDICATION

À mon fils Milan. Suis ta curiosité, le reste viendra naturellement.

To my son Milan. Follow your curiosity, the rest will come naturally.

ACKNOWLEDGEMENTS

I would like to first thank my research director professor Carl-Éric Aubin for welcoming me in his laboratory and providing me with this opportunity. It was on honor to study under his guidance and leadership within a group of skilled researchers and student colleagues at the TransMedTech Institute. Thank you as well to Dr A. Noelle Larson for the valuable exchanges at the beginning of this project. I would also like to thank the laboratory research assistants Christian Bellefleur, Nikita Cobetto, and Nathalie Bourassa for their support in integrating the laboratory environment and sharing their precious knowledge. A special thank to Christiane Caouette, who's technical guidance and finite-element modeling expertise were tremendously helpful in my learning curve and the realization of this study. Lastly, I would like to thank my family and friends who encouraged me to follow through my idea of going back to school and who helped daily to maintain sanity while studying at home during two historic years of a global pandemic.

This project was funded by NSERC (NSERC/Medtronic Industrial Research Chair in Spine Biomechanics)

RÉSUMÉ

Les déformations sévères du rachis telles que la scoliose, le spondylolisthésis ou les traumatismes aux rachis varient quant à leur étiologie, mais lorsque la chirurgie orthopédique est nécessaire les patients seront généralement positionnés sur une table opératoire spécialisée afin de faciliter les différentes étapes de la chirurgie. Les patients sont sécuritairement installés sur cette table grâce à différentes composantes d'aide au positionnement telles que des coussins, coussinets et sangles pour assurer la stabilité du rachis, donner accès à la zone chirurgicale et aux appareils d'imagerie, minimiser le saignement, stabiliser les structures vitales (e.g. organes, nerfs), assurer une ventilation adéquate et faciliter les procédures d'instrumentation. Cette étape de positionnement du patient sur la table opératoire a un effet démontré sur la correction du rachis et offre un potentiel démontré de moduler les courbes du rachis avant même de débuter la chirurgie de correction. Pendant la chirurgie, le clinicien exécute des manœuvres de correction qui imposent des charges importantes sur l'instrumentation de correction et le rachis, mais le potentiel de réduction de ces charges, au bénéfice du clinicien et du patient, par une manipulation ciblée du rachis via le positionnement patient n'a jamais été documenté et doit être plus approfondi.

Ce projet a tenté de répondre à la question suivante : en comparaison à la pratique courante, est-ce qu'une manipulation ciblée du rachis via le positionnement patient permet d'améliorer et de faciliter davantage la correction des déformations du rachis, ainsi que de réduire les forces requises pour exécuter les manœuvres de correction? Les hypothèses suivantes ont été émises : 1) Un modèle biomécanique du rachis humain calibré à l'aide de données cliniques préopératoires peut simuler à 5 degrés près les changements de courbure du rachis résultants du positionnement en décubitus ventral sur un cadre chirurgical standard à 4 montants avec l'ajustement sagittal du bassin et du torse; 2) Le modèle biomécanique du rachis humain validé au préalable à l'aide de données cliniques préopératoires peut simuler les changements de courbures du rachis et les forces exercées aux vertèbres résultants d'une instrumentation postérieure du rachis avec tiges et vis pédiculaires, et ce à 5 degrés près pour les courbes et à des niveaux de forces aux vis comparables aux études déjà publiées; 3) Le positionnement du patient sur un cadre chirurgical standard à 4 montants avec l'ajustement du bassin et du thorax durant les procédures d'instrumentation peut réduire jusqu'à 25% les forces d'interface entre les vertèbres et les vis pédiculaires.

Trois objectifs spécifiques ont été élaborés afin de guider la stratégie de réponse à la question de recherche et de tester les hypothèses : 1) Développer un modèle biomécanique par éléments finis (MEF) du rachis humain capable de simuler le décubitus ventral intra-opératoire et la chirurgie corrective du rachis avec instrumentation par approche postérieure; 2) Vérifier et valider le modèle avec des cas cliniques existants et quantifier les effets associés aux incertitudes du modèle; 3) Caractériser l'influence du positionnement du patient sur la correction du rachis et les forces résultantes de la chirurgie avec instrumentation, ceci étant l'objectif principal du projet.

Afin d'atteindre l'objectif 1, un modèle par éléments finis personnalisé du rachis humain comprenant les vertèbres thoraciques et lombaires, les disques intervertébraux, les côtes, le sternum, les cartilages costaux, les tissus mous de l'abdomen et le bassin a été adapté pour inclure un cadre chirurgical et l'instrumentation corrective aux déformations du rachis. L'instrumentation corrective était faite de tiges et de vis pédiculaires. Des procédures de simulation avec conditions limites ont été développées pour le modèle afin de simuler le patient en décubitus ventral et la chirurgie corrective du rachis via une technique de translation. Le modèle a permis de mesurer les courbes du rachis et les forces axiales à l'interface os-vis issues des simulations.

Afin d'atteindre l'objectif 2, un plan de vérification, validation et quantification des incertitudes a été implémenté. Cinq patients atteints de scoliose idiopathique de l'adolescent et issus de la base de données de patients du CHU Sainte-Justine ont été utilisés pour comparer les résultats de simulation avec les mesures de données cliniques intra-opératoires. Des études *in vivo* et *in silico* ont aussi été utilisées afin de comparer les résultats. Les incertitudes associées au modèle ont été quantifiées à l'aide d'une série d'études de sensibilité des paramètres du modèle associés au positionnement, au patient et à l'instrumentation.

Afin d'atteindre l'objectif 3, le modèle a été utilisé pour mesurer l'influence d'une élévation des coussins thoraciques sur les forces intra-opératoire exercées aux vis pédiculaires sur les patients instrumentés.

Nos simulations ont permis de constater que :

- Le modèle a permis de représenter en moyenne les changements de courbes du rachis résultants du positionnement intra-opératoire en décubitus ventral selon l'objectif donné ($\leq 5^{o}$).

- Le modèle a permis de simuler un déplacement vertical de 50-mm des coussins thoraciques avec des résultats moyens comparables aux études utilisant des patients sains. Le déplacement vertical des coussins thoraciques a eu une influence significative sur la cyphose thoracique, soit un changement de 9º en moyenne, ce qui correspond à une augmentation de 67% de la cyphose.
- Le modèle a permis de représenter les changements de courbes du rachis et les forces exercées aux vertèbres résultants d'une instrumentation par approche postérieure utilisant des tiges et des vis pédiculaires, selon l'objectif donné (≤ 5º) pour les courbes et à l'intérieur d'une plage de valeurs issues d'études *in silico* comparables pour les forces d'arrachement aux vis.
- Le cadre chirurgical standard à 4 montants a favorisé la mobilité du rachis dans le plan sagittal tout en restreignant la mobilité dans le plan coronal. La rotation du bassin a été efficace pour manipuler les courbes sagittales passant d'une réduction moyenne de 32º (pour représenter la flexion maximum des membres inférieurs) à une augmentation de 14º (en extension maximum) pour la lordose. Le positionnement longitudinal des coussins thoraciques a exercé une influence significative sur la cyphose thoracique passant d'une réduction moyenne de 6º pour un déplacement de 50-mm en direction crâniale à une augmentation de 4º pour un déplacement de 50-mm en direction caudale. En accord avec les études existantes, les résultats obtenus des simulations ont confirmé que la combinaison de la rotation du bassin dans le plan sagittal et du placement des coussins thoraciques est pertinente pour la manipulation des courbes sagittales avant la procédure d'instrumentation.
- De légères variations (3 mm) associées à la modélisation de la connexion tige-vis ont impacté significativement les valeurs moyennes (jusqu'à 30%) et maximales (jusqu'à 69%) des forces d'arrachement des vis. Cette observation a confirmé comment des ajustements à l'instrumentation de l'ordre du millimètre jouent un rôle significatif sur les niveaux de force mesurés.
- Les simulations d'instrumentation réalisées avec le modèle ont révélé des modifications variées des forces d'arrachement aux vis avec l'augmentation de la cyphose thoracique via le positionnement du patient. Les résultats ont varié d'une réduction de 23 N ou 28% à une augmentation de 13 N ou 17% pour les valeurs moyennes et d'une réduction de 80 N ou

37% à une augmentation de 52 N ou 27% pour les valeurs maximales. Pour les forces d'arrachement, il a donc été observé que la correction sagittale imposée par les tiges cintrées peut s'agencer favorablement ou défavorablement avec la courbure sagittale induite par le positionnement du patient. Il est donc proposé de poursuivre les efforts pour détailler comment la stratégie de correction par instrumentation peut intégrer la manipulation du rachis issue du positionnement du patient pour déduire des formes de tiges qui réduiraient les forces intra-opératoires aux implants. Il a été noté qu'afin de pouvoir étudier les forces aux vis durant les différentes étapes de la chirurgie, certains changements à la modélisation de la connexion tige-vis seraient nécessaires.

Le modèle numérique proposé dans le cadre de ce projet est le premier à combiner les manipulations intra-opératoire des courbes du rachis via le positionnement du patient avec la possibilité de simuler la chirurgie corrective et de mesurer les forces résultantes aux implants. Notre MEF a le potentiel d'être intégré au développement rapide et à l'essai de nouvelles composantes d'aide au positionnement cherchant à optimiser la manipulation des courbes du rachis afin de faciliter et d'améliorer la correction de ses déformations.

ABSTRACT

Severe spinal deformities requiring orthopedic surgeries such as scoliosis, spondylolisthesis or spinal trauma vary in etiology, but generally for their treatment patients need to be positioned on a specialized operating table to facilitate the various stages of surgery. Patients are secured on this operating table via a set of positioning components such as cushions, pads, and straps to ensure spine stability, provide surgical and radiological imaging access, minimize bleeding, stabilize and preserve vital structures (e.g., organs, nerves), provide proper ventilation and facilitate instrumentation procedures. The simple act of positioning the patient has been shown to have an influence on spinal correction and offers a demonstrated and documented potential to leverage the patient's body kinematics to segmentally adjust the shape of the spine prior to any surgical correction. During surgery, corrective maneuvers are performed by the clinician which impose important loads on the corrective instrumentation, but the potential of targeted position induced spine manipulations on reducing these intraoperative loads, benefiting both the clinician and patient, has never been documented and must be further researched.

This project looked to answer the following question: when compared to the current practice, can position induced spine manipulations further improve and facilitate the correction of spinal deformities, as well as reduce the forces required to perform corrective maneuvers? It was hypothesized that: 1) a biomechanical model of the human spine calibrated with preoperative clinical data can simulate the changes in spinal curvatures resulting from being prone on a typical 4-post adjustable surgical frame with sagittal adjustment of the pelvis and torso, to within 5 degrees; 2) the previously validated biomechanical model of the human spine calibrated with preoperative clinical data can simulate the changes in spinal curvatures and the forces exerted on the vertebrae resulting from posterior instrumentation with rods and pedicle screws to within 5 degrees of accuracy for curvatures and within the measured range of comparable studies for forces; 3) perioperative patient positioning with pelvic and thoracic adjustments on a 4-post operating frame can reduce interface loads between the vertebral bone and the pedicle screws by up to 25% during instrumentation procedures.

From there three specific objectives guided the strategy to answer this question and test these hypotheses: 1) develop a biomechanical finite element model (FEM) of the human spine capable of simulating the intraoperative prone position and posterior spinal instrumentation surgery; 2)

verify and validate the model with existing clinical cases and quantify the effects of model uncertainties; 3) characterize the influence of patient positioning on the correction and forces resulting from instrumentation surgery, which was the principal objective of this project.

To achieve objective 1, a personalized finite-element model of the human spine which included the thoracic and lumbar vertebrae, intervertebral discs, ribs, sternum, costal cartilages, abdominal soft tissues, and pelvis was adapted to include a surgical frame and spine deformity correction instrumentation. The correction instrumentation consisted in contoured rods and pedicle screws. Model simulation procedures with associated boundary conditions were developed to simulate the patient prone position and the instrumentation surgery via a translation technique. The model allowed to measure the resulting spine curvatures and axial forces at the bone-screw interface.

To achieve objective 2, a verification, validation and uncertainty quantification plan was developed and followed. Five patients with adolescent idiopathic scoliosis from the Sainte-Justine University Hospital patient database were used to compare the simulation results with intraoperative clinical data measurements. Published *in vivo* and *in silico* studies were also used to compare results. Model uncertainty was quantified via a series of parameter sensitivity studies with a varied set of positioning, patient-related and instrumentation parameters.

To achieve objective 3, the model was used to measure the influence of raising the surgical frame's thoracic cushions on the intraoperative post-instrumented pedicle screws loads.

Our simulations yielded the following results:

- The model allowed to simulate the changes in spinal curvatures resulting from the intraoperative prone position within clinical significance ($\leq 5^{o}$) on average.
- The model allowed to simulate a 50-mm vertical displacement of the thoracic cushions with comparable results as previous experiments with healthy patients. The thoracic cushions vertical displacement had a significant influence on thoracic kyphosis with an average change of 9^{o} corresponding to a 67% increase in kyphosis.
- The model allowed to simulate the changes in spinal curvatures and forces exerted on the vertebrae resulting from posterior instrumentation with rods and pedicle screws within clinical significance ($\leq 5^{o}$) on average for curvatures and within the measured range of comparable *in silico* studies for screw pull-out forces.

- The studied standard 4-post surgical frame favored spine mobility in the sagittal plane and restricted mobility in the coronal plane. Pelvic rotation was effective at manipulating the sagittal curves with an average reduction of 32º (at maximum flexion of lower limbs) to an increase of 14º (at maximum extension) in lordosis. Longitudinal positioning of the thoracic cushions had a significant influence on thoracic kyphosis with an average 6º reduction for a 50-mm cephalad displacement to a 4º increase for a 50-mm caudal displacement. The combination of pelvic rotation in the sagittal plane and thoracic cushions placement was shown as pertinent for manipulating the sagittal curves prior to instrumentation, in accord with published studies.
- Small variations (3 mm) in screw-to-rod connection modeling assumptions had a significant impact on screw pull-out forces average (up to 30%) and maximum (up to 69%) values. This finding confirmed how millimeter level adjustments in the instrumentation play a significant role in measured load levels.
- The instrumented simulations using the model revealed a varying effect on intraoperative post-instrumented screw pull-out forces resulting from an increase in thoracic kyphosis using patient positioning. Results ranged from an average reduction of 23 N or 28% to an increase of 13 N or 17% in average forces and a reduction of 80 N or 37% to an increase of 52 N or 27% in maximum forces. It was observed that the sagittal correction objective imposed by the contoured rods shape may work in combination with or against the position induced correction. From this finding it was proposed to further investigate how the correction strategy could integrate the position induced correction to deduce contoured rod shapes that would minimize intraoperative forces. It was noted that further model developments would be required to also measure screw loads at intermediate stages of the instrumentation surgery which would involve a refinement of the screw-to-rod connection modeling.

The proposed numerical model is the first to combine intraoperative position-induced spine manipulations with the capability to simulate instrumentation surgery and measure resulting implant forces. Our FEM has a great potential in the rapid development and testing of novel positioning modalities which aim to advantageously manipulate the spine to further facilitate and improve the correction of spinal deformities.

TABLE OF CONTENTS

LIST OF TABLES

LIST OF FIGURES

LIST OF ACRONYMS AND ABBREVIATIONS

2D	Two dimensions
3D	Three dimensions
AIS	Adolescent idiopathic scoliosis
AP	Anteroposterior
ASME	American Society of Mechanical Engineers
C1-C7	Cervical region
CC	Concave
cm	Centimeter
CoCr	Cobalt-Chrome
COU	Context of use
CV	Convex
DDD	Degenerative disc disease
DPF	Dynamic positioning frame
EX	Young modulus
FA	Favored angle
FEA	Finite-element analysis
FEM	Finite-element method or Finite-element model
IVD	Intervertebral disc
L1-L5	Lumbar region
LAT	Lateral
LL	Lumbar lordosis
LLD	Lateral leg displacer
Max	Maximum

MBM	Multibody modeling or multibody model
MBS	Multibody simulation
MFPF	Multi-functional positioning frame
Min	Minimum
mm	Millimetre
MPa	Mega Pascal (kg/mm^2)
MT	Main thoracic
N	Newton ($kg.m/s^2$) or Number (statistics)
OTS	Off-the-shelf
PA	Posteroanterior
PCO	Posterior column osteotomies
pFEM	Patient specific finite-element model
Post	Posterior
POVL	Perioperative visual loss
PT	Proximal thoracic
PTD	Pelvic torsion device
RMSE	Root mean square error
Rx	Radiograph
S1-S5	Sacrum region
SD	Standard deviation
Sim	Simulation
SRS	Scoliosis Research Society
SVA	Sagittal vertical axis
SVD	Sternum vertical displacer

T1-T12	Thoracic region
Ti	Titanium
TK	Thoracic kyphosis
TLIF	Transforaminal lumbar interbody fusion
TL/L	Thoracolumbar/lumbar
V&V	Verification and validation
VVUQ	Verification, validation, and uncertainty quantification

LIST OF APPENDICES

CHAPTER 1 INTRODUCTION

In the context of orthopedic surgeries, the operating table plays an essential role in patient safety as it provides body stability, surgical and radiological imaging access, minimizes bleeding, preserves vital structures from potential damage, provides proper ventilation and facilitates instrumentation procedures. Perioperative patient support on the operating table is achieved with the use of positioning modalities such as cushions or pads at targeted locations and a table hinge for body segment rotation. For the treatment of severe spinal deformities such as scoliosis, spondylolisthesis or spinal trauma, the patient is securely positioned on the operating table to facilitate surgical area exposure and corrective instrumentation maneuvers. Operating tables for corrective spine surgeries have evolved over the last decades, with several studies documenting how their design influences the patient's spine geometry. These studies have shown how perioperative patient positioning can significantly modify the spine sagittal curves (i.e., lumbar lordosis, thoracic kyphosis) and coronal curves (i.e., Cobb angles) when compared to standing radiographs (Delorme et al., 2000; C. Driscoll, Aubin, Canet, Labelle, & Dansereau, 2012; Sebastian et al., 2018). Indeed, by varying positioning modalities, intraoperative manipulation of the spine can be achieved with some level of deformity correction prior to instrumentation. Permanent deformity correction is then achieved by a series of maneuvers performed by the surgeon with the aid of instrumentation anchored to the patient's bone structure. Many combinations of maneuvers and instrumentation strategies are possible to achieve the desired correction outcome, with studies evaluating how these combinations can influence loads acting at the instrumentation to bone structure interface. The potential in providing pre-instrumented spinal deformity correction via patient positioning has been hypothesized to facilitate the instrumentation phase for the clinician and potentially reduce intraoperative loads at the bone-anchor interface (C. Driscoll, 2010; Duke, 2005; Vedantam et al., 2020), but never measured.

A patient's preoperative standing radiographs can be used to create a personalized virtual spine on which patient positioning and corrective spine surgery simulations can be performed to study *in silico* new surgical technique and spine corrective instruments. To this end, the finite-element method (FEM) enables the calculation of displacement, stress, strain and reaction forces on the virtual spine to evaluate potential innovations prior to any form of *in vivo* testing.

The general objective of this project was to use the FEM to develop a biomechanical model of the human spine capable of simulating the prone position on a typical surgical operating frame for instrumented spine surgery via posterior approach. The model allowed for the variation of positioning, corrective instrumentation, and patient specific parameters, with the ability to measure the resulting spine sagittal and coronal curves, and bone-anchor interface loads. Of particular interest was the possibility of manipulating the thoracic kyphosis through positioning prior to instrumentation to improve and facilitate the correction of spinal deformities, as well as potentially reduce the forces acting at the bone-anchor interface. The credibility of the proposed model was assessed using a risk management-based verification, validation, and uncertainty quantification plan (VVUQ).

This master's thesis is organized in seven chapters including this introduction. Chapter 2 contains a literature review on the fundamentals in spine anatomy, spinal pathologies, corrective instrumentation and techniques, positioning modalities, and biomechanical simulation of the human spine. It is followed by a presentation of the project's problematic, hypotheses and objectives in Chapter 3. Chapter 4 details the methodology employed including the VVUQ plan, with results obtained described in Chapter 5. Chapter 6 contains a discussion of the results, with conclusion and perspectives presented in Chapter 7. An appendix is also provided which contains supplementary results to complement the Chapter 5 findings.

CHAPTER 2 LITERATURE REVIEW

In order to contextualize this project, a review of the fundamentals in anatomy, spine pathologies and surgical interventions is first presented. The patient positioning concept and biomechanical simulation of the spine follow to conclude this chapter.

2.1 Descriptive and functional anatomy and biomechanics of the human spine

The human spine is a complex structure which houses a portion of the nervous and vascular systems. It supports the weight of the head, trunk, and superior members and transfers these loads to the legs via the pelvis. It anchors the rib cage and several muscles for posture and body movement and protects the prolongation of the central nervous system. Furthermore, important blood vessels pass through or in proximity of the spine. Before detailing the anatomy of the human spine and its anatomical landmarks, a spatial orientation convention for describing the different features must first be defined. To this end, a three-axis coordinate system exists. It consists of the posterior-anterior (X), medial-lateral (Y) and caudal-cranial (Z) directions. Three planes are also defined in accordance with this system: coronal plane (YZ), sagittal plane (XZ) and transverse plane (XY) (Figure 2.1).

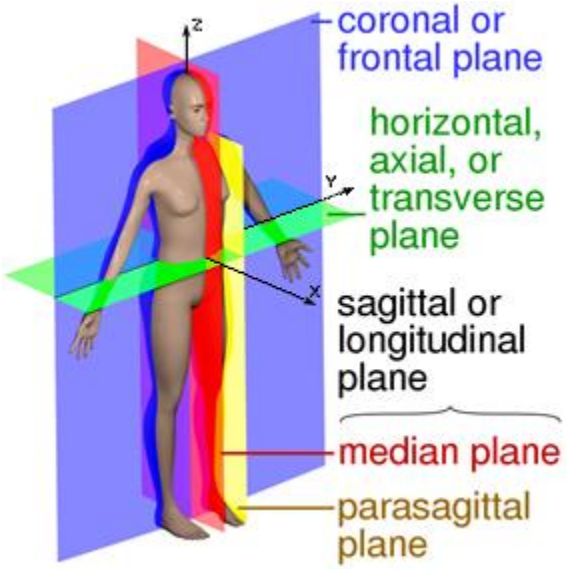

Figure 2.1 Human anatomical planes and coordinate system (Source: Wikipedia, 2021, license free)

This mechanically complex column of the human body is composed of 24 interlinked non fused vertebrae starting at the base of the skull down to the top of the sacrum, followed by the sacrum and its 5 fused vertebrae and finally the coccyx with 4 fused vertebrae for a total of 33 vertebrae. The vertebrae are grouped into regions: cervical (C1-C7), thoracic (T1-T12), lumbar (L1-L5), sacrum (S1-S5) and coccyx (tailbone), with the combination of thoracic and lumbar referred to as the thoracolumbar region (Figure 2.2).

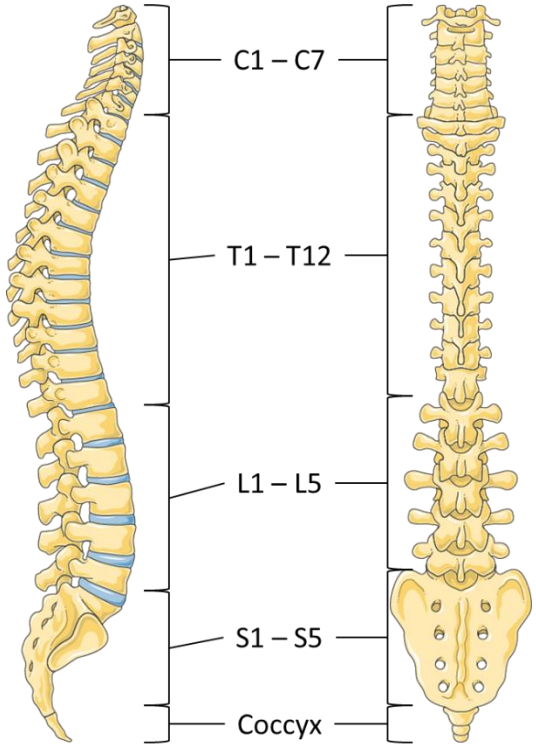

Figure 2.2 The human spine and vertebral regions (adapted from Server Medical Art, license free)

The rib cage is composed of 10 pairs of ribs anteriorly fused with the sternum and 2 pairs of floating ribs. Each pair connects posteriorly with a thoracic vertebra at a facet interface and are also interconnected via the intercostal muscles (Figure 2.3).

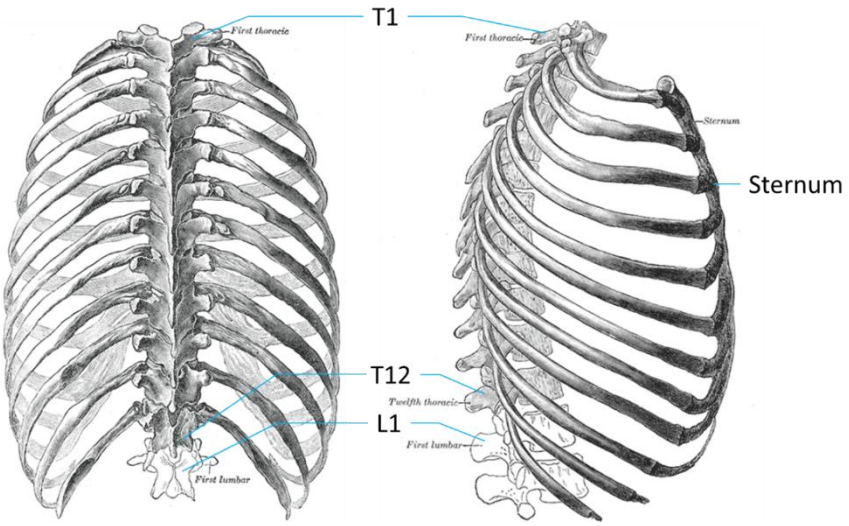

Figure 2.3 Rib cage posterior and lateral views (adapted from bartleby.com, license free)

The pelvis is formed by the sacrum, ischium, ilium, and pubis bones. It connects with the lower members (i.e., legs) via the coxo-femoral articulation comprised of the acetabulum and femoral head of the femur (Figure 2.4).

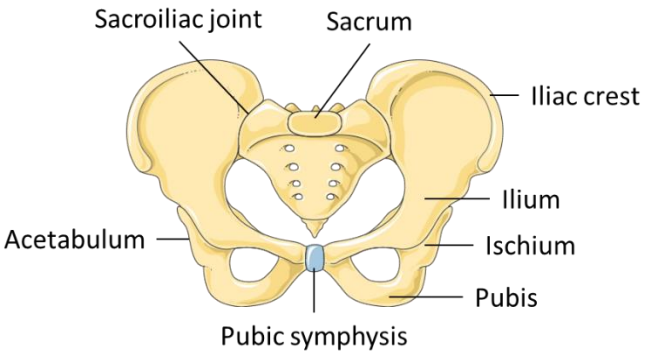

Figure 2.4 Pelvis anterior view (adapted from Server Medical Art, license free)

Neck, abdominal, back, pelvis and leg muscle groups are responsible for spine movement. Several layers of muscle with various insertion points along the spine, including muscle groups interconnections (e.g., thoracolumbar fascia) grant the spine the following movements: flexion-extension in the sagittal plane, flexion in the coronal plane and rotation in the transverse plane (Figure 2.5 and Figure 2.6). The interconnected flexible structure of the trunk formed by the T1-S1 segment has a varying range of motion depending on region (see Table 2.1). The rib cage and thoracic vertebra articular facets orientation stiffen the thoracic region and restricts its local amplitude of motion as compared to the lumbar region for global flexion-extension in the sagittal

plane. In the coronal plane, global lateral flexion is more evenly distributed along the thoracic and lumbar regions. In the transverse plane the lumbar vertebrae articular facets orientation restrict rotation, hence relying more on the thoracic vertebrae to rotate the trunk. The muscles associated with the pelvis allow for tilt (or rotation) in the sagittal plane, elevation-depression in the coronal plane and rotation in the transverse plane.

Table 2.1 Spine regions functional rotation angles from litterature (T12-L1 not shown)

Spine region	**Flexion-extension**	**Lateral flexion**	**Axial rotation**	**References**
T1-T12	28º	36º	45º	(Borkowski et al., 2016)
L1-S1	77º	50º	6º	(Dvorak et al., 1991; Ochia et al., 2006)

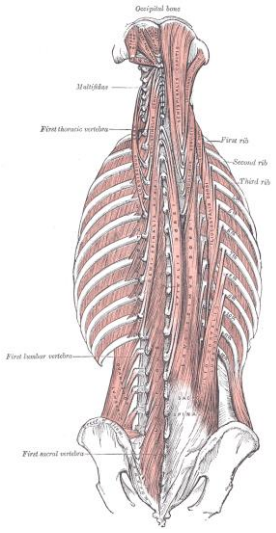

Figure 2.5 Deep muscles of the back, posterior view (Source: bartleby.com, license free)

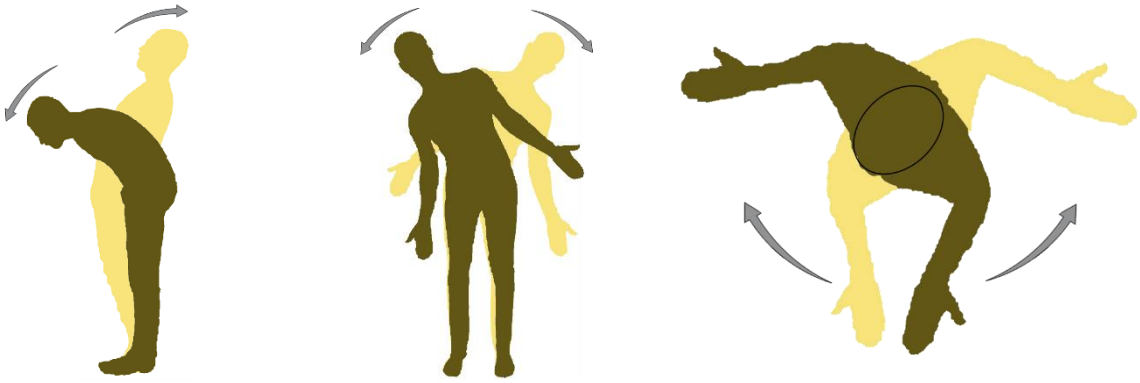

(a) (b) (c)

Figure 2.6 General spine movements (a) Flexion-extension; (b) Lateral flexion; (c) Rotation

The thoracic aorta begins around the T4 level and follows a gradual left anterolateral to anteromedial trajectory anterior to the spine until it divides into the common iliac vessels at the L3-L6 level (Figure 2.7a) (Egea-Gámez et al., 2021). The spine also hosts the external and internal vertebral venous plexuses comprised of a network of longitudinal veins interconnected via an anastomotic (connecting) system of veins. In situations where the vena cava is obstructed, these venous plexuses have been shown to effectively divert the venous return through its network to compensate the rise in caval pressure (Schonauer et al., 2004). The peripheral nervous system is intricately hosted by the spine through a complex network of nerve roots extending laterally outwards of the spinal canal which is housed within the vertebrae's foramen (Figure 2.7b). The spinal cord enters the spinal canal at C1 until the L1-L2 junction, where it branches out into the lumbar and sacral plexuses. The brachial plexus (C5-T1) caters for the upper limbs and the thoracoabdominal nerves regroup the intercostal and genitofemoral regions.

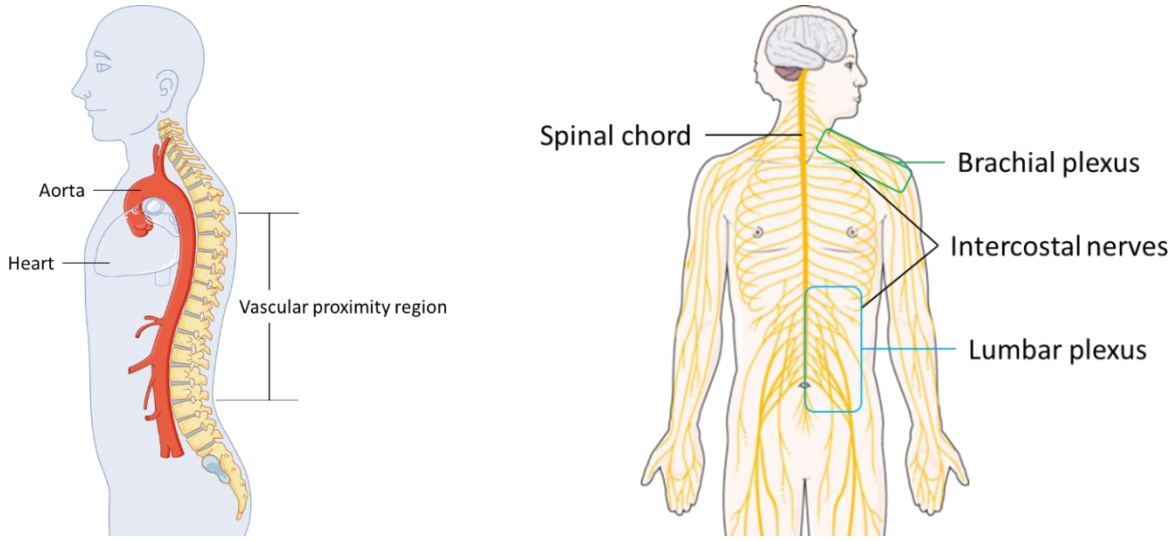

(a) (b)

Figure 2.7 (a) Vascular proximity region; (b) Peripheral nervous system (adapted from Server Medical Art, license free)

A functional segment of the C1-S1 section of the spine is composed of two adjacent vertebrae, their intervertebral disc, facet joints and ligaments (Figure 2.8). A vertebra is composed of cortical and cancellous bone, with the vertebral body in the anterior section and processes (i.e., spinous and transverse) and facets in the posterior section. Pedicles bridge the two sections and together with the lamina, spinous process, and vertebral body they define the vertebral foramen (Figure 2.9). The facet joints allow movement continuity between vertebrae in the transverse plane. Ligaments contribute to the segment stability and maintain adequate tension between vertebrae to prevent hyperextension.

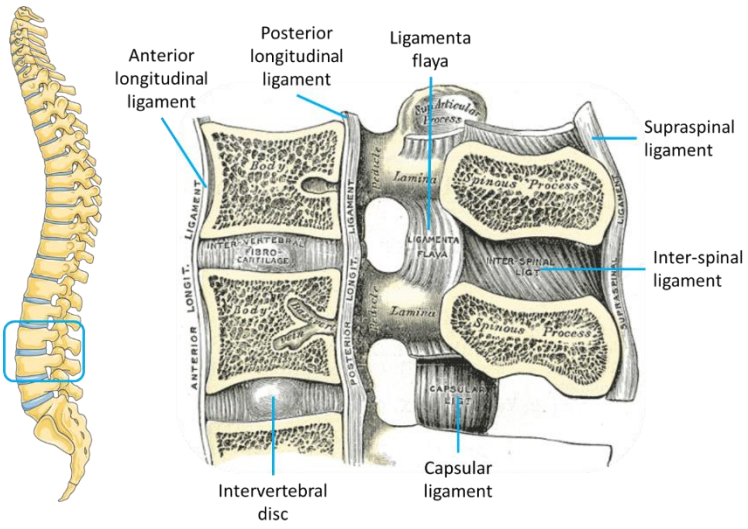

Figure 2.8 Spine functional segment and lateral cross-section (adapted from Server Medical Art and bartleby.com, license free)

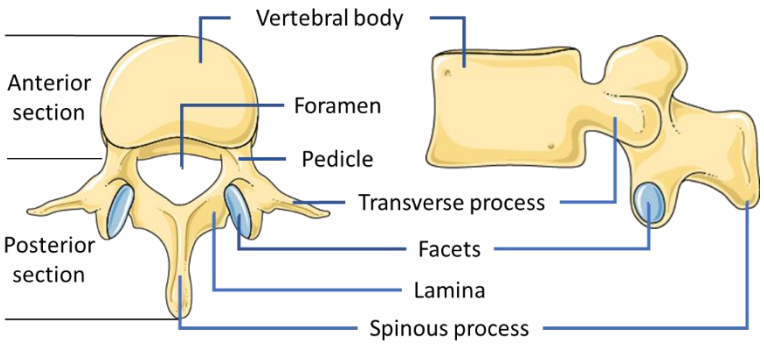

(a)

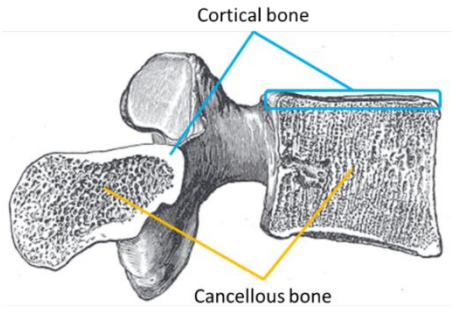

(b)

Figure 2.9 Vertebra features (a) Anatomical features, top and lateral views; (b) Bone features, lateral cross-section (adapted from Server Medical Art and bartleby.com, license free)

The intervertebral disc (IVD) is composed of the outer anulus fibrosus and inner nucleus pulposus. This fibrocartilaginous joint is anchored at the inferior and superior plateaus of adjacent vertebral bodies. Together with the vertebrae, the IVDs form a continuous link from head to sacrum making up the flexible load bearing column on which the trunk exercises its motion. The IVDs are also reported to greatly contribute to human gait by transferring axial torque along the spine and not solely acting as a shock absorber during locomotion (Gracovetsky SA, 1997).

In comparison with great apes, the hominin bipedalism, driven by adaptation, has led to the appearance of distinct spine curvatures. In the sagittal plane, they are defined as cervical lordosis, thoracic kyphosis, lumbar lordosis, and sacral kyphosis (Figure 2.10a). The average normal sagittal alignment is: 15° cervical lordosis (C2-C7), 20-40° thoracic kyphosis (T1-T12), and 40-60° lumbar lordosis (T12-S1) (Ouellet, n.d.). In the coronal plane, a healthy spine in the stand-up position is straight and exhibits minimal curvatures. In scoliosis cases, lateral spine curvatures are characterized using the Cobb angle measurement technique. The technique consists in measuring the angle between two straight lines drawn from the proximal and distal vertebral body end plates of a selected segment (Figure 2.10b and c). In the sagittal plane, a similar method is used to measure the physiological kyphosis and lordosis. In the transverse plane, a healthy spine exhibits minimal intervertebral rotation, but in scoliosis the vertebrae are rotated in the transverse plane, and their measurement is made by the axial rotation angle (generally maximum at the apex of the curve).

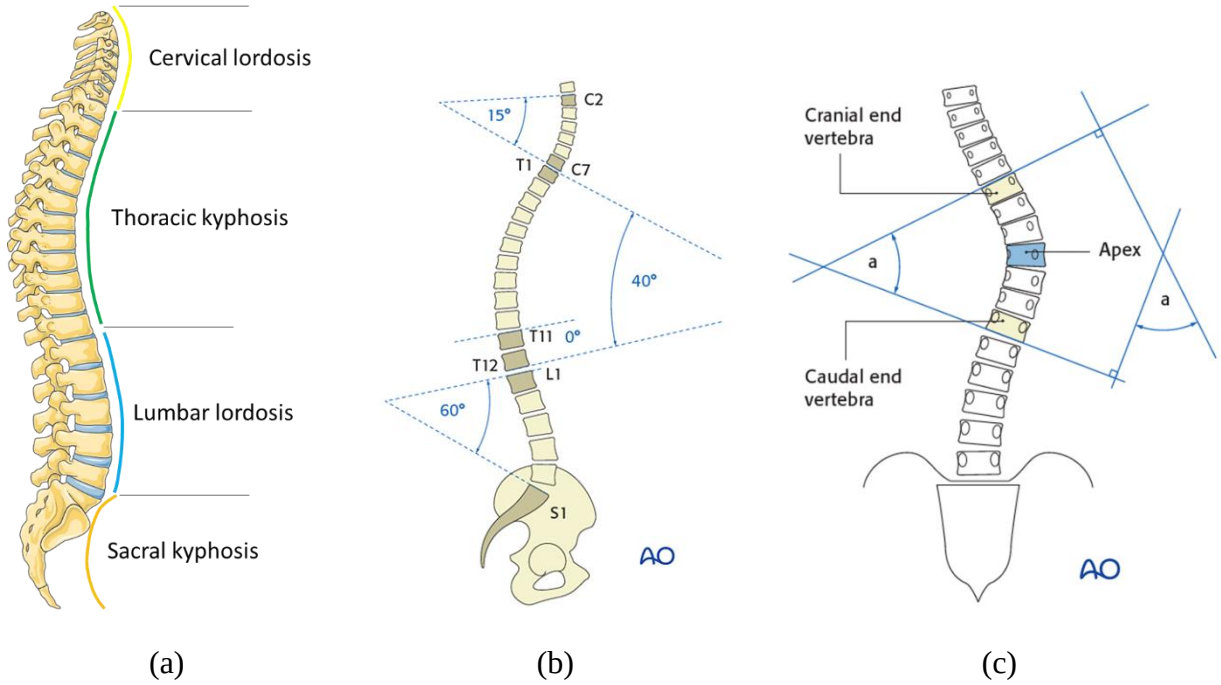

(a) (b) (c)

Figure 2.10 Spine physiological curvatures (a) Sagittal curvatures (adapted from Server Medical Art, license free) (b) Normal sagittal angles (c) Coronal Cobb angles measurement technique (Source: AO Surgery Refence, www.aosurgery.org, copyright with permission)

For the pelvis, the sacral slope, pelvic tilt, and pelvic incidence establish a geometrical relationship between the sacrum, lower limbs, and horizontal plane (Figure 2.11). This relationship is of importance given that the pelvis is responsible for transferring loads between the spine and lower limbs.

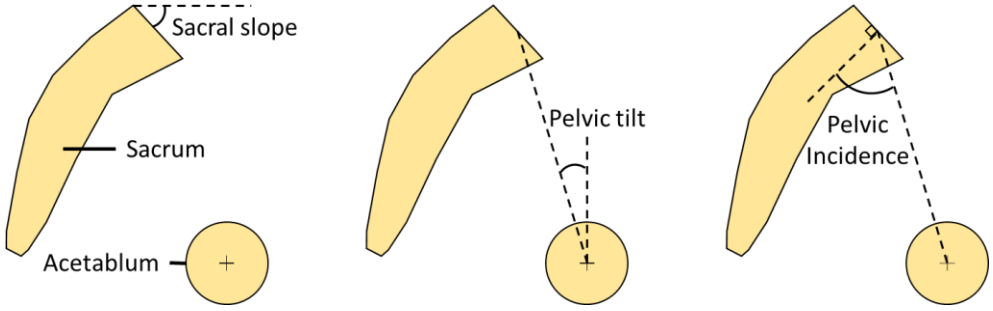

Figure 2.11 Pelvic geometrical parameters, lateral view

Sagittal balance, or sagittal vertical axis (SVA), is defined as the anterior-posterior distance between the C7 vertebral body and the posterior-superior corner of S1 (Figure 2.12). Neutral balance is +/- 5 cm, positive balance > 5 cm anterior to S1 reference, and negative balance < -5 cm

posterior to S1 reference (Oxland, 2016). This balance, or lack thereof, has been shown to correlate with clinical symptoms and is considered in the correction strategy of spines afflicted with deformity pathologies (Abelin-Genevois, 2021; Glassman et al., 2005; Schwab et al., 2010).

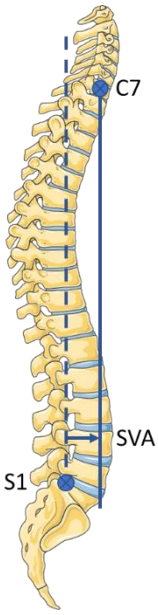

Figure 2.12 Sagittal vertical axis (SVA) (adapted from Server Medical Art, license free)

2.2 Spine pathologies

The proper functioning of the human spine can be affected by multiple pathologies ranging from mild backpains to severe deformations which affect millions of people worldwide (Kassebaum et al., 2016). Of particular interest for this project, the following section presents pathologies which affect the spine curvature and can lead to an instrumented spine correction surgery via posterior approach.

2.2.1 Scoliosis

Scoliosis is characterized by a 3D structural, lateral, rotated curvature of the spine (Figure 2.13). Causes of scoliosis can be vertebral malformation, neuromuscular disorder, or idiopathic (i.e., unknown cause). It is important to note that adolescent idiopathic scoliosis (AIS), which is manifested at or around puberty, represents more than 80 percent of pediatric scoliotic cases. According to the Scoliosis Research Society (SRS), adolescent idiopathic scoliosis occurs in both girls and boys, but upon entering adolescence, scoliosis in girls are five to eight times more likely

to increase in size and require treatment. The general guideline for observable onset of scoliosis is a curve measurement in the coronal plane greater than 10 degrees in Cobb angle. Using this criteria, epidemiological studies show that 1 to 3% of the 10 to 16 years old age group will develop some level of scoliosis (Weinstein et al., 2008). A lateral curvature less than 20 degrees is monitored, which is most cases, above 20 degrees to 40 degrees requires bracing, and above 40-45 degrees requires surgical intervention.

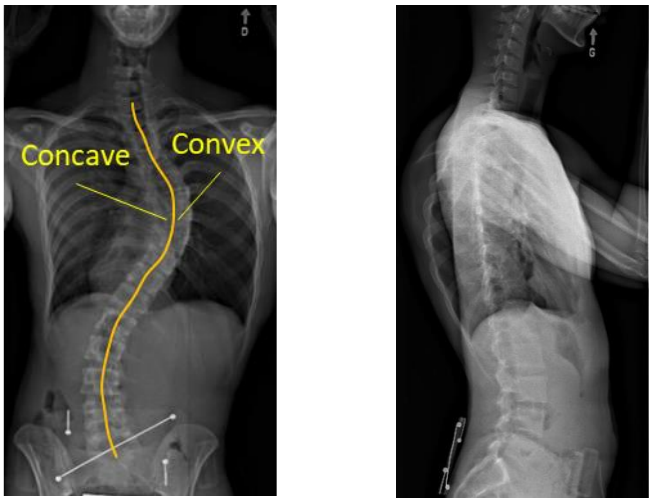

Figure 2.13 Posterio-anterior and lateral radiographs of AIS patient with identification of concave and convex sides in coronal curvature (Source: Sainte-Justine University Hospital database)

This progressive change in spine curvature results in a series of observational characteristics. The most externally apparent is general trunk deformity, consisting in a varying combination and magnitude of transverse and coronal rotation of the shoulders, lateral and postero-anterior shift of C7 with respect to S1, rib hump, and overall “S-shape” spine (Mac-Thiong et al., 2002). Lateral and postero-anterior radiographs of the trunk reveal the skeletal construct of the three-dimensional deformation, with high inter-patient variability. In the coronal plane, each spine curvature is delimited by region; proximal thoracic (PT), main thoracic (MT), and thoracolumbar/lumbar (TL/L). A lateral curvature presents a concave and convex side, with an apical vertebra (most lateral within the curve) and its periapical region (adjacent vertebrae) (Figure 2.13). Lenke introduced in 2001 a classification system to regroup curve types into six groups with the addition of a lumbar modifier based on the position of the center sacral vertical line with respect to the lumbar apical vertebra (Ovadia, 2013). A thoracic sagittal profile modifier is also included in the classification

based on the T5-T12 kyphosis angle. This system remains the gold standard for classification but does not address the observed variations in transverse plane axial rotation deformity (Labelle et al., 2011; Stokes et al., 2009). The cosmetic appearance of scoliosis is linked to psychological distress amongst patients and reduced quality of life, but also back pain and for severe cases diminished lung function due to the rib cage deformation (Johnston et al., 2011; Weinstein et al., 2008).

2.2.2 Hypo/hyperkyphosis

Deviations from the normal thoracic kyphosis may be characterized by excessive rounding (hyperkyphosis or roundback) or flattening (hypokyphosis or straight back syndrome) of the back (Figure 2.14). Kyphosis disorders can be congenital, developmental, post-traumatic (i.e., resulting from injury) or the result of the aging spine. Congenital kyphosis refers to bone malformation occurring in utero, while developmental kyphosis occurs later during growth and can either be postural (flexible) or structural (rigid). Typically associated with puberty and exhibiting vertebral wedging in the sagittal plane, structural hyperkyphosis is also referred to as Scheuermann's kyphosis. Age-related hyperkyphosis may also occur from several spine aging related processes like degenerative disc disease, muscle weakness and vertebral fractures (Katzman et al., 2010). A healthy spine having a typical thoracic kyphosis angle ranging from 20 to 40°, hypokyphosis will be less than 20° and hyperkyphosis above 40°.

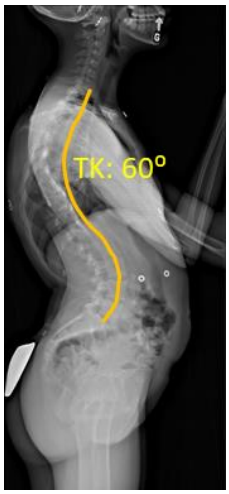

Figure 2.14 Lateral radiograph of AIS patient with hyperkyphosis (Source: Sainte-Justine University Hospital database)

For hyperkyphosis, all patients with angles less than 80° are generally treated nonsurgically with anti-inflammatory medications, physical therapy, and possibly bracing for younger patients still growing. Above 80°, surgical intervention is indicated due to higher risks of pain, neurological impairment, diminished lung function and cosmetic impact.

Hypokyphosis is mostly seen in AIS patients with primary thoracic scoliosis and can also be the result of a significant spinal correction in the coronal plane by surgical treatment via posterior approach without sufficient sagittal correction (Acaroglu et al., 2019). Post-operative sagittal imbalance can result in compensatory mechanisms which have been linked to proximal junctional kyphosis and adjacent segment degeneration events (Cheung, 2020). Corrective surgery to re-establish sagittal balance may be advised. There are also documented cases of congenital straight back where the anteroposterior narrowing on the rib cage has been shown to lead to a compression of the heart and diminished cardiac function (Davies et al., 1980).

2.2.3 Spondylolisthesis

Spondylolisthesis is characterized by the anterior displacement of a vertebra with respect to the one below it (Figure 2.15). The main causes are isthmic (i.e., fatigue or stress fractures of pars) and degenerative (e.g., facets arthrosis, disc degeneration). Isthmic cases occur mostly at the L5-S1 level, while degenerative cases are at the L4-L5 level. Isthmic spondylolisthesis is one of the most common conditions treated by spinal surgeons, affecting 4.6% to 7.7% of the population (Noorian et al., 2018). A grading scale ranging from 1 to 5 is used to assess the condition’s severity. A measurement of the anterior displacement of the upper vertebra is taken and presented as a percentage of slipped distance over the lower vertebral body diameter. Grade I is <25%, II is 25% to 50%, III is 50% to 75%, IV is 75% to 100%, and V is complete fall off referred to as spondyloptosis. Higher grades are also characterized by a sagittal rotation of the displaced vertebra.

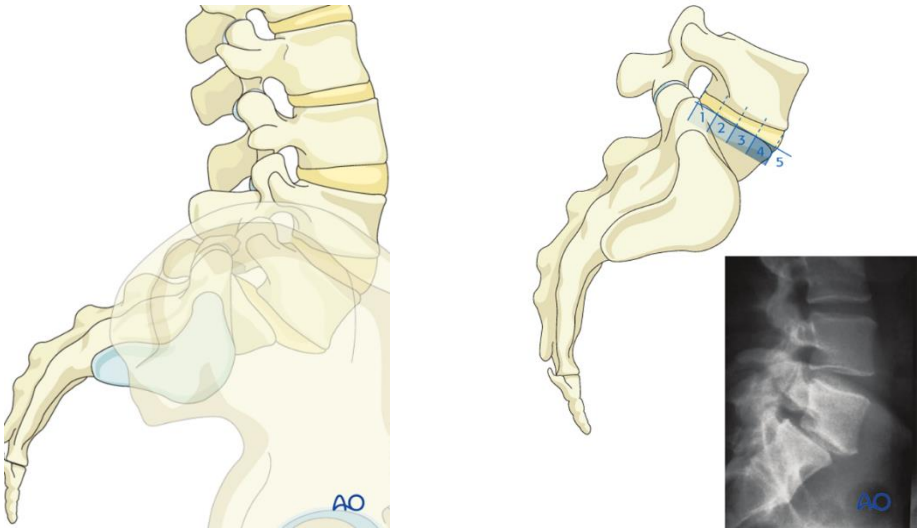

(a) (b)

Figure 2.15 Illustration of spondylolisthesis (a) General slip at the L5-S1 level, lateral view; (b) Grading system (Source: AO Surgery Refence, www.aosurgery.org, copyright with permission)

This spinal disorder is a common cause of low back and leg pain. Symptomatic patients may first be treated via physical therapy, pain medication, epidural steroid injections, and transforaminal injections. If the degeneration is too severe, surgery may be necessary.

2.2.3.1 Disc degeneration

Lumbar degenerative disc disease (DDD) is characterized by the progressive and irreversible deterioration of the intervertebral disc structure. Typically linked to time related wear and tear, the onset of the degeneration is multifactorial and tends to be more prevalent in elderly patients. This condition can slowly lead to degenerative spondylolisthesis, bulging disk and disk herniation, the latter occurring when the inner nucleus pulposus ruptures out of the annulus (Figure 2.16). Standard non-surgical treatments include physical therapy and pain medication. For more severe symptoms, epidural steroid injections, lumbar fusion (arthrodesis), and total disk arthroplasty may be considered (Madigan et al., 2009). Recent studies are also investigating the molecular characteristics of DDD in the hope of one day leveraging stem cells and tissue engineering to repair degenerated discs (Bydon et al., 2020).

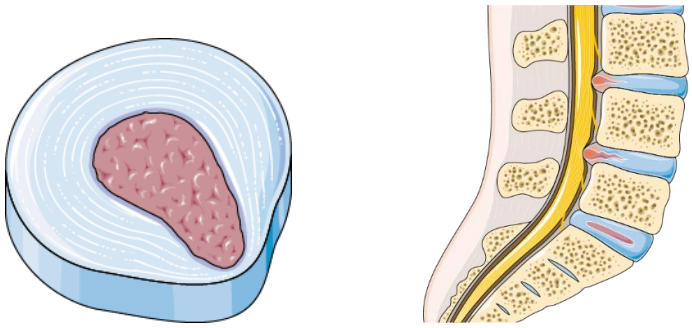

(a) (b)

Figure 2.16 Illustrative examples of disc degeneration (a) IVD bulging (b) Spinal canal compression from IVD building (adapted from Server Medical Art, license free)

2.2.4 Trauma

Trauma covers a wide range of instances where the spine integrity is compromised following low or high energy events. Low energy events are best defined by the "wear and tear" effect over a long period of time observed in activities such as sports training and repetitive motions solicitating the trunk. High energy events encompass vehicle accidents, falls, gunshots, and high impact incidents. The affected bones, intervertebral discs, muscles, and ligaments can generate local instabilities which if mild may be treated by physical therapy, but more severe scenarios may require surgical intervention.

2.3 Corrective surgical interventions

For the previously presented pathologies, spine correction surgery can vary greatly in approach, instrumentation, and technique. Regardless of the methods, the surgical goals remain to restore stable sagittal and coronal balance for the patient, and sometimes to correct spinal deformity. Surgery can either be performed using a posterior (i.e., incision on the patient's back) or anterior (i.e., lateral incision) approach. For this project, focus is given on the posterior surgery approach. With the patient laying in the prone position, surgical access to the spine is gained through a posterior incision, followed by removal of ligaments and bone (osteotomy) at selected locations to increase spine flexibility, placement of anchoring instruments, contoured rod insertion, stabilisation and/or corrective maneuvers followed with construct fixation, and finally the addition of osteoinductive substitutes to promote bone grafting (arthrodesis).

2.3.1 Instrumentation

The operated segment is instrumented to provide spinal stability and/or spinal curvature correction. During surgery, the surgeon will shape and anchor to the bone structure a rigid metallic structure using anchoring implants fixed to selected vertebrae and interconnected with rods and fixators (Figure 2.17).

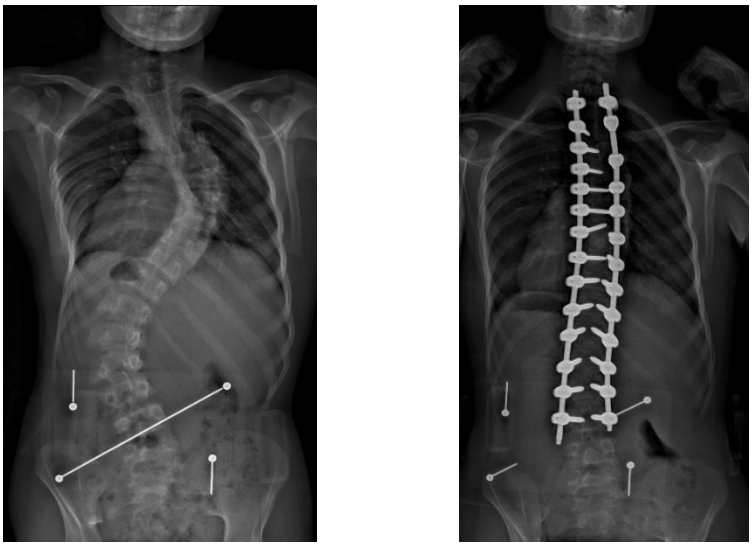

Figure 2.17 PA radiographic example of pre-operative to post-operative correction of AIS with an instrumented construct (Source: Sainte-Justine University Hospital database)

To create the vertebral bone to implant interface, different anchoring devices can be used, including hybrid constructs by combining several. A hook can be placed on the lamina, pedicle, or transverse process. Sublaminar wiring is also used, and more recently sublaminar and subtransverse bands using metal clamps and polyester belts were developed (Hongo et al., 2009; Strickland et al., 2016). Lastly, specially designed screws can be inserted in the vertebra, with pedicle screws recognized for their high pull-out strength and demonstrated capability in providing a 3D correction of the spine as part of the instrumentation set (Kadoury et al., 2009) (Figure 2.18).

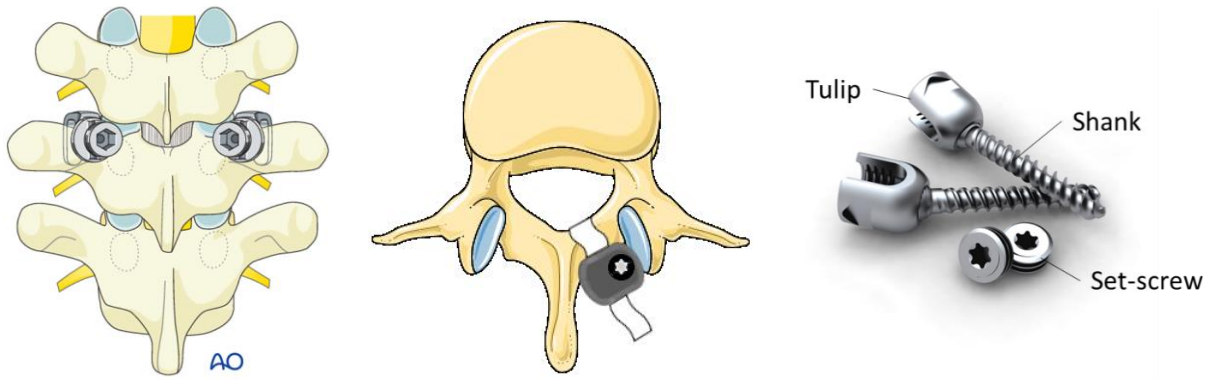

(a) (b) (c)

Figure 2.18 Anchoring devices (a) Transverse hooks (Source: AO Surgery Refence, www.aosurgery.org, copyright with permission); (b) Laminar band (adapted from Server Medical Art, license free); (c) Multiaxial pedicle screws (Source: Wikipedia, 2021, license free)

The insertion of the pedicle screw shank follows a linear trajectory through the pedicle. Once the implants are in place, contoured cylindrical rods and implants are connected to provide the desired curvature correction. Made of stainless steel, titanium, or cobalt-chrome, the rod diameter generally vary between 4.5 and 6.35 mm (Le Naveaux, 2016). The rods are contoured by the surgeon based on the desired post-operative curvature correction in the sagittal plane (Figure 2.19). The screw-to-rod connection is achieved by securing the rod in the screw tulip saddle and locking using a set-screw. Different screw types are available, the most popular being monoaxial, uniaxial, and multiaxial. Each type offers varying levels of freedom at the screw-to-rod connection which have been shown to influence stresses at the bone-screw interface. By increasing the connection's level of freedom, less force is required to properly seat the rigid rod with the screw tulip geometry, thereby reducing the loads transferred at the bone-screw interface (M. Driscoll et al., 2015; Wang et al., 2012). The pedicle screw is now the implant of choice for spinal fusion corrective surgeries by posterior approach in the context of minimally invasive surgery which leverages the advances in computer navigation and robotics over the last 15 years (Stull et al., 2019).

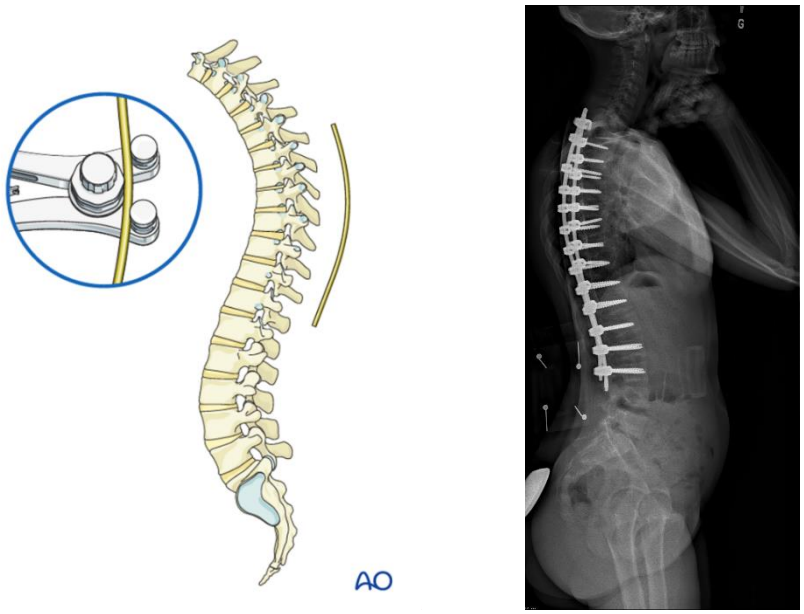

(a) (b)

Figure 2.19 Contoured rods (a) Contouring with French bender (Source: AO Surgery Refence, www.aosurgery.org, copyright with permission); (b) Post-operative lateral radiograph of the instrumented spine with pedicle screws, hooks and contoured rods (Source: Sainte-Justine University Hospital database)

When looking at the overall instrumented region, a more rigid construct will deform less and favor more control on the correction, but no optimum screw pattern has been established within the medical community (Le Navéaux et al., 2016; Wang et al., 2012). Rod contouring is typically performed manually using a French bender, but recent innovations include the introduction of a computer-assisted system (Bendini) (Tohmeh et al., 2014). A higher level of instrumented segments with spinal fusion is synonymous to an overall reduced range of motion for the patient, since the fused segments are no longer mobile.

2.3.2 Corrective maneuvers

Correction of the spine deformity is achieved intra-operatively by a series of maneuvers performed by the surgeon and involves the use of instrumentation. The maneuvers presented in this section remain at the discretion of the surgeon. As a result, there is some variability in techniques for correcting the spine. The surgeon may proceed with the removal of ligaments and bone

(osteotomies) to increase local vertebral mobility prior to the correction of the deformity. The connection between the implants and the contoured rods can be achieved using different correction methods.

Rod rotation consists in placing and contouring the concave rod to approximately follow the curvature of the scoliotic spine in the coronal plane (Figure 2.20a). The rod is then rotated 90 degrees to have its curvature now laying in the sagittal plane, therefore correcting the coronal deformity, and achieving sagittal correction in one movement. A convex rod rotation can also be done in conjunction with the concave rod.

For the translation maneuver, the concave contoured rod is first fixed to have the contour in the sagittal plane using the proximal and distal vertebrae. Implants are then sequentially pulled towards the rod using a reduction device to achieve both coronal and sagittal alignment (Figure 2.20b).

The cantilever maneuver consists in first fixing the contoured rod at the proximal or distal end of the instrumented segment, followed by the application of a downward force by the surgeon at the unfixed extremity (Figure 2.20c). As the rod progressively reaches the unfixed implants, the cantilever effect created will contribute to the sagittal and transverse alignment, especially when combined with differential rod contouring.

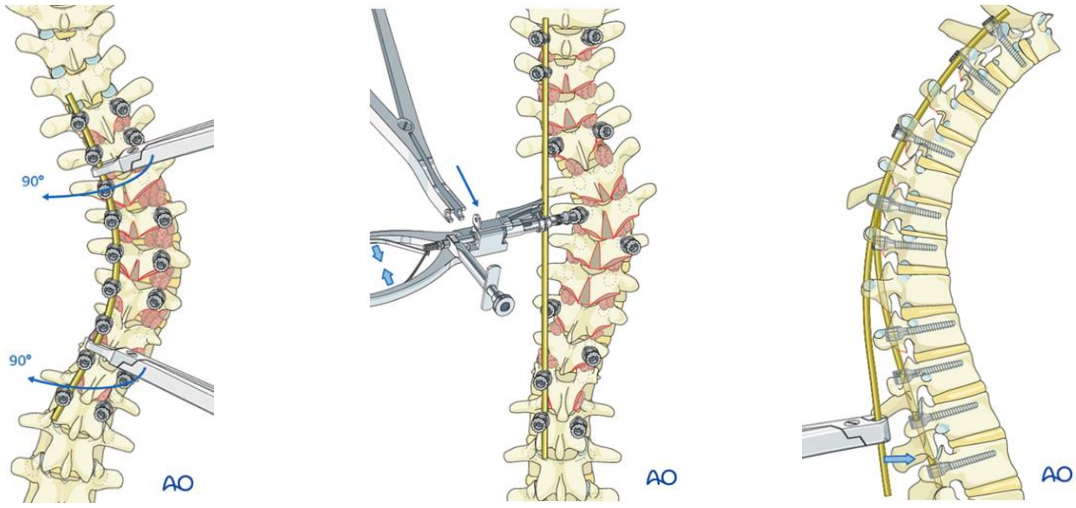

(a) (b) (c)

Figure 2.20 Intraoperative corrective maneuvers (a) Rod rotation; (b) Implant translation; (c) Cantilever maneuver (Source: AO Surgery Refence, www.aosurgery.org, copyright with permission)

Differential rod contouring consists in creating a curvature difference between the concave and convex rods. A higher curvature is used for the concave side and lower curvature for the convex side. This difference will provide posterior traction on the concave implants and anterior compression on the convex implants, thereby creating a moment along the cranio-caudal axis for derotation of the spine on the transverse plane (Figure 2.21). Higher differential rod contouring increases transverse correction but has been shown to result in higher screw pull-out forces (Wang et al., 2016).

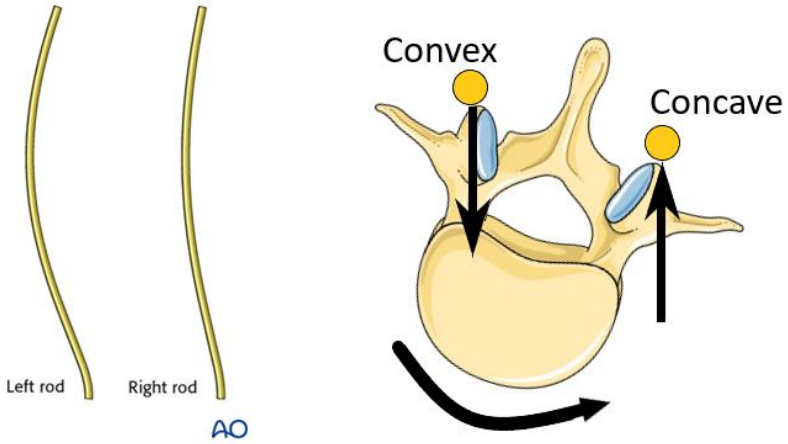

(a) (b)

Figure 2.21 (a) Differential rod contouring (Source: AO Surgery Refence, www.aosurgery.org, copyright with permission); (b) rotational effect in transverse plane, top view (adapted from Server Medical Art, license free)

Derotation of the spine can also be achieved by direct vertebral rotation (DVR). This technique introduced by Lee et al. (2004) uses metallic tubes called screw derotators temporarily fixed to the pedicle screws to carefully apply a torque to the vertebra along the cranio-caudal axis (Figure 2.22). It can be performed at each segment (segmental derotation) or for a group of vertebrae (en bloc derotation). En bloc derotation is typically performed in the apical and periapical regions of the curve.

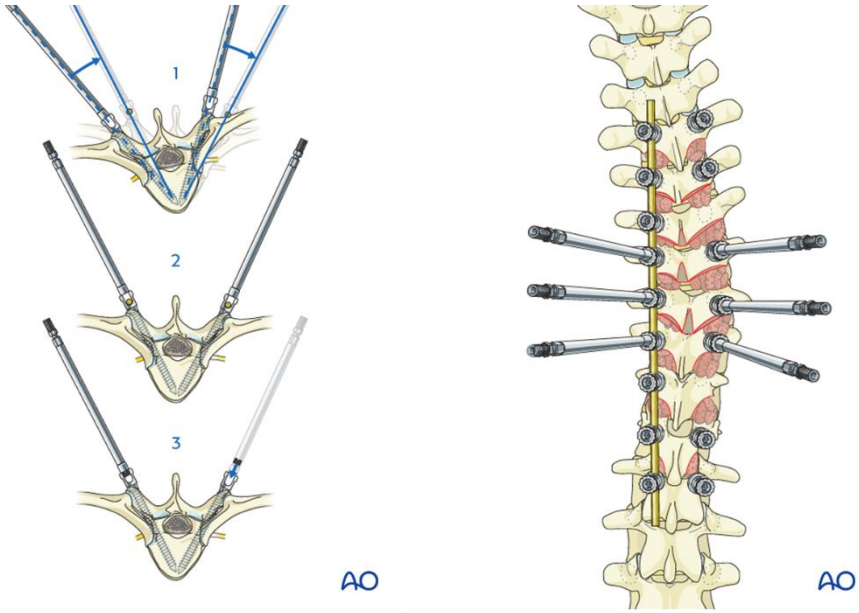

(a) (b)

Figure 2.22 Direct vertebral rotation (a) Segmental; (b) En bloc (Source: AO Surgery Refence, www.aosurgery.org, copyright with permission)

The above correction techniques are typically executed with pedicle screw heads closed using set screws, but not locked to the rods, allowing rod mobility and translation of the screw along the rod longitudinal axis at each instrumented segment. To complement global coronal, sagittal and transverse corrections, a combination of compression and distraction maneuvers can be applied to locally adjust each vertebra incrementally (Figure 2.23a and b). Compression is applied to the convex screws and distraction to the concave screws using pliers. These adjustments improve intervertebral alignment uniformity, residual deformity, and transition to non-instrumented vertebrae. Finally, *in situ* rod contouring can also be done to plastically reshape the rod to the desired shape at each instrumented level (Figure 2.23c). Once the final desired correction is obtained, screws are locked to the rods to fix the construct and proceed with the bone graft.

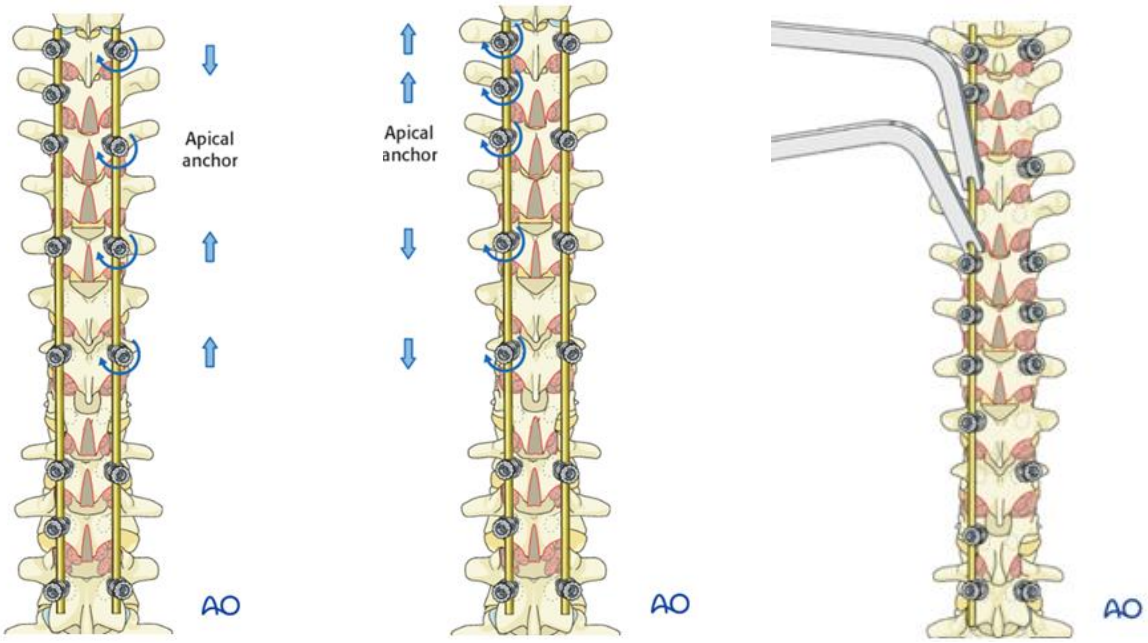

(a) (b) (c)

Figure 2.23 Local adjustment techniques (a) Compression; (b) Distraction; (c) *In situ* rod contouring (Source: AO Surgery Refence, www.aosurgery.org, copyright with permission)

2.4 Perioperative patient positioning

With any surgery, patient positioning is of upmost importance. Intraoperative positioning objectives can be listed that best describe a safe intervention: to facilitate exposure, surgical and radiological access, minimize bleeding, stabilize and preserve vital structures (e.g., organs, nerves), and provide proper ventilation to the patient. As detailed in previous sections, spine surgeries deal with a complex biological structure protecting the nervous and vascular systems, combined with deep soft tissue removal, high surface area surgical site, and lengthy interventions which can last several hours. In this context, the patient positioning strategy during surgery cannot be overlooked.

The original intent for a dedicated spine surgery table design was the intraoperative relief of abdominal pressure and preservation of lumbar lordosis. As shown in section 2.1, the spine's vertebral venous system plays an integral role in the global venous return, compensating when the vena cava is obstructed. When laying in the prone position on a regular horizontal mattress the patient's abdomen is compressed and so is the vena cava, therefore promoting a diversion in blood flow to the vertebral venous system (Schonauer et al., 2004). The surgical site for a posterior

approach surgery will expose the vertebral venous system, putting the patient at risk of excessive bleeding. To prevent this undesirable, but necessary vascular compensation mechanism, the contact area between the patient and the table had to be reduced to free the abdomen from contact pressure. It was in 1967 that the first dedicated spine operating frame was reported by Relton and Hall (1967) (see section 2.4.2 for details).

The operating tables and positioning modalities presented in this section have been developed and optimized over the last 60 years to improve surgical outcomes and minimize risks of intraoperative and postoperative complications. Even today, common positioning complications remain. The first one being skin pressure sores, which are the result of a prolonged contact pressure at the patient's skin to table interface combined with friction and shear stress. High probability incidences of peripheral nerve damage in the form of compression neuropraxia (mild injury) or meralgia paresthetica (numbness) to the brachial plexus and lateral femoral cutaneous nerve have also been reported in the literature (DePasse et al., 2015; Kwee et al., 2015; Schonauer et al., 2004). More severe complications associated with patient positioning for spine surgery, while uncommon, are reported. A systematic review by Shriver et al. (2015) showed a positive correlation between operation time and occurrence of position complications, resulting from the excessive pressure applied to ventral or lateral structures for a prolonged period. The most commonly reported complication from the Shriver et al. review was vision loss, also referred to as perioperative visual loss (POVL) which can be irreversible is some cases.

2.4.1 Patient positions

Before surgery, the patient is put under general anesthesia on a standard hospital rolling bed, in the supine position (laying on his back). The patient is then transported into the operating room and transferred on the operating table. Safe and efficient patient transferring is a delicate step requiring the synchronized effort of the medical staff since the patient is in a completely relaxed muscular state. As reported by Asiedu et al. (2018), the anthropometry of the patient may be a source of anxiety and physical stress to the medical staff, especially when dealing with positioning on a spinal surgery frame which involves a patient rotation to its intraoperative position. Depending on the selected surgical approach and levels to be instrumented, several positioning strategies are possible.

In the context of spinal surgery, the two main patient positions are prone and lateral decubitus. The prone position will have the patient laying face down or to the side with his back exposed to the

ceiling (Figure 2.24a). The patient's head, arms and legs are independently supported to distribute the contact pressure between the patient and operating table. Limbs are placed in a moderately flexed position to avoid ligament, muscle, or nerve tensions. The abdomen is free of contact to relieve vascular pressure, therefore relying on the rib cage and pelvis's iliac crests to support the trunk. This position is suited for posterior approach surgeries and is the most used. Variations of the prone position include the kneeling, knee-chest and knee-elbow positions, which are used to reduce the lumbar lordosis through hip flexion, thus facilitating surgical access at the lumbar levels. Surgeons may also decide to perform a reverse Trendelenburg with the prone position by tilting the table with respect to the horizontal plane. This technique improves the patient's intraocular pressure by lowering the heart, as increased intraocular pressure is associated with optical injuries such as POVL.

The lateral decubitus has the patient laying on his side, most often with a 90 degrees angle between the patient's back and the table (Figure 2.24b). An independent head support helps maintain neutral spine alignment, with the arms placed on an arm board structure facing forward of the patient. Lower leg flexion sometimes combined with antero-posterior hip supports are used to stabilize the torso against ventral tilt. With the patient's side facing upwards, this position promotes surgeries by lateral approach and facilitates access to the anterior features of the vertebra (i.e., vertebral body and intervertebral disc). Spine surgeries by lateral approach are considered minimally invasive, since they preserve the back's soft tissues as compared to traditional posterior approach surgeries. They do imply a thoracotomy and deflation of the upper lung to gain access to thoracic vertebral levels. This approach is also not suited for instrumenting the L5-S1 segment since the iliac crest prevents access. The presented positions and associated tables must also allow intraoperative radiographic capture of the surgical site to dynamically monitor the instrumentation's integration and resulting spine deformity correction. Mobile fluoroscopic imaging modalities such as C-arms, U-arms and O-arms are used to that effect.

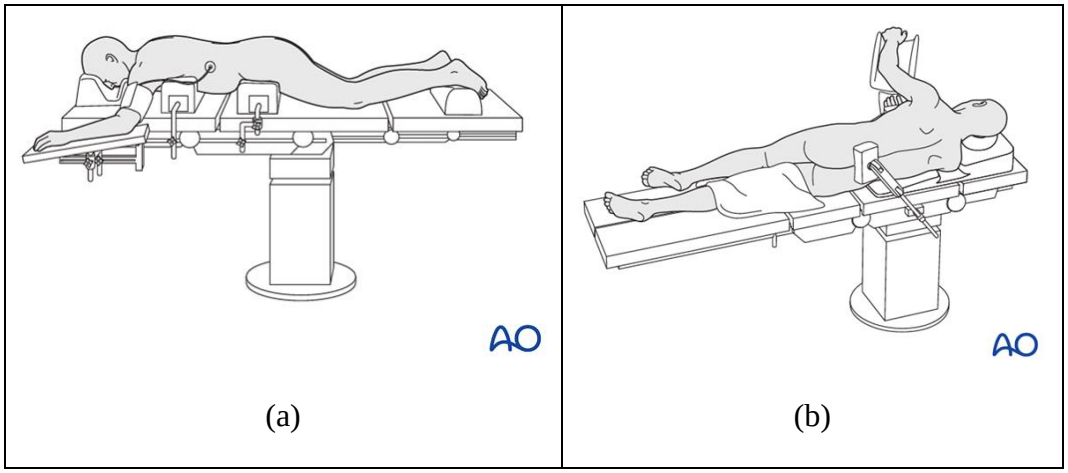

(a) (b)

Figure 2.24 Main positions in spinal surgery (a) Prone; (b) Lateral decubitus (Source: AO Surgery Refence, www.aosurgery.org, copyright with permission)

2.4.2 Patient positioning modalities

Briefly discussed in the introduction to section 2.4, the Relton-Hall operating frame, as reported in 1967, was the first tailored patient positioning system for posterior approach spinal fusion (Anderton, 1991). It consists of a simple rectangular metallic structure equipped with four individual inclined V-shape cushioned pads (Figure 2.25). The frame can be set on a standard operating table and the pads secure the thorax and pelvis in the lateral and anterior directions while leaving the abdomen free of contact pressure. With its simple and economical design, the Relton-Hall frame quickly became the standard of care in posterior approach spine surgery for many years and is still actively used today with several studies documenting outcomes associated with its use (see section 2.5.5).

(a) (b)

Figure 2.25 Examples of Relton-Hall 4-poster frames (a) Standard metallic (Source: Surgmed, www.surgmed.com, copyright with permission); (b) Modified non-metallic (Source: Sainte-Justine University Hospital database)

The Hastings frame, described in 1969 by Hastings, was developed to provide a more secured modified knee-chest prone position. The Wilson frame, still frequently used today, consists in a rigid frame with two curved lateral pads running the full length from the thorax to the pelvis (Figure 2.26). The center opening maintains the abdomen free of pressure and the curved design promotes a continuous sagittal curvature of the spine in accordance with the curvature of the cushion, thus reducing lumbar lordosis.

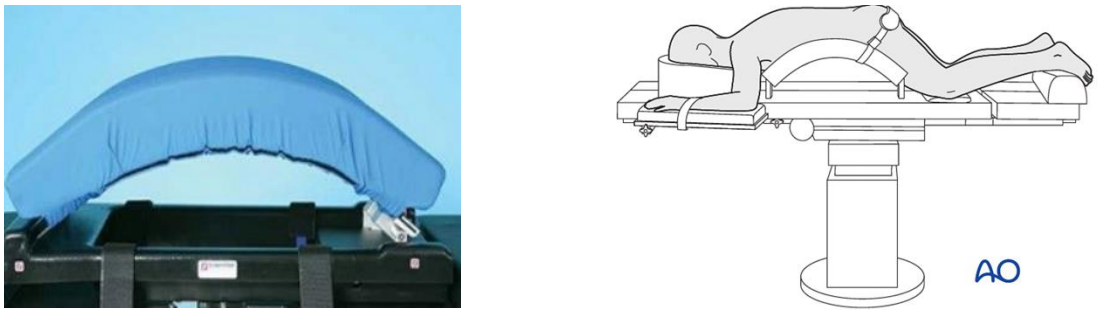

(a) (b)

Figure 2.26 Wilson frame (a) Close-up lateral view (Source: Merivaara, www.merivaara.com, copyright with permission); (b) Use in prone position (Source: AO Surgery Refence, www.aosurgery.org, copyright with permission)

With the evolution of positioning modalities came modular operating tables integrating spinal surgery accessories and dedicated spinal surgery tables. The Trumpf Medical TruSystem™ 7500,

or the Merivaara Practico™ systems, are examples of modular operating tables which can be outfitted for spinal surgery (Figure 2.27). These systems offer a range of adjustments for supine, lateral or prone positions with a large set of interchangeable modular sections to accommodate a wide range of general and orthopedic surgeries, including spinal. For posterior approach spinal surgery, the integration of a Wilson frame with dedicated head and arm rests is possible, as well as different options of pads and cushions.

Figure 2.27 Modular operating table with prone spine surgery accessories (Source: Merivaara, www.merivaara.com, copyright with permission)

The Andrews SST-3000 table is a spinal surgery table which specializes on the prone knee chest position for lumbar surgeries. The knees are maintained flexed at 90 degrees and the pelvis is secured in the caudal direction using a posterior cushion. Hip flexion can be adjusted via the table's rotation of the lower limbs. The table allows for Trendelenburg, reverse Trendelenburg and a 10° lateral tilt (Figure 2.28).

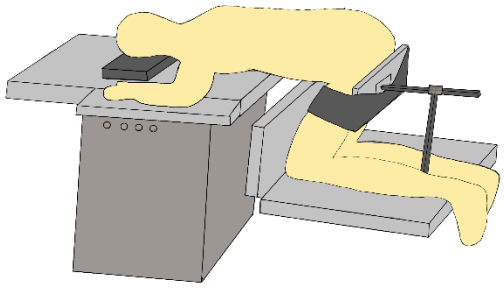

Figure 2.28 Prone knee chest position on Andrews table

An important evolution in operating table design for spinal surgery came with the Jackson table invented in 1992 by Dr. Roger Jackson (1992). This table introduced an open frame design combined with dual supporting columns suitable for supine, prone and lateral approach surgeries (Figure 2.29a). The system relies on an open rectangular ladder frame with the longitudinal

structural members acting as railings to mount different positioning accessories, including a full-length radioluscent top for supine and lateral positioning. The radioluscent top combined with the prone positioning surgery top allowed to reposition a patient from supine to prone (i.e., 180° rotation along the horizontal axis). The height of the support columns was adjustable for Trendelenburg, reverse Trendelenburg, and overall table height variations. 12° lateral roll was also possible via the two support column hinges. From this design the Axis Jackson System® followed, now equipped with a central hinge on the railings which allowed for intraoperative patient articulation within a range of 35° hinge up to 20° hinge down (Figure 2.29b). The supine to prone horizontal rotation feature was no longer supported by this model. The latest evolution of the Jackson table is the ProAxis® spinal surgery table from Mizuho OSI® launched in 2013. This version replaced the support columns table base system with two triple hinged robotic arms for precise control of the central hinge absolute position during its rotation. The degree of flexibility and adjustments enabled by the presented Jackson table models also come with a level of complexity in operation for the medical staff, as reported by Asiedu et al. (2018) who reviewed positioning and repositing procedures with the Jackson table. Mizuho OSI® also offer the Trios® and Modular Table System (original Jackson) tables still based on the dual columns table base system without the central hinge.

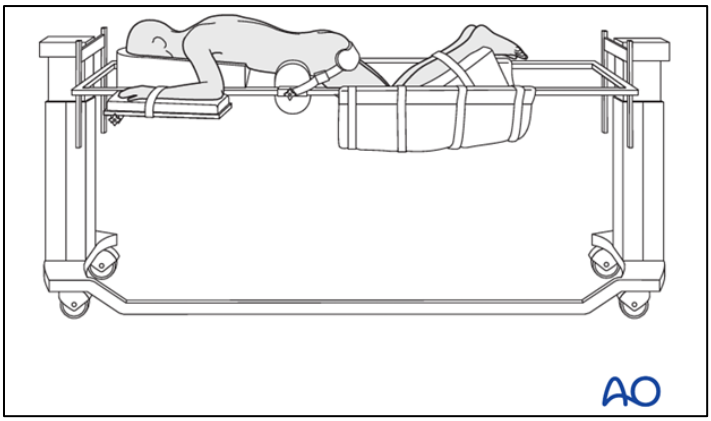

(a)

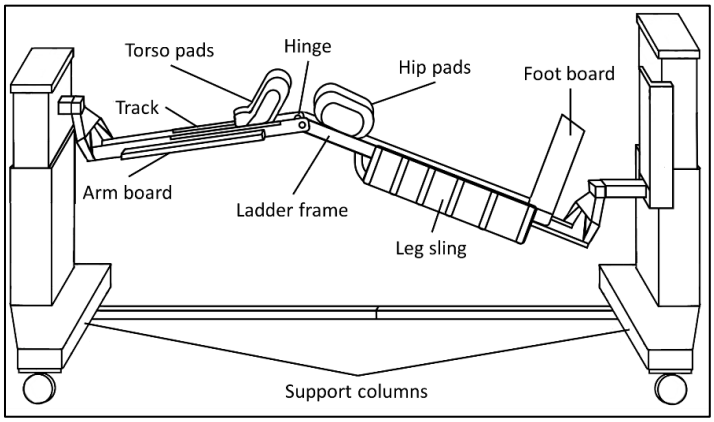

(b)

Figure 2.29 Jackson tables (a) Original (Source: AO Surgery Refence, www.aosurgery.org, copyright with permission) (b) Axis Jackson System® with central hinge

Other currently available modern positioning modalities include the Hillrom™ Trumpf Medical specialty tabletop Carbon Spine based on the ladder frame concept without a hinge. The Hillrom™ Allen® Advance table is capable of manually repositioning an anesthetized patient from supine to prone and the Hillrom™ Allen® Spine system is a module which attaches to a standard operating table and can benefit from the table's adjustments to provide some hip rotation. Lastly, the Mizuho OSI® Insite® table is a cantilevered surgery table with ladder frame and no hinge.

The previously discussed frames and specialized operating tables all employ a combination of accessories to achieve safe positioning of the patient. Pads, pillows, and rolls constitute the first essential set. Since contact pressure is accentuated on the pelvis and thorax to compensate for the

relief of the abdomen, visco-elastic foam or gel cushioning materials are selected for support. Pillows and pads come in a variety of shapes and sizes to conform to the patient's morphology and will be placed by the medical staff to best redistribute the patient's weight and avoid overextension of joints (i.e., knees, ankles, shoulder, elbows). Head cushions are designed to permit ventilation and minimize contact pressure on the eyes. Straps and belts are used to firmly secure cushions and/or positioning frames on operating tables, and a leg sling can used to support lower limbs on ladder frame designs like the Axis Jackson System® or Hillrom™ Allen® Advance table. Tables equipped with a central hinge enable the surgeon to intraoperatively modulate the alignment of the spine, with focus on the lumbar lordosis when in the prone position. This dynamic positioning enables the surgeon to facilitate exposure of the lumbar segment by reducing lordosis, followed by restoration of physiological lordosis to finalize the construct fixation and arthrodesis phases. Dynamic positioning using a hinge is complemented by a thorax translation device to avoid excessive skin shear forces and spine distraction or compression. Lastly, if head traction is determined necessary by surgeons as a mean to intraoperatively align and stabilize the cervical spine, operating tables can be outfitted with Mayfield, bivector, or halo ring skull clamping devices.

Innovations are still under development for positioning modalities, as can be seen by the Warsaw Orthopedic Inc. patents filed in recent years. This child company of Medtronic plc describe a modular surgical table made of the joining of two single column systems which can operate independently or in unison to adapt to several patient positioning scenarios (Jackson, 2020). When joined, the dual support system can be equipped with a central hinge and would permit supine to prone repositioning. It is designed to be compatible with prone, prone knee chest, supine, and lateral decubitus positions. They also have another patent specific to spine surgery which describes a dual support column surgical frame with a main longitudinal support beam which would host pelvic tilt, leg adjustment and torso lifting mechanisms, and a coronal adjustment assembly (R. Lim et al., 2017). A torso sling is also presented as an alternate mean of securing the patient (R. K. Lim et al., 2020). This surgical frame would be compatible with prone and lateral decubitus positions. In the area of academic research, the Multi-Functional Positioning Frame (MFPF) system was a research only test bed developed at Polytechnique Montreal also based on the open ladder frame design. This frame, compatible with the Jackson's dual column support table base, served to explore new positioning modalities and manipulation of the spine in all three planes. The

MFPF exploratory modalities included the chest raise, lateral thorax, lateral leg, and hip torsion devices (Figure 2.30). Refer to section 2.5.5 for more details on positioning studies.

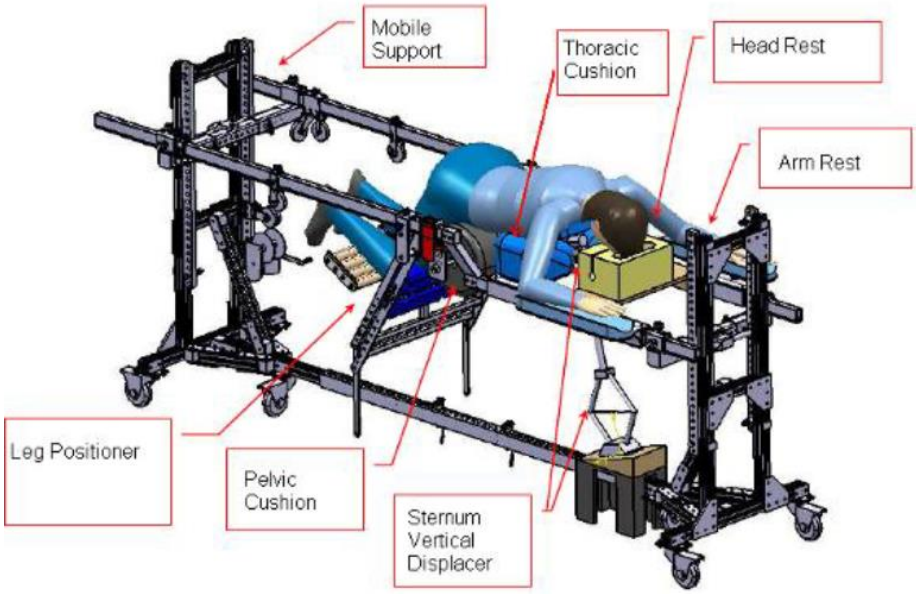

Figure 2.30 Computer-aided design image of MFPF (C. Driscoll, 2010)

2.5 Biomechanical simulation of the human spine

2.5.1 3D reconstruction of the spine

Computational modelling of the human anatomy enables the creation of a virtual patient on which explorative studies can be performed. The computer model, although an abstraction of the actual biological system of interest, can be made sufficiently credible to assist researchers in developing new devices, software tools or changes in clinical practices. When studying the biomechanical behavior of a system using a virtual model, the first step typically involves the creation of a visual representation. In the context of the human spine, as discussed previously, a healthy spine has distinct curvatures in the sagittal plane, but pathologies can alter its geometry in all three planes. Combined with large range of motion in translation and rotation, and a significant number of moving parts, the need for an accurate 3D representation of the spine becomes evident. For the biomechanical study of spine deformities, the biplanar reconstruction technique using stand-up radiographs is frequently used. This technique uses the 2D posterio-anterior (PA) and lateral (LAT) radiographs of a patient to semi-automatically segment the bone structure of the vertebrae and

pelvis using anatomical landmarks. This validated process generates a 3D representation with an error of less than 1.5mm (Humbert et al., 2009) (Figure 2.31). In recent years, the EOS imaging system (EOS Imaging, France) has permitted the creation of biplanar radiographs using 8 to 10 times less radiation compared to conventional radiographic modalities (Deschênes et al., 2010; Wybier & Bossard, 2013), making it a modality of choice to collect imaging data from younger cohorts more sensible to radiation. The rib cage can also be reconstructed using a semi-automatic technique using anatomical landmarks of the ribs and sternum (Bertrand et al., 2008). Once generated, this reconstruction can first be used to extract specific geometrical measurements in a 3D context, but also serves as the basis to develop physics-based models to simulate the spine behavior under different loading conditions.

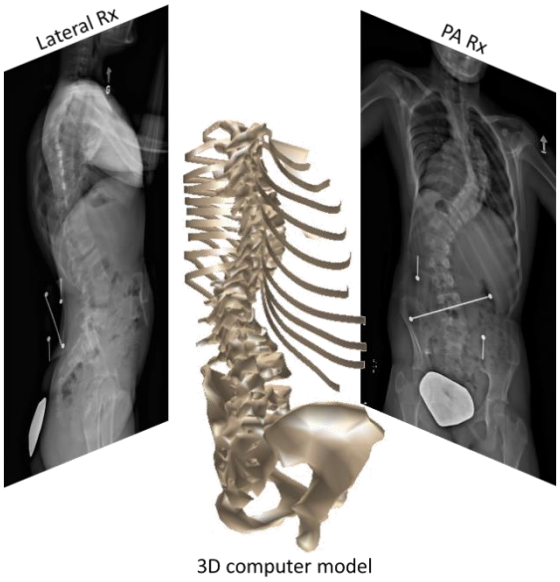

Figure 2.31 3D reconstruction concept using biplanar radiographs (lateral and PA) (Radiographic source: Sainte-Justine University Hospital database)

2.5.2 Material properties

A system's material properties must be understood and assigned to conduct a physics-based simulation. For the spine, the respective contribution of bone, intervertebral disc, muscle, fascia, and ligament to the overall system's mechanical properties can be explicitly defined or grouped. An extensive body of knowledge on material properties of the human trunk has been accumulated over the years by several researchers. Vertebrae, IVDs, ribs, cartilage, sternum, and pelvis

properties have been obtained experimentally and properties grouping in a stiffness matrix form have been proposed (Gardner-Morse et al., 1990; Panjabi et al., 1976; Pintar, 1986). The stiffness matrix can be adjusted using pre-operative spinal flexibility tests to optimize the segmental spinal stiffness to match radiographs taken under test (Cobetto et al., 2018; C. Driscoll, Aubin, Canet, Labelle, & Dansereau, 2012).

The explicit inclusion of features like muscles, fascia, and ligaments in the model versus grouped properties will depend on the study objectives and whether they play a significant role in the system's behavior (computational cost of modelling vs. effect). For example, in his study detailing the influence of lower limb positioning on the spinal geometry during intraoperative prone position, Driscoll et al. (2012) modeled the lower limbs including major muscles and connective ligaments using beam elements with linear properties. For another study looking into the sacroiliac joint biomechanics with implant fixation under physiological loads, Bruna-Rosso et al. (2015) focused on modelling bone, ligaments, and joint cartilage material properties.

Biological materials are known to have nonlinear material behaviors. Soft tissues will tend to exhibit viscoelastic properties and nonlinear phenomena like creep, relaxation, and remodelling which are time dependent. Bone's anisotropic behavior (i.e., direction dependent) is often simplified into a single isotropic value. Simplifying biological tissue behavior using linear relationships is common practice to improve computational efficiency and has yielded satisfactory accuracy when models are well adapted to their context of use. With the exponential improvement in computer's processing power over the years, integration of nonlinear material properties is an active field of research in spine biomechanics (Ghezelbash et al., 2018; Mills & Sarigul-Klijn, 2019).

2.5.3 Finite-element method

The finite-element method or finite-element modelling (FEM) is a numerical method for solving partial differential equations. By discretizing a large system into a subset of smaller finite elements with physical behavior bounded by known mathematical equations, one can analyze the resulting behavior of the larger system subjected to a given set of initial conditions. This method is applicable in a wide range of engineering domains like structural, fluid flow, heat transfer and electromagnetic analyses. The computerized geometry of the large system is discretized into a mesh of interconnected finite elements of various shapes and function. Each element consists of a set of

nodes (points) and element equations that enables to calculate how the nodes are meant to behave with respect to each other. The element equations will utilise the material properties defined by the user to solve them. For a steady-state structural analysis, the combination of all the interconnected finite elements will result in a global stiffness matrix which will be used in solving for the system's node displacements for a given set of initial conditions (i.e., loads and constraints applied at selected nodes).

In the context of the spine biomechanics, the FEM is an established method with documented studies dating back to the 1970s when Andriacchi et al. (1974) proposed a mathematical model combining the rib cage and spine. In the 1980s Shirazi-Adl et al. (1986) modeled the 3D motion of a L2-L3 segment as compared to experimental measurements. Since then, a considerable number of studies investigating a wide range of objectives have been published. Spine models can be regrouped into three main categories: global, refined and hybrid. Global models consider a geometrically simplified representation of the complete spine, with or without elements for the rib cage. These models will use a reduced set of finite elements to generally represent the vertebrae, pelvis, ribs, IVDs, ligaments, muscles, and fascia. This modelling abstraction is particularly useful to measure whole spine deformations and point loads at lower computational cost, but do not provide any means of measuring mechanisms internal to an anatomical system (e.g., vertebra internal stress distribution). For example, in their work Driscoll et al. (2012) used a global spine beam element model and integrated another global model of the lower limbs to study the influence of lower limbs positioning on spinal geometry (Figure 2.32). This *in silico* study allowed to characterize the influence of lower limb positioning on spinal geometry which was shown to improve intraoperative control of spine curvatures, especially lumbar lordosis.

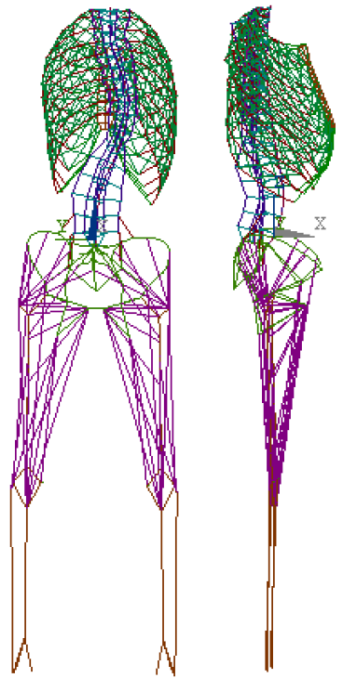

Figure 2.32 Example of global spine FEM with lower limbs (C. Driscoll, Aubin, Canet, Labelle, Horton, et al., 2012)

Refined models will concentrate on providing greater details on a selected sub-structure of the spine by creating a denser mesh more representative of the real geometry and assigning different mechanical properties based on internal features of the system that a global model would agglomerate. For example, a vertebra meshed with sufficient finite elements to distinguish between cortical and cancellous bone (Bruna-Rosso et al., 2015). This approach allows to measure with more details the internal stresses and strains distributions within a structure but comes at the cost of mesh generation complexity and computational time to solve the scenarios. Bianco et al. (2019) used refined models of the thoracic vertebrae to characterize pedicle screw performance under several loading conditions taking morphology and surgical choices into account. Sterba et al. (2019) used a refined model of the L1-L3 segment to determine how impact velocity and ligament properties variability can influence the lumbar spine response in traumatic flexion-shear conditions. Recently, El Bojairami et al. (2020) developed a comprehensive FEM of the T1-Sacrum spine with the inclusion of 273 tissues representing muscles, tendons, fascia and the abdominal cavity.

Hybrid models will integrate both the global and refined modelling approaches. They are used to measure detailed local effects influenced by global spine conditions. In her work, Cobetto

combined a global model of the spine with a refined model of the vertebrae including IVDs and bone growth modulation to model the evolution in time of the scoliotic spine following anterior vertebral body tethering (Figure 2.33) (Cobetto et al., 2018).

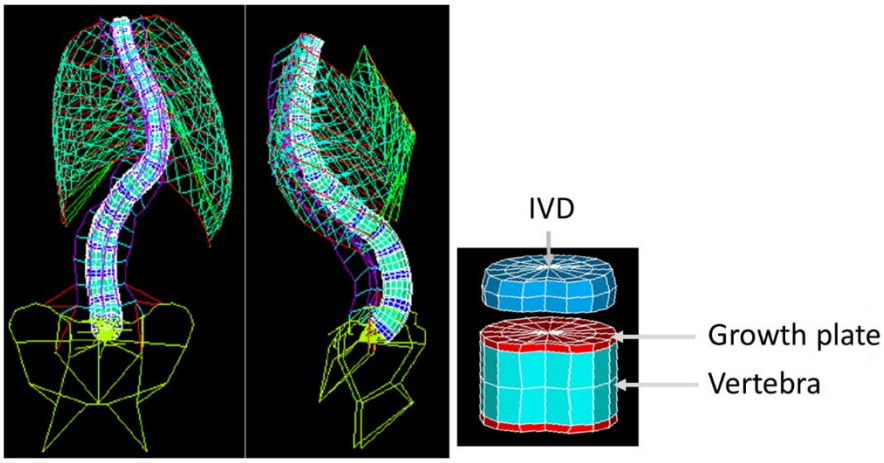

Figure 2.33 Hybrid model example of global spine FEM with refined vertebrae modelling (Cobetto, 2017)

The finite-element method is not the only means to computationally study spine biomechanics. Another popular method called multibody modelling (MBM), or multibody simulation (MBS), considers the spine as a series of interlinked mass-spring-damper systems that can be connected by flexible or kinematic links. The system's state for given initial conditions is then numerically solved via the equations of motion for rigid bodies. This method is much faster computationally thanks to the reduced number of degrees of freedom but does not provide stress or strain analysis capability. This modeling technique has found many uses in simulating instrumented spine correction surgeries and analyzing resulting forces acting at bone-screw and rod-screw interfaces (Le Navéaux et al., 2016; Wang et al., 2016). Studies have also coupled MBM with FEM into hybrid models that exchange feedback to change model properties or conditions during simulation (Fradet et al., 2016; Rajaee et al., 2021).

The FEM developer sits where Art and Engineering meet, having to balance the need for accurate representation of a real-life nonlinear complex system with finite computational capabilities. Geometry, mesh, elements selection, material properties, initial conditions, inclusions, and deliberate exclusions make up the mathematical abstraction which hopefully will result in a practical and credible representation. For its results to be meaningful, a computational model must be verified and validated to demonstrate its credibility in simulating the real-life phenomenon it

attempts to represent. To that effect, in the context of medical devices, international guidelines have been established which are discussed in greater details in section 4.3.

2.5.4 Instrumented spine surgery biomechanical studies

Numerical models have proven very useful in evaluating the performance of corrective spinal devices in correcting deformities, and the devices load-sharing capability within the instrumented construct. Biomechanical numerical studies have reported the effects on spine correction and instrumentation loading of implant selection, implant density (i.e., number of implants per level), instrumented levels, rod materials and dimensions, and surgical maneuvers in posterior approach surgeries. In his work using a T1-pelvis MBM, Wang et al. looked to determine minimum corrective forces for scoliotic patients and how the screw-to-rod kinematic connection influenced bone-screw forces (Wang et al., 2012). They measured the corrective forces in spinal instrumentation for three pedicle screw designs using 10 AIS patients undergoing concave rod attachment, rod derotation, apical vertebra derotation, convex rod attachment and compression/distraction maneuvers. Their findings showed how the type of screw-to-rod kinematic connection significantly influences bone-screw forces, but cannot completely eliminate the extra forces required to properly secure the screw-to-rod connection. In a later study using the same MBM model to evaluate how differential rod contouring influenced vertebral rotation correction, they reported that increased differential rod contouring had a significant impact on transverse plane correction, on thoracic kyphosis increase and on pedicle screw pull-out forces increase (Wang et al., 2016). They also reported how alternative screw patterns can achieve similar deformity correction with 23% fewer screws, but with 25% higher bone-screw forces when performing a simultaneous segmental translation technique (Wang et al., 2017).

Le Navéaux et al. (2016) used the same T1-pelvis MBM to study the influence of implant density and instrumentation configurations on spine correction and bone-screw forces. They sought to determine whether lowering implant density in targeted regions could maintain spine deformity correction while lowering overall instrumentation loads. Using 9 AIS patients with patient-specific screw types, they simulated the concave rod attachment, rod rotation, en bloc DVR, and convex rod attachment maneuvers. They reported higher bone-screw load levels with higher implant density in the post-instrumented state, with the capacity for similar spine correction using a lower implant density. Maximum peak bone-screw loads were reported to occur during the execution of

the surgical maneuvers. Boyer (2017) used a comparable MBM to simulate segmental and en bloc DVR with derotation tools and measure the impact of DVR on bone-screw forces and spine correction. They quantified apical vertebral rotation correction from DVR and associated screw pull-out forces and medio-lateral torques. They found that segmental derotation increased screw pull-out forces and medio-lateral torques as compared to en bloc derotation and that the surgeon's instrumentation strategy played a significant role on resulting implant forces. Delikairis et al. (2018) used MBM as well to analyze how screw pattern variations can influence spine correction and bone-screw forces using rod derotation and en bloc DVR. They reported similar corrections in coronal and sagittal planes with lower implant density, correlation between screw density in the apical region and apical vertebral rotation correction, and higher bone-screw load levels with higher implant density. Using a FEM with a similar approach, Driscoll et al. (2013) and Clin et al. (2019) found similar correction and bone-screw force results for low and high implant density configurations, but significant variations across screw types. Tachi et al. (2021) developed a T1-Pelvis FEM to simulate posterior approach surgeries in AIS with multiaxial screws and established its potential as a surgical planning tool. Through a prospective study using 47 AIS patients and a standardized surgical protocol including a catalog of pre-bent rods, they used the model to simulate the surgical protocol and obtain a prediction of postoperative spine correction within 5°, rod stresses and bone-screw forces reaching their peak near the apex of the MT curve and near the lower instrumented vertebra.

2.5.5 Patient positioning biomechanical studies

As elaborated in the previous sections of this chapter, the human spine shape is characterized by a set of specific curvatures and a range of motion which can be greatly affected by spine deformities. The importance of patient positioning in spine surgery was also discussed, but further to that, several researchers have been documenting the relationship between patient positioning and its influence on spine geometry. A vast number of studies detail measurements of spine geometry, estimated stress, strains, and displacements for static and dynamic scenarios, but only a reduce set have focused on spine biomechanics related to intraoperative positioning.

Studies evaluating the impact of prone positioning on lumbar lordosis vary in objectives and methodologies. Five studies looked at quantifying variations in lumbar lordosis between preoperative standing upright and intraoperative prone on different positioning modalities. It was

reported that the prone knee chest position typical of the Andrews table or Hasting frame significantly reduced total lordosis (> 35%) (Peterson et al., 1995), with three studies concluding that the knee-chest prone position does not adequately reproduce the physiologic value of standing lordosis due to excessive hip flexion (Guanciale et al., 1996; Peterson et al., 1995; Stephens et al., 1996). Peterson et al. (1995) reported that the Jackson table preserved total lumbar lordosis and Guanciale et al. (1996) reported how the 4-poster frame on average preserved lumbar lordosis within 3º. Using the Jackson table, Harimaya et al. (2009) showed how patient physiological variability in preoperative upright lordosis for a similar intraoperative position can yield either no change (≤5º) or increase in intraoperative lordosis (>5º), with a correlation between high upright lordosis and no change in intraoperative lordosis. Lastly, Miyazaki et al. (2019) reported how for single-level (L4-5) transforaminal lumbar interbody fusion (TLIF), the total lumbar lordosis (LL) can be preserved when using a 4-poster frame with hip flexed at 30° and a Jackson table with hip flexed at 0°, but with lower measured segmental LL using the 4-poster frame, noting that loss in segmental lordosis will result in increased upper adjacent segments loading as a compensation mechanism to preserve total LL. Care should therefore be applied in selecting the surgical table and manipulating hip position for the intended surgery.

Five studies expanded on prone positioning spine measurements with added metrics to study the spine in the sagittal and coronal planes. Using 58 scoliotic patients and a 4-poster frame, Delorme et al. (2000) determined that positioning, anesthesia and surgical exposure were responsible on average for a 37% reduction in coronal curves (half of total correction) and a 58% reduction in thoracic kyphosis before instrumentation, with no significant effect on lordosis. Duke et al. (2002) obtained comparable results for coronal curves with two scoliotic patients. Canet (2008) and Driscoll et al. (2012), both using scoliotic patients measured the influence of prone positioning with two surgical frames; preoperative MFPF and intraoperative Relton-Hall (RH). In the sagittal plane, the two studies reported for the MFPF reductions of 11% and 12% in lordosis, and 19% and 24% in kyphosis, as compared to reductions of 21% and 42% in kyphosis for the RH (no lordosis measurement). In the coronal plane they reported reductions of 25% and 26% for TL/L, and both 15% for MT curves with the MFPF, and reductions of 35% and 38% for TL/L, and 25% and 29% for MT curves with the RH frame. These studies highlighted how the act of positioning the patient can have a significant influence in reducing both sagittal and coronal plane curves and that a variation in operating table design has also an influence on results, noting that the effect of

anesthesia and surgical opening could not be isolated. Lastly, Mac-Thiong et al. (2002) focused on the influence of prone positioning on trunk deformity in AIS. The results in part showed how the 4-poster frame, by virtue of contact with the cushions, restricted the rotation of the shoulders with respect to the pelvis, and constrained the alignment of C7 to S1 in the postero-anterior and lateral directions without reducing trunk deformity.

With the understanding that prone positioning and operating table design influenced the spine geometry, several studies looked to characterize how variations in positioning parameters can enable adjustments of the spine. Benfanti & Geissele (1997) using the Wilson frame, Canet (2008), Prophète (2012), and Driscoll et al. (2012) using the MFPF and Sebastian et al. (2018) using the Axis Jackson System® concentrated on hip movement as a mean to influence lumbar lordosis. By varying the hip rotation using the patients' lower limbs position, these studies reported significant influence in manipulating lordosis while keeping the patient safe. The MFPF and Jackson table, with dedicated mechanical systems to position the lower limbs across a wide range of motion, proved more effective at varying lordosis (up to 37° with MFPF, 20° with Jackson), as compared to the Wilson frame combined with added cushions for hip extension (10° variation). Canet (2008) and Driscoll et al. (2012) also reported a 6° variation in thoracic kyphosis with the lower limb positioning system range of motion. Prophète (2012) showed how design improvements made to the MFPF lower limb positioning system could achieve better leg rotation for a given leg support rotation with lower femoral head displacement, showcasing the advantage of adapting the positioning system kinematics based on the pelvis and lower limb biomechanics. Lastly, Vedantam et al. (2020) showed that for posterior column osteotomies (PCO), a hinged table can be used intraoperatively during the surgical process to manipulate the spine. They were able to first create spine decompression (i.e., reduced lordosis) to facilitate exposure for pedicle screw insertion, osteotomy, and interbody graft. Then by returning the table to neutral, they closed the PCO and compressed the interbody graft, followed by rod insertion and construct locking. Although screw head forces were not measured, it showed that the hinged table produced no statistically significant differences in segmental lordosis as compared to the traditional manual technique.

Three studies leveraged thoracic cushions placement as a mean to influence thoracic kyphosis. With their Dynamic Positioning Frame (DPF) prototype, which would later evolve into the MFPF, Duke et al. (2002) showed the ability to maintain physiological thoracic kyphosis by creating a vertical offset between the thoracic and pelvic cushions to increase thoracic kyphosis. Canet (2008)

and Driscoll et al. (2010) used the MFPF's sternum vertical displacement device (SVD) on healthy unanesthetized volunteers and showed a significant increase of up to 14° in thoracic kyphosis and an average thorax vertical displacement of 8 cm. These thoracic spine manipulation studies also measured increases in cushion contact pressures during manipulations and recommended to consider time limitations in the 20 to 30 minutes range to avoid potential pressure sores.

With the MFPF, Driscoll et al. (2011) used two novel mechanical systems aimed at coronal curves correction of the scoliotic spine via positioning: the lateral leg displacer (LLD) and pelvic torsion device (PTD). The LLD allowed for lateral bending of the legs up to 60°, thereby allowing for elevation and depression of the pelvis in the coronal plane. The PTD allowed for transverse plane twisting of the pelvis by 30° combined with a 5 cm thoracic cushion vertical offset. With scoliosis patients pre-operatively positioned on the MFPF, both devices were most effective at correcting TL/L curves, with an average additional reduction of 39% (LLD) and 19% (PTD). Apical vertebra rotation was also measured, with reductions of 33% (LLD) and 48% (PTD).

Numerical models of the human spine were developed using some of these above experiments to further explore the potential of patient positioning. Duke et al. (2005) developed a global spine model of the trunk using FEM to simulate the prone positioning on a RH frame and adjust spine flexibility parameters to adapt to the patient's spine flexibility based on side bending radiographs, including an anesthesia factor. Their model allowed to be within 10° of coronal plane measurements for two AIS patients, but with large variations in the anesthesia factor applied. Driscoll et al. (2012) built upon this methodology to develop a FEM to simulated prone positioning on the MFPF and were able to be within 5° of radiographic measurements with the patient's spine flexibility calibrated based on prone radiographs with no anesthesia factor. Their model sensitivity study showed how both positioning and patient-related parameters have an important impact on resulting spine curvatures. In a separate study, Driscoll et al. (2012) used the FEM to simulate the positioning of the lower limbs and explored the impact of intermediate and more extreme lower limb positions (30° in hip extension to 90° in flexion) with four healthy patients. Personalization of hamstring properties proved necessary to be within 6° of radiographic measurements and they reported a potential manipulation of 59° in lordosis and 13° in kyphosis using the more extreme range of positions. Prophète (2012) used the model from the work of Driscoll et al. (2012) to study position induced spine corrections in the lateral decubitus position using an MFPF mechanism to manually perform lateral bending of the spine. Numerical model validation with *in vivo*

experiments showed that the FEM could not adequately reproduce the lateral decubitus position and spine manipulations (>6°). This was attributed to modeling simplifications in the assignment of soft tissue and IVD material properties, missing anatomical features like trunk muscles in the model and simplified patient weight distribution assumptions. These studies all applied boundary conditions directly on the patient to model contact with the operating table (i.e., no table systems modeled). They also highlighted how modeling the patient's spine flexibility using pre-operative data did not result in an improved prediction once positioned; model calibration using intraoperative radiographs remained required.

Finally, two studies leveraged the potential of a numerical model in proposing an optimized position for a given set of objectives. Duke (2005) with the DPF model looked at a single scoliotic patient and recorded ten geometric measures from the individual and combined variations of three positioning parameters (pelvic inclination, chest cushion longitudinal location and chest cushions height offset) and three external correction forces parameters (rib hump, lateral thoracic and lateral lumbar). Driscoll et al. (2010) with the MFPF looked at three scoliotic curve types and recorded eleven geometric measures from the individual and combined variations of five positioning parameters: lower limb position, thorax vertical and lateral displacements, LLD, and PTD. Results from both studies showed that a combined use of the varied parameters allowed for a wider range of correction as compared to an independent use, with 70% to 75% improvement in overall spinal geometrical measures reported. Optimized combinations varied with curve types and cost function buildup. These studies did not validate the results with *in vivo* experimental data nor attempted to predict patient's comfort under the prescribed combinations.

The review of these studies highlights how intraoperative patient positioning can influence the spine geometry. The effects of safely leveraging the patient's body kinematics using the thorax, pelvis and legs have been demonstrated experimentally and simulated numerically and have shown how a table or frame's specific mechanical design, cushion contact zones and offset options, and dynamic adjustment can provide significant pre-instrumentation correction. From these observations, it is reasonable to believe that intraoperative patient positioning can aid the surgeon in achieving his/her desired spine correction objective and can influence the forces at the bone-screw interface.

CHAPTER 3 HYPOTHESES AND OBJECTIVES

3.1 Rationale of the project

As outlined in Chapter 2, for orthopedic surgeries necessary for the treatment of severe spinal deformities such as scoliosis, spondylolisthesis or spinal trauma, patients need to be positioned on a specialized operating table to facilitate the various stages of surgery such as exposure and surgical instrumentation maneuvers. The positioning system components ensure spine stability and patient safety through the positioning of the head and upper limbs, thorax, hips, and legs. Using modalities like cushions or pads at targeted locations, a table hinge for body segment rotation, and head traction, it is possible to leverage the patient's body kinematics to segmentally adjust the shape of the spine. Various studies have shown that prone and lateral surgical positioning of patients allows for adjustment of the spine shape prior to surgical correction maneuvers (Canet, 2008; C. Driscoll et al., 2011; C. Driscoll, Aubin, Canet, Labelle, & Dansereau, 2012; C. Driscoll, Aubin, Canet, Labelle, Horton, et al., 2012; Prophete, 2012). Access to the vertebrae at the appropriate angle is important to perform implant placement and correction maneuvers. Corrective maneuvers impose important loads on the implants, which can lead to weakening of the screw anchors in the bone, with a risk of failure (Hicks et al., 2010; Suk et al., 2001). The study of bone-screw forces in instrumentation surgery using pedicle screws has been an active field of research, with the objective of improving patient safety and outcomes, while reducing surgery costs (Clin et al., 2019; Delikaris et al., 2018; Le Navéaux et al., 2016).

Although the positioning modalities available to surgeons remain rudimentary, it is known that positioning can generate some level of correction prior to instrumentation, and facilitate the surgical steps, but this has been poorly documented, and it has not been possible to quantify whether the forces acting on the screws and their anchorage in the bone are influenced by this position-induced correction. With the consensus on ensuring that surgical techniques and associated instrumentation maintain bone-screw forces within safe levels, we believe that targeted position-induced correction is an underexploited way to facilitate and improve the correction of spinal deformities.

Of particular interest was the possibility of manipulating lumbar lordosis by flexing or extending the legs (Canet, 2008; C. Driscoll, Aubin, Canet, Labelle, Horton, et al., 2012; Miyazaki et al.,

2019; Sebastian et al., 2018; Vedantam et al., 2020). Also, thoracic kyphosis could be manipulated through positioning, as explored by Duke (2005), Canet (2008), and Driscoll et al. (2012). This latter study showed how prone positioning tended to reduce the physiologic thoracic kyphosis by 42% on average, which may affect the surgeon's strategy when shaping and installing the rods. Furthermore, the sagittal overbending of the rods affects the risk of increasing the stress on the implants during surgery. Using an experimental positioning device, Canet (2008) and Driscoll et al. (2010) showed that thoracic kyphosis could be increased respectively by 40% and 53% on average as compared to the neutral prone position. Reducing intraoperative stresses on the instrumentation and its anchorage in the bone while achieving the goals of correction is a difficult task, but not yet addressed. By incorporating sagittal plane adjustment through patient positioning prior to instrumentation, it is intended to facilitate the correction maneuvers and reduce intraoperative stresses at the bone-screw interface. This situational review led us to a general question: can the biomechanical understanding of intraoperative patient positioning be further exploited to facilitate and improve spinal correction instrumentation procedures?

3.2 Research Question, Hypotheses and Objectives

Specifically for this master project, we propose to exploit biomechanical modeling tools of patient positioning to answer the following principal research question: can sagittal spine manipulations performed through patient positioning further improve and facilitate the correction of spinal deformities, as well as reduce the forces required to perform intraoperative corrective maneuvers when compared to the current practice?

For this project, three hypotheses derived from this research question are addressed:

- **Hypothesis 1 (H1):** A biomechanical model of the human spine calibrated with preoperative clinical data can simulate the changes in spinal curvatures resulting from being prone on a typical 4-post adjustable surgical frame with sagittal adjustment of the pelvis and torso, to within 5 degrees. For this hypothesis, the surgical frame and pelvis orientation are the independent variables, and the spine curvature the dependant variable.
- **Hypothesis 2 (H2):** The previously validated biomechanical model of the human spine calibrated with preoperative clinical data can simulate the changes in spinal curvatures and the forces exerted on the vertebrae resulting from posterior instrumentation with rods and

pedicle screws to within 5 degrees of accuracy for curvatures and within the measured range of comparable studies for forces. For this hypothesis, the independent variables are the instrumentation configuration (i.e., number and type of screws, rod contour, diameter, and material), while the dependent variables are the sagittal curvatures and resulting forces at the bone-screw interface.

- **Hypothesis 3 (H3):** Perioperative patient positioning with pelvic and thoracic adjustments on a 4-post operating frame can reduce interface loads between the vertebral bone and the pedicle screws by up to 25% during instrumentation procedures. For this hypothesis, the pelvic and thoracic adjustments are the independent variables, and the resulting spine curvature and forces at the bone-screw interface the dependant variables.

Previous studies have demonstrated the pertinence of numerical simulation tools to study position-induced corrections and bone-screw forces from instrumentation surgery, but these two topics have been studied independently up to now. Our study looked to establish a novel simulation method to link both topics and characterize the influence of positioning on bone-screw forces. With the ongoing development of new specialized operating tables and positioning modalities, an integrated numerical simulation tool can represent a valuable complement to leverage the full potential of these devices and explore new design concepts.

A series of three objectives were elaborated to test these hypotheses:

- **Objective 1 (O1):** Develop a biomechanical finite element model of the human spine capable of simulating the intraoperative prone position and posterior spinal instrumentation surgery.
- **Objective 2 (O2):** Verify and validate the model with existing clinical cases and quantify the effects of model uncertainties.
- **Objective 3 (O3):** Characterize the influence of patient positioning on the correction and forces resulting from instrumentation surgery.

For this project, objectives 1 and 2 were specific objectives necessary to achieve our principal objective 3.

CHAPTER 4 METHODOLOGY

4.1 General approach

The overall approach of this modeling and computational simulation project can be summarized by the process map in Figure 4.1. Objective 1, which consists in developing the numerical model and the simulation of the positioning, is carried out from pre-operative radiographs of 5 available AIS patients, and by the 3D reconstruction of the bone anatomy of the spine, the rib cage and the pelvis. From there, a personalized finite-element model (pFEM) is generated and adapted to include the operating table and spine deformity correction instrumentation. The simulation of the positioning and instrumentation is then performed through a sequence of model manipulations with associated boundary conditions. For objective 2, which is to ensure the consistency and credibility of the model for the specific objectives of this study, we followed the framework of the new ASME standard (V&V40:2018). Thus, a verification, validation and uncertainty quantification (VVUQ) plan was developed and followed. This step was based mainly on comparing the simulations with clinical data measurements and analogous results from published studies, and performing a sensitivity study of the parameters. For objective 3, which consisted in characterizing the influence of patient positioning on the correction and forces resulting from instrumentation surgery, the model was exploited to analyze changes in sagittal spine correction and pull-out forces at the pedicle screws between the simulation of a reference (baseline) position and a positioning configuration that targeted thoracic spine manipulation.

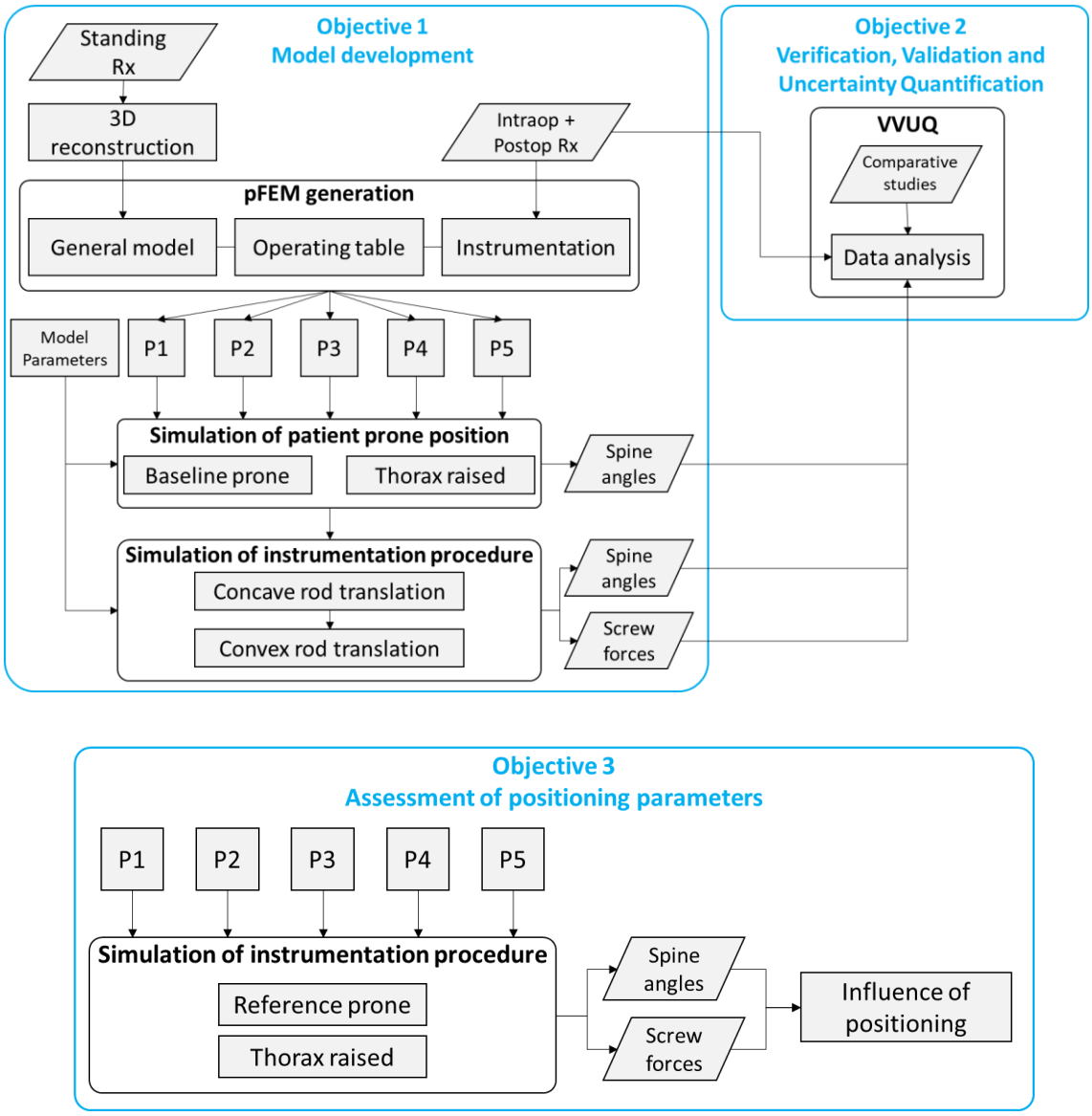

Figure 4.1 Project objectives and simulation process strategy

4.2 Development of a finite element model for patient positioning and instrumentation simulation

4.2.1 3D reconstruction of the patients' trunk bone anatomy

A three-dimensional (3D) reconstruction of each patient's spine, rib cage and pelvis was created using calibrated pre-operative biplanar standing radiographs (Figure 4.2) obtained with the low-dose x-ray EOS imaging device (EOS Imaging, France). The imaging device proprietary software

IdefX (version 2017-07-11, LIO) was used to semi-automatically identify bony structures and provide control points for further adaptations. Control points on anatomical landmarks of the T1 to L5 vertebrae, rib cage and pelvis were manually adjusted to provide a more accurate representation of the patient and exported as a database of control points enabling 3D visualization. This reconstruction technique has a reported mean accuracy of 1.1 mm (SD = 0.2 mm) with 95% confidence interval of 1.7 mm (Glaser et al., 2012; Humbert et al., 2009).

The 3D reconstruction was then used to create a patient specific physics-based numerical model. For this study, the finite element approach was taken given its previously demonstrated ability to simulate the intraoperative prone position and the posterior spinal instrumentation surgery (Clin et al., 2019; C. Driscoll, Aubin, Canet, Labelle, & Dansereau, 2012; Duke et al., 2005; Tachi et al., 2021).

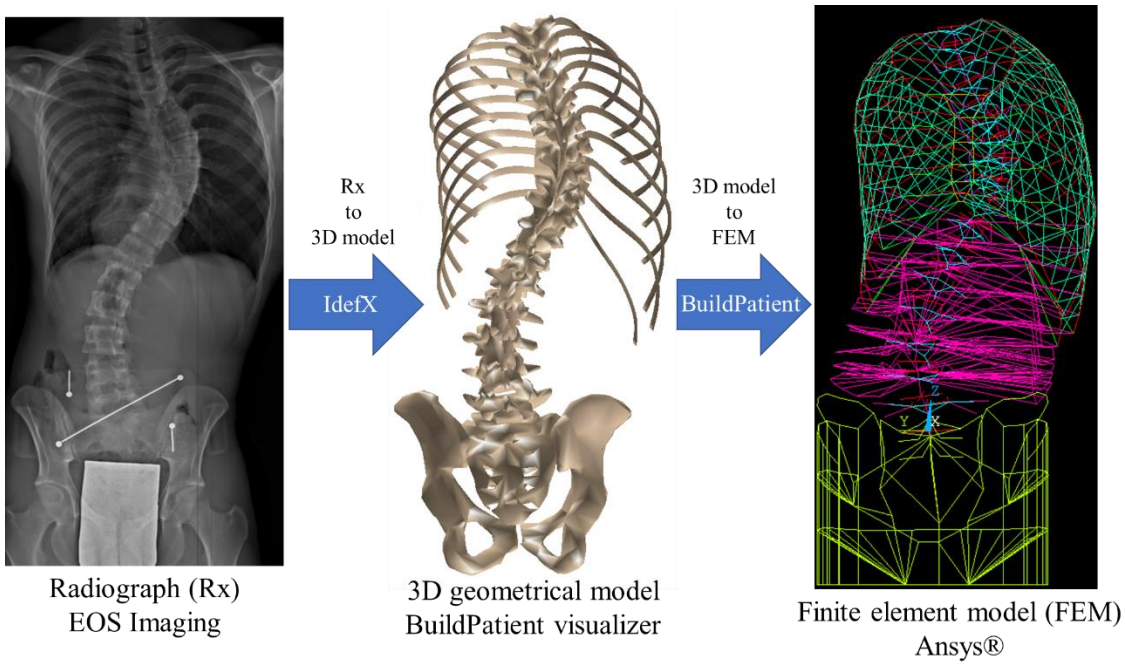

Figure 4.2 3D geometrical model and personalized FEM from patient's radiographs. (Source: Sainte-Justine University Hospital database)

4.2.2 Finite-element model of the patients' trunk

4.2.2.1 General model description

The pFEM was automatically generated from the 3D reconstructed patient's trunk using the *BuildPatient* in-house software and associated modules (i.e., LIScorrect, v3.0. LIScaldef, v2.0. LISModNds, v2.0. LISgeoparam, v2.0, LISgenS3D3. LISgeopersocv, v2.0. LISmodmov). This numerical model of the human spine, rib cage and pelvis has served in previous studies; more specifically, we have chosen as base model the one used in brace design studies of scoliotic patients (Cobetto et al., 2014, 2016, 2017; Dupuis et al., 2018; Pea et al., 2018). In theses studies, the spine deformity correction was achieved by simulating the transmission of brace pressures to the internal bone structures (i.e., ribs and vertebrae) via the thorax and abdomen. Through these studies, the model has been shown to adequately represent the correction of spine deformity within clinical significance ($\leq 5^{o}$) for both coronal and sagittal curves. It was therefore assumed as a relevant baseline model for the purpose of our patient positioning study, and we made necessary context specific adaptations.

The general model is described here with project specific adaptations detailed in later sections. The pFEM was built using the Ansys® scripting language and version 16.1 was used to conduct the simulations. The pFEM was made of 6263 nodes and 10 111 elements. The assigned mechanical properties were taken from published and experimental data (Clin et al., 2011; C. Driscoll, Aubin, Canet, Labelle, & Dansereau, 2012; Périé et al., 2004). Refer to Table 4.2 for a description of material properties and element types assigned for each modeled anatomical feature.

The general pFEM included the thoracic and lumbar vertebrae, intervertebral discs, ribs, sternum, costal cartilages, and abdominal soft tissues, without the skin. Thoracic and lumbar vertebrae were represented by a series of beam elements connecting the following anatomical landmarks: upper and lower endplates centers, body center, pedicle centers, lamina, and spinous/transverse processes (Figure 4.3). The inter and intravertebral ligaments were not represented in the model but this simplification was evaluated as part of the parameter sensitivity study (cf. section 4.3.4.3). The zygapophyseal joints (i.e., facet joints) were not represented in the model based on their low probability of contact (Gignac, 1998) during patient positioning and the facetectomies typically performed by the surgeons in the instrumented segment. The intervertebral discs (IVD) were

modeled as a beam element connecting the lower vertebral endplate to the upper endplate of the adjacent vertebrae.

The rib cage was modeled by the ten levels of true rib bones connected to the sternum including the sternocostal cartilage, all using beam elements. The intercostal muscles were modeled with tension-only link elements, and the costotransverse and costovertebral joints using beam elements.

The pelvis was modeled as a series of beam elements geometrically representing the iliac crest, ilium, ischium, sacrum, and pubis bone. Abdominal cavity soft tissues were modeled as a series of beam elements connected to both anterior and posterior sections of the L4 to T11 vertebral levels. Adjacent levels were also interconnected anteriorly at the abdominal wall. The abdominal cavity soft tissues model also connected the L3 to T11 vertebral levels to rib levels 8 to 10 through beam elements to represent the diaphragm (Figure 4.3) (Périé et al., 2004). This beam element representation of soft tissues contributes to the overall flexural strength of the abdomen region and provides an additional load path between the selected vertebral and rib levels.

The pFEM axis system follows the same convention as presented in Section 2.1, namely: posterior-anterior (X), medial-lateral (Y) and caudal-cranial (Z) directions. Three planes are also defined in accordance with this system: coronal plane (YZ), sagittal plane (XZ) and transverse plane (XY)

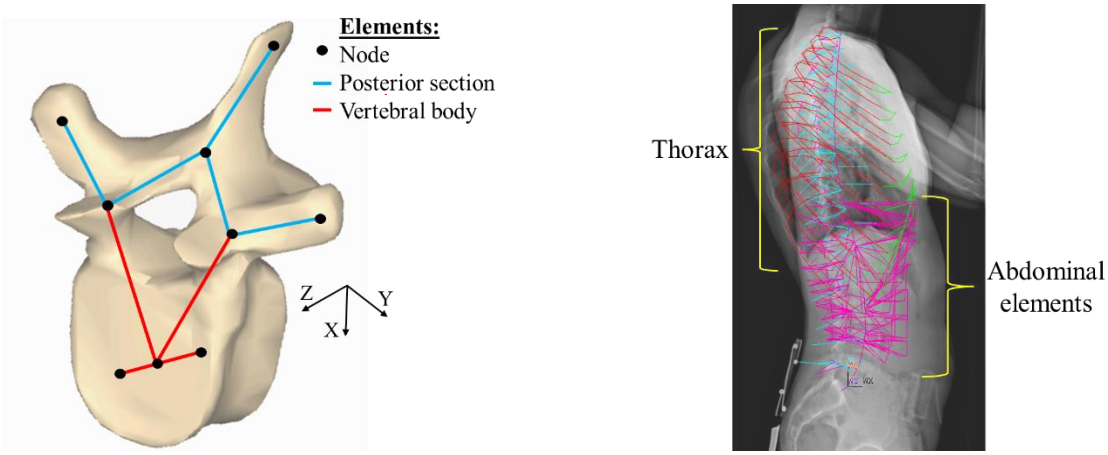

(a) (b)

Figure 4.3 pFEM visual representations (only subset of elements showed for clarity). (a) Vertebra modeling (adapted from Wikipedia, 2021, license free). (b) Abdominal elements (in pink) overlayed with lateral Rx for spatial reference (source: Sainte-Justine University Hospital database).

4.2.2.2 Modeling of the prone position on the operating table

The pFEM was obtained from radiographs in the standing position, hence gravitational forces had to be appropriately modeled. An intermediary model geometry without gravity was first estimated, so that when the gravitational loads were applied the model geometry matched that of the X-ray images (Clin et al., 2011; C. Driscoll, Aubin, Canet, Labelle, & Dansereau, 2012). Next, the model was oriented from the standing to the intraoperative prone position, and the gravitational forces were applied consistently over this new model orientation. The prone position gravitational forces were modeled as follow. The head and upper limbs were assumed to be independently supported; their effects were removed. Gravitational forces were applied on the spine based on body mass fractions at each vertebral level and pelvis. These fractions and points of application were based on the study from Driscoll et al. (2012) (Table 4.1). For the T1 to T10 levels, one third of the total force acting at each segment was placed at the vertebral body center node, with the remaining two thirds distributed equally along the connecting left and right ribs of the segment. For T11 to L5, the total force acting at each segment was placed at the vertebral body center node. The pelvis weight was distributed equally on the most anterior left and right iliac crest nodes.

Table 4.1 Body mass fraction and center of mass assignment per vertebral level

Vertebral level	Body mass (%)*			Sagittal center of mass (cm anteriorly from vertebral body)*		
	Trunk	Head	Upper Limbs	Trunk	Head	Upper Limbs
T1	1.1	6.94		0.8	-0.5	
T2	1.1			1.3		
T3	1.4		3.29	2.0		2.0
T4	1.3		3.29	2.8		2.0
T5	1.3		3.29	3.4		2.0
T6	1.3			3.9		
T7	1.4			4.3		
T8	1.5			4.6		
T9	1.6			4.6		
T10	2.0			4.6		
T11	2.1			4.4		
T12	2.5			4.1		
L1	2.4			3.5		
L2	2.4			2.7		
L3	2.3			1.8		
L4	2.6			1.1		
L5	2.6			0.4		
Pelvis	10.7			NA		

*Source: (De Leva, 1996; Pearsall et al., 1996)

A simplified 4-post positioning system was modeled by creating four 20 mm thick cushions that matched the length and width specifications of a typical frame: 133 mm and 165 mm respectively (Imperial Surgical, n.d.). Each cushion was made of 2 layers of 8-node linear brick elements with material properties of a linear elastic foam (C. Driscoll, 2010). Each cushion bottom surface was rigidly connected to a node of the table to impose displacement constraints during the simulation. The rotation angles of the cushions along the longitudinal or vertical axis of the table (i.e., allowing angulations in the transverse and coronal planes, about the Z and X axes respectively) can be adjusted as required (Figure 4.4). Cushions were modeled to be symmetric along the sagittal plane. Point-to-surface contact elements between selected rib nodes and thoracic cushion surfaces were generated based on the vertebral levels used to assign longitudinal placement of the thoracic cushion. A contact friction coefficient of 1.16 was imposed on these contact elements based on a medical gown friction test (C. Driscoll, 2010). Target elements were assigned to the thoracic cushions upper surface to support node-to-surface contact simulation. Pelvic cushions were created for visual reference only and were positioned to align with the pelvis iliac crest anterior nodes, with no contact modeling. Lower limb positioning was represented by the sagittal rotation of the pelvis.

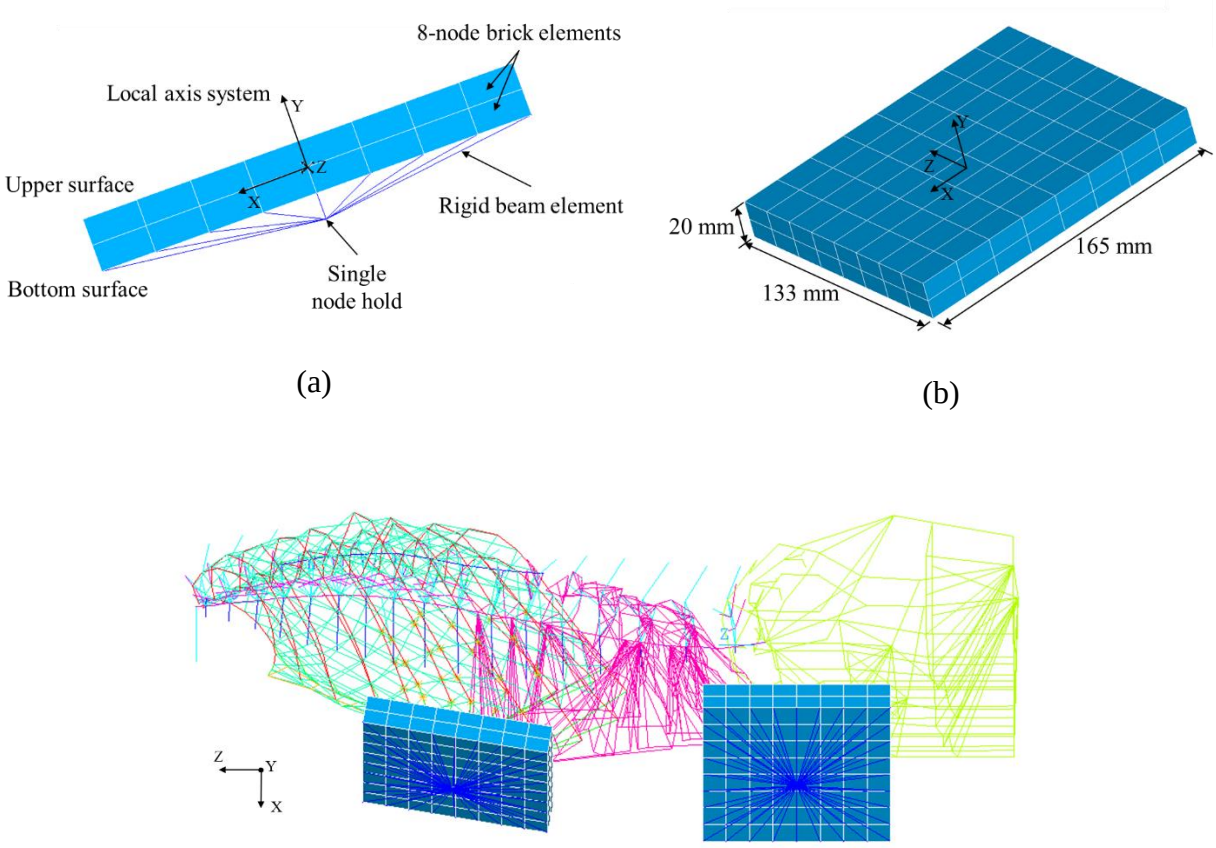

Figure 4.4 Cushion model of the positioning system. (a) Side view of a cushion. (b) Dimensions of a cushion in isometric view. (c) Example of thoracic and pelvic cushion integration with the pFEM (lateral view). The thoracic cushion has an inclination of 20° along the Z axis and 10° along the X axis, while these angles are respectively 35° and 0° for the pelvic cushion.

4.2.3 Spine correction instrumentation modeling

The modeling of the surgical instrumentation was based on the data deduced from the intra-op and post-op radiographs of the patients to determine instrumented levels and spatial location of the screws, as well as the rods contour. The concave and convex contoured rods sagittal shapes of each patient were deduced from lateral intraoperative post-instrumented radiographs in the prone position and converted into points which spatially defined the relative position of the screw tulips as a function of the instrumented level (Figure 4.5). The medical imaging software Surgimap® version 2.3.2.1 was used to collect the shape of the rods and position of each screw tulip head, using the intraoperative radiographs.

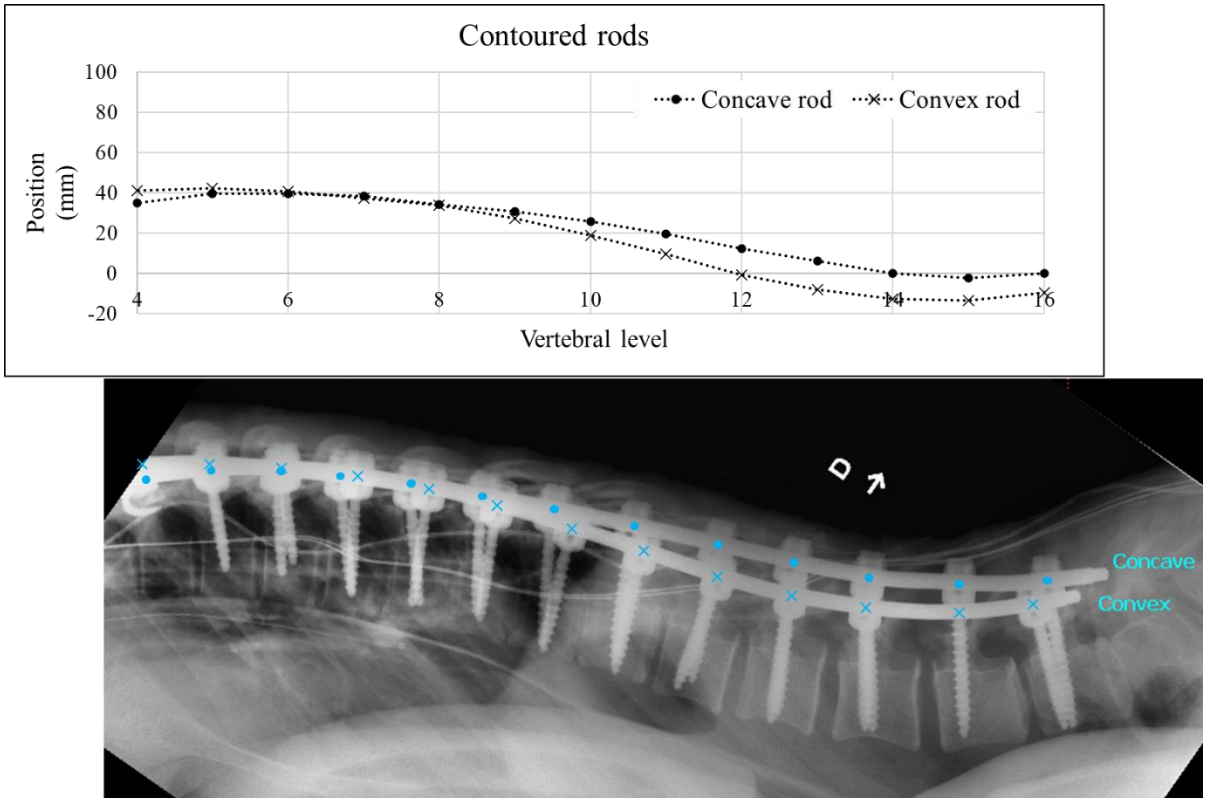

Figure 4.5 Example of contoured rod sagittal profile reconstruction from a lateral intraoperative radiograph (source: Sainte-Justine University Hospital database)

The screws were modeled by representing the screw shank with respect to the pedicle and by defining the position of the tulip head, and its kinematic behavior. The screw shank (body) was modeled as a 6 mm diameter beam element connected to the pedicle centroid and extending to the screw tulip's position (Figure 4.6). In the reality, the multi-axis screw allows for five degrees of freedom (DoF) movement; its kinematic chain consists in one spherical joint at the screw body to tulip (i.e., 3 DoF) and one cylindrical joint between the tulip and contoured rod (i.e., 2 DoF) (Figure 4.6). Once the tulip is locked in place to the rod via a set screw, only the spherical joint remains. In the model, these permissible movements between the vertebra and contoured rod were simplified by using one MPC184 cylindrical joint element (i.e., 2 DoF) at the screw tulip node with small resistances on joint motion to facilitate model convergence. This joint allowed for rotation around a local Z axis at the tulip with a 50 N.mm/rad resistance stiffness (Figure 4.6). Translation along the same Z axis was allowed within a +3 mm to -3 mm distance with a resistance stiffness of 25 N/mm. Locking of the tulip to the rod via a set screw was simulated by fixing the joint with the rod elements. Contoured rods were modeled as a series of 6.35 mm diameter beam elements. Cobalt-

Chrome (CoCr) material properties were assigned to the screws and rods elements (i.e., Young's Modulus: 240 GPa). The elements of the rods were placed to connect adjacent screws (Figure 4.7).

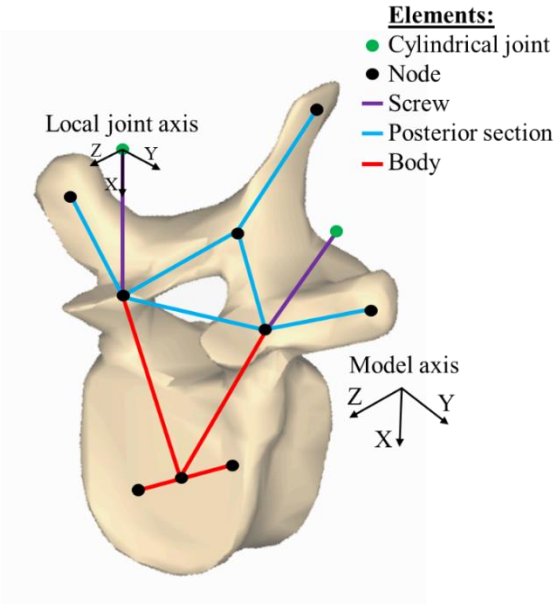

(a)

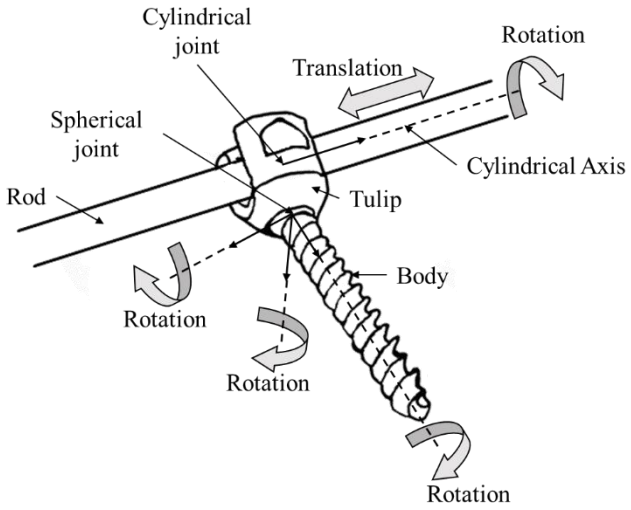

(b)

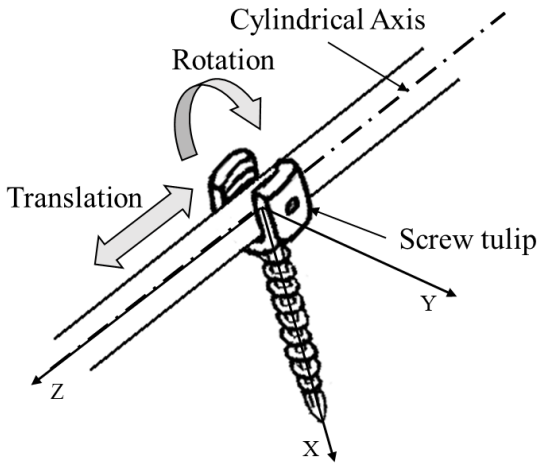

(c)

Figure 4.6 Modeling of the screw-to-rod connexion. (a) Model of the screw body fixed to the pedicle centroid and to the tulip head with a 2 DOF cylindrical joint (adapted from Wikipedia, 2021, license free). (b) Actual multi-axis screw-to-rod joints with 5 DoF movement. (c) Model of the screw tulip-to-rod cylindrical joint with 2 DoF movement.

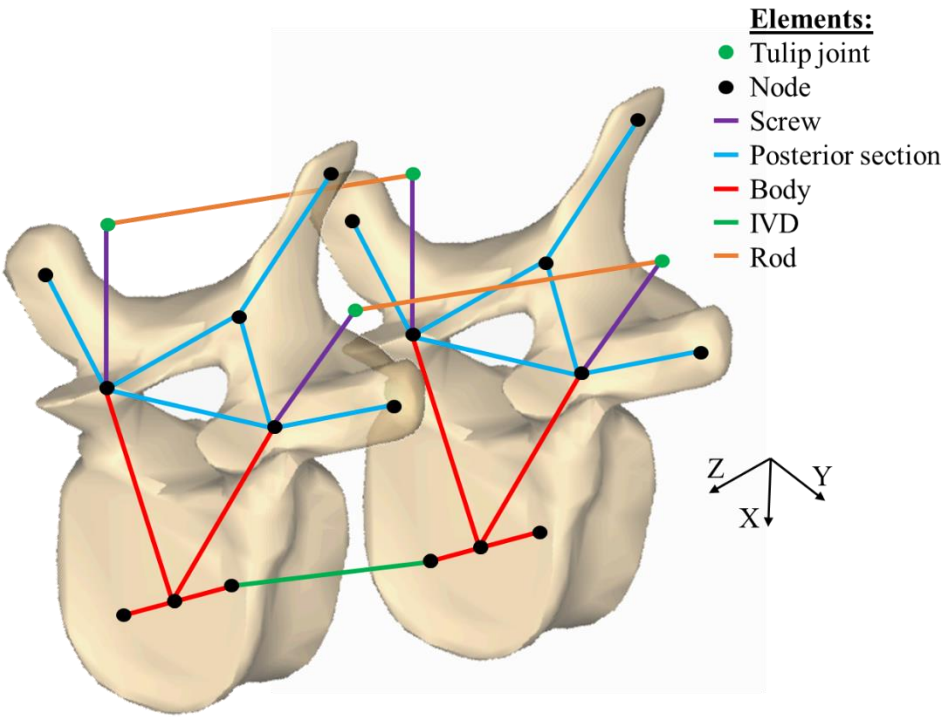

Figure 4.7 Visual representation of pFEM modeling details of an instrumented spine functional unit. Isometric view (adapted from Wikipedia, 2021, license free). Elements for the costovertebral and costotransverse joints not shown for clarity.

Table 4.2 Material properties and element types of the finite element model

Body	Young's Modulus (GPa)	Poisson's Ratio	Element type
Vertebral body	10	0.3	BEAM 189
Pedicles	5	0.3	BEAM 188
Laminae	1	0.3	BEAM 188
Spinous processes	3.5	0.3	BEAM 188
Transverse processes	5	0.3	BEAM 188
Intervertebral discs	4.2 E-3	0.3	BEAM 189
Ribs	5	0.1	BEAM 188
Intercostal muscles	0.1 E-3	0.3	LINK 10
Costovertebral joints	3.3 E-3	0.2	BEAM 188

Table 4.2 Material properties and element types of the finite element model (continued)

Body	Young's Modulus (GPa)	Poisson's Ratio	Element type
Costotransverse joints	0.33 E-3	0.2	BEAM 188
Sternum	5	0.1	BEAM 188
Sternocostal cartilages	0.25	0.1	BEAM 188
Abdominal soft tissues	2-20 E-3	0.3	BEAM 188
Pelvis	1	0.3	BEAM 188
T1 control: baseline prone anterior control*	0.1	0.3	LINK180
T1 control: thorax raised posterior control*	Adjusted	-	COMBIN39
T1 control: post-instrumented anterior control*	Adjusted	-	COMBIN39
Operating table cushion	0.1	0.3	SOLID185
Screw and spinal rod, cobalt chrome	240	0.3	BEAM 188

*: See section 4.2.4 for element description

4.2.4 Simulation of the patient positioning and instrumentation

4.2.4.1 Boundary conditions

The model was solved in a series of load steps which included large-deflection effects. Boundary conditions were defined at various stages of the simulation to represent the interactions between the pFEM and the positioning components, as well as to represent the behavior of the patient position during the instrumentation surgery.

To represent the longitudinal alignment of the patient, as well as the behavior of the upper and lower ends of the body not explicitly modeled (i.e., head, upper and lower limbs), boundary conditions have been applied to T1 and the pelvis, in addition to the pFEM to cushion contacts. The control of T1 and pelvis displacements during the simulations was handled in different ways according to the different stages of simulation: 1) baseline prone position; 2) position when manipulating the thoracic positioning pads; 3) during the instrumentation procedure. Simulation stages and associated boundary conditions are presented in the following sections. In all stages of

the simulation, the pelvis was controlled using three nodes: the S1 superior plate and the left and right iliac crest most anterior nodes.

4.2.4.2 Baseline prone position on the positioning frame

The generic 4-poster frame was adjusted in all three translations (X, Y, and Z) and angled to fit the rib cage anatomy of the patient using their rotation angles; 35º in the transverse plane was used based on specifications of a typical frame, and 0º or 5º in the coronal plane to better follow the rib cage. To determine the cushions position, the following method was followed. For the pelvic cushions, the most anterior pelvic node out of one right and one left iliac crest nodes was set as the reference to position the geometrical center of the pelvic cushion, with the opposite side cushion generated from a symmetry in the sagittal plane. For the thoracic cushions, their vertical position was set 10 mm higher than that of the pelvic cushion. The lateral position (Y axis) was defined according to the width of the patient's rib cage, and cranio-caudal position (Z axis) was defined according to the vertebral levels covered by the cushions as identified on intraoperative coronal radiographs.

Baseline prone position simulation was performed in a series of three steps with associated boundary conditions. The first step consisted in aligning the pelvis on the horizontal plane by displacement using the left or right iliac crest node selected for the placement of the pelvic cushions. At the same time the thorax was moved laterally according to a lateral adjustment factor to simulate the lateral adjustment of the trunk by the medical staff placing the patient on the table.

In the second step, the gravity distributed forces were applied (section 4.2.2.2) and the contact with the thoracic cushions was set. The anterior displacement of T1 was controlled with a LINK180 tension element to allow resistance free anterior movement up to 50 mm posterior of the thoracic cushion's center.

With the patient rested on the cushions, the third step was to fix T1 in the AP and lateral directions and consistently adjust the pelvic rotation via a displacement constraint. The pelvis axis of rotation was assumed to coincide with the left and right iliac crest nodes used to align the pelvis on the horizontal plane in the first step (Figure 4.8). The rod model, defined at the beginning of the simulation, was only activated during the instrumentation simulation step.

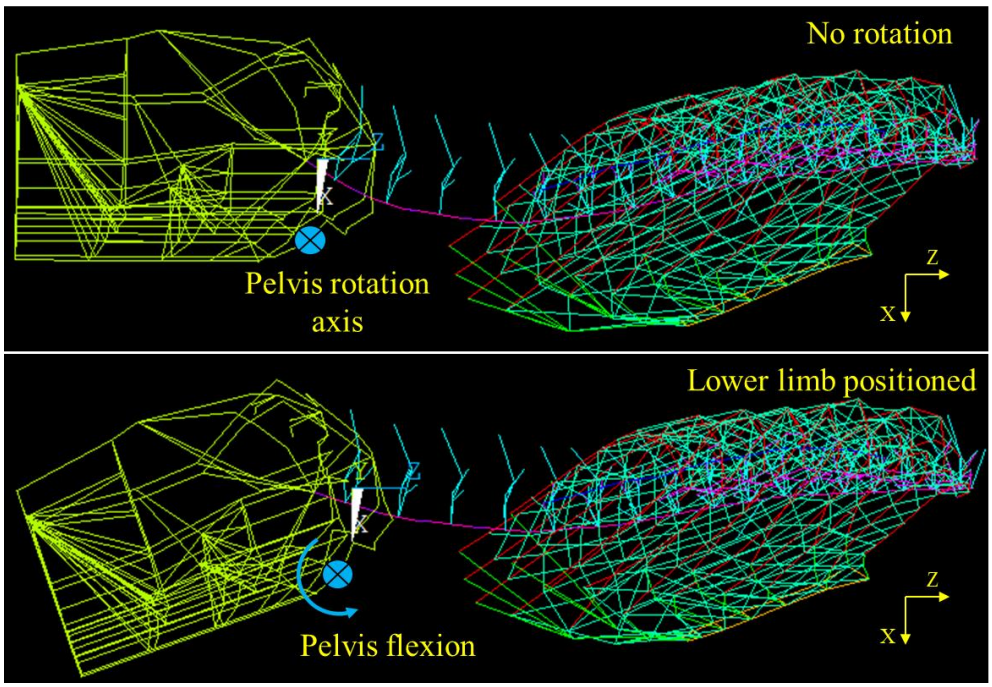

Figure 4.8 Details of pelvis positioning modeling to represent the flexion of the lower limbs (some pFEM elements have been hidden to improve visualization).

4.2.4.3 Modeling the effect of raising the thoracic cushions

In our study, we also modeled the effect of raising the thoracic cushions by 50 mm (Figure 4.9), a positioning strategy to manipulate the thoracic kyphosis. To do so, the thoracic cushions were longitudinally positioned to have the proximal edge of the cushion aligned with T7, and raised 50 mm. During the raise, the thoracic cushions were allowed to adjust longitudinally (Z axis) to minimize the contact shear stresses at the cushion to ribs interface and pelvis rotation was adjusted between 10º and 20º in flexion.

During the raise, a non-linear spring was created to exert an anterior pulling force on T1 to simulate the lifting of arms and head as the thorax is raised (C. Driscoll, Aubin, Canet, et al., 2010). The resistance force was based on the upper body weight (i.e., head and upper limbs: 16.81% of body weight as per Table 4.1) as a function of T1 posterior displacement from its baseline prone position (Figure 4.10).

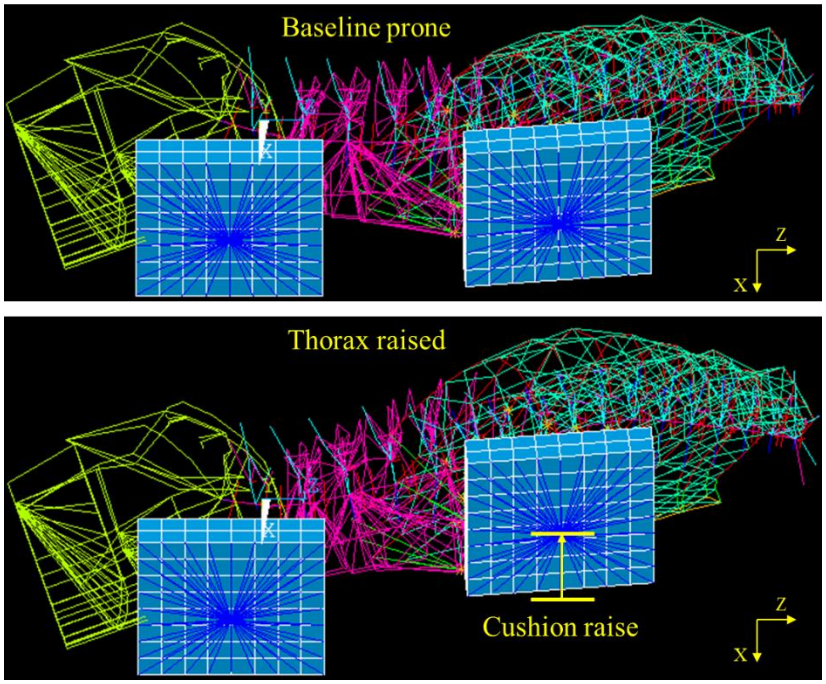

Figure 4.9 Modeling the 50-mm elevation of the thoracic cushions

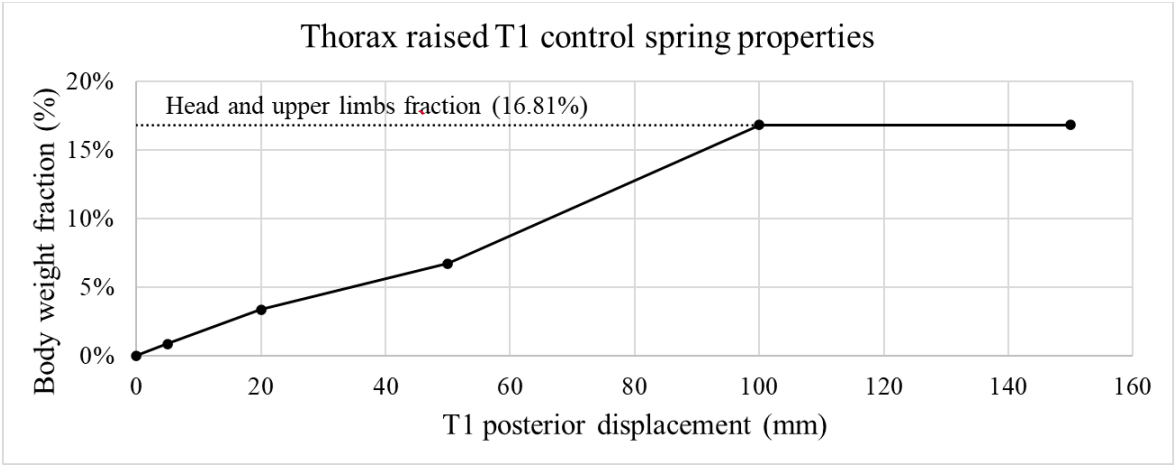

Figure 4.10 T1 control spring properties: thorax raised posterior control

4.2.4.4 Simulation of the instrumentation procedure

The actual correction maneuvers were simplified using a translation technique, with the concave rod first, followed by the convex rod and in-situ contouring. Starting with the patient in the prone position (baseline or with the thoracic cushions raised by 50 mm), a 20% reduction in IVD stiffness attributed to anesthesia was applied only at the vertebral levels of interest (i.e., instrumented levels) and the instrumentation procedure was modelled as follow.

The translational correction maneuver was performed by first applying a relative displacement between the concave rod and the proximal and distal instrumented vertebrae. Then, the apical vertebra was connected to the concave rod. During this step, the abdominal elements linking the T11 to L2 vertebrae to the rib cage were momentarily relaxed to allow local adjustments. The geometry of the provisional corrected spine allowed to deduce the remaining translation to apply to each screw to be connected to the rod as inferred from the intraoperative coronal reference radiograph. From there, the screw tulips on the concave side were translated one by one to the rod, starting with the distal vertebra to the proximal instrumented one. Local screw-to-rod adjustments were simulated using a temporary orient joint (i.e., 3 DoF in translation) at each tulip to automatically find an optimized position within a 4 mm x 4 mm x 4 mm volume.

The connection of the convex side rod was made in the same way. Then, all screw-rod joints were locked, and all other temporary displacement constraints were released (Figure 4.11). Abdominal elements and boundary conditions at T1 were reactivated. For T1 control at this step, a non-linear spring with a stiffness of 1 N/mm and a limited resistance upward force of 60 N was connected to T1 to allow some anterior displacement of the upper thorax following the correction of the spine (Figure 4.12).

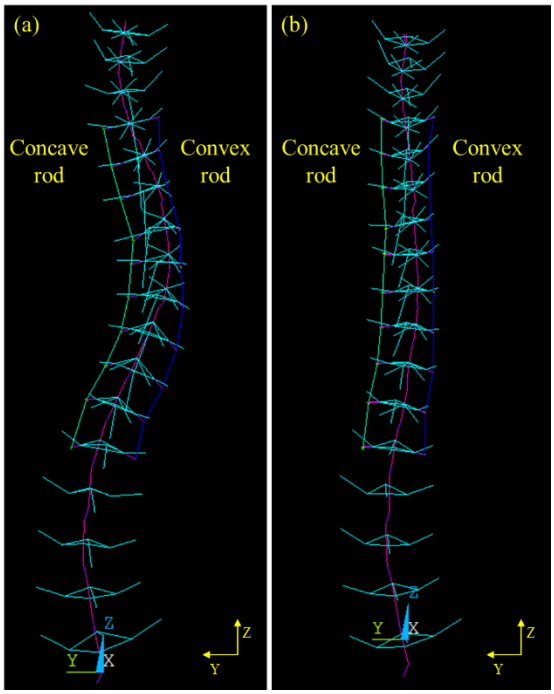

Figure 4.11 Simulation of the translation maneuver, before (a) and after (b) the correction (PA view). Elements removed for visual clarity.

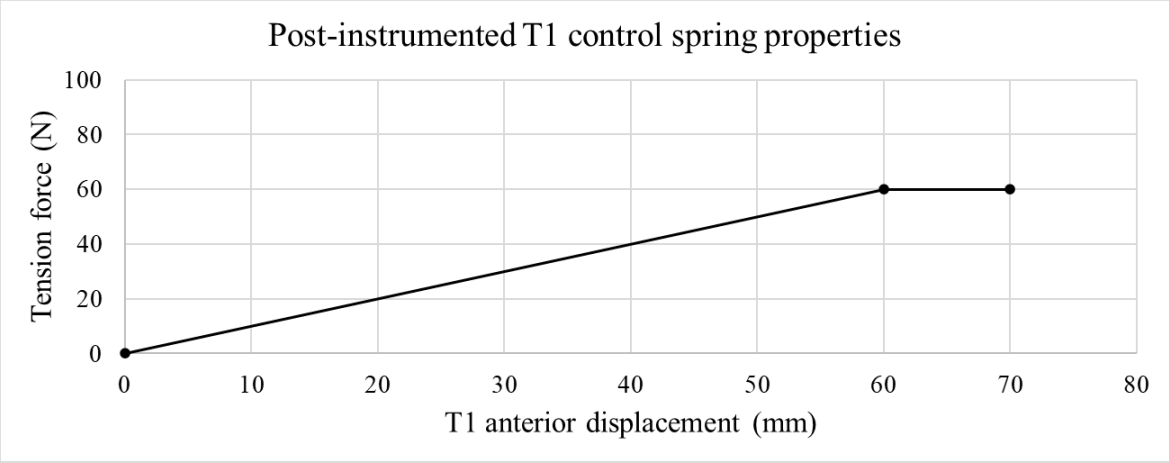

Figure 4.12 T1 control spring properties: intraoperative post-instrumented anterior control

4.3 Model Verification and Validation (V&V)

To verify the credibility of the developed model for positioning and spinal instrumentation, a verification and validation plan was used based on the guidelines of the recent American Society of Mechanical Engineers (ASME) V&V40 standard (V&V40, 2018). This standard provides a framework for the various approaches required for this purpose and allows for the derivation of a risk management-based verification, validation, and uncertainty quantification plan (VVUQ).

The ASME V&V40:2018 framework defines a VVUQ workflow to aid in establishing and documenting model credibility (Figure 4.13). The workflow starts with the question of interest (i.e., can sagittal manipulations of the spine improve and facilitate the correction of spinal deformities, as well as reduce the forces required to perform intraoperative correction maneuvers?), which is addressed through a series of steps performed under three main activities: establishing risk-informed credibility, V&V activities and model credibility assessment.

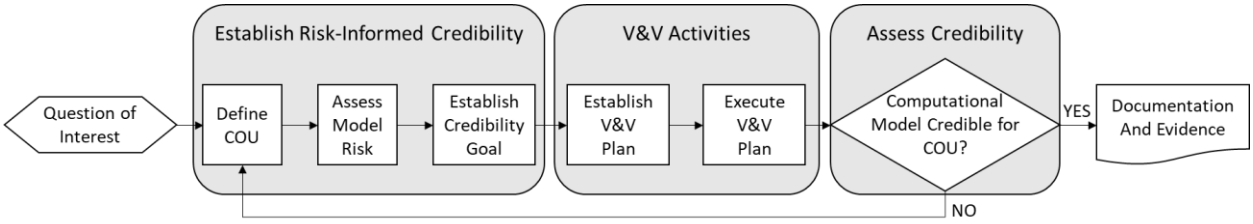

Figure 4.13 The VVUQ workflow

4.3.1 Context of Use

As per the standard, *the context of use (COU) is the specific role and scope of the computational model used to address a question of interest* (V&V40, 2018). The computational model developed in this study aims at exploiting the potential of positioning modalities to improve and facilitate instrumentation surgeries. The COU was defined as a comparative study to analyze the influence of different positioning components on spinal deformity instrumentation correction and forces at the screw-bone level, allowing to address the stated research question. Finite element analysis (FEA) was used to simulate the patient prone position on the operating frame and characterize whether a variation in positioning parameters influenced spine geometry and reduced intra-operative loads at the vertebral anchoring implants during corrective spine instrumentation surgery.

4.3.2 Model Risk

The V&V framework is based on model risk, which is *the possibility that the computational model leads to an incorrect decision that results in an adverse outcome, such as patient harm or device malfunction* (V&V40, 2018). Model risk was determined by evaluating the model influence on a safety decision and the potential consequence of a poor decision on patient safety.

Model influence investigates how the model outputs are to be considered in the decision-making process of the decision makers (i.e., clinicians). Conclusions drawn from this biomechanical study are relying on the model results. Yet, the consequence of these results is low because no clinical decision will be made from the study, and final clinical decision is balanced between these biomechanical information and clinician's knowledge and experience. The clinician would remain in complete control of the positioning adjustments on the operating frame. Any new positioning modality concepts resulting from the computational model explorative capabilities would go through a separate validation process which would support future model calibration and validation. Based on these considerations, the model influence as defined in this project is ranked as LOW.

Decision consequence is used to characterize the severity of an incorrect decision which relied on the computational model. As explained above, the computational model developed for this project remained a research only tool with no clinical decision to be made from the study. Incorrect positioning of the patient during surgery may increase contact pressures at the patient to cushion interfaces leading to skin pressure sores and peripheral nerve damage. Spine curvature and overall

patient stability is monitored by the medical staff throughout the operation. Newer operating frames could be equipped with cushion pressure sensors for live intraoperative monitoring, but models currently on the market do not. Based on these considerations, the decision consequence for this project is ranked as LOW.

The model risk is determined to be LOW-LOW, which based on the V&V40 five-level risk scheme, corresponds to a Level 1 (Table 4.3).

Table 4.3 Model risk matrix for project

Decision Consequence				
	High	3	4	5
	Medium	2	3	4
	Low	1	2	3
		Low	Medium	High
		Model Influence		

4.3.3 Verification plan

Analysis of the pFEM combined with a typical 4-post simplified frame was performed with the off-the-shelf (OTS) Ansys® version 16.1 software using the structural static analysis module. A user-developed script was used to generate the pFEM and its adaptations described in section 4.2. The model consisted in 3116 elements and 7684 nodes and was solved in a series of load steps (section 4.2.4) which included large-deflection effects. The commercial software's ability to numerically solve the mathematical problem was verified by first ensuring that a solution was produced and converged through a review of the solution's output files. These output files contained the convergence levels of overall displacements, forces, and moments as well as any warnings and errors which might have been encountered. Solutions were considered converged when error-free and below the forces and moments convergence criterion of 5 N and 50 N.mm respectively. Then, a calculation verification was performed by reviewing the summation of reaction forces acting at the constrained nodes for a match with the known imposed prone position

gravitational forces. Overall model element distortion was qualitatively reviewed. Thoracic cushion elements mesh density was doubled as compared to baseline to assess impact on results and solution convergence time.

4.3.4 Validation plan

4.3.4.1 Baseline prone position simulation

The validity of the simulated baseline prone position was assessed by comparing the simulated Cobb angles and sagittal curves for the 5 AIS patients used in this study (cf. section 4.5). Intraoperative radiographs were used to measure MT and TL/L Cobb angles for comparison, as well as the thoracic kyphosis and lumbar lordosis angles when the sagittal radiographs were available.

The tested thorax raised simulation results were compared with *in vivo* experimental results from the SVD studies undertaken with the MFPF system (Canet, 2008; C. Driscoll, Aubin, Canet, et al., 2010) (section 2.5.5). Canet (2008) used four healthy volunteers, while Driscoll et al. (2010) used six healthy volunteers, all without anesthesia. Average variation in thoracic kyphosis angle was compared to their results to verify its agreement.

4.3.4.2 Instrumentation construct simulation

The validity of the simulated instrumentation was assessed by comparing the simulated Cobb angles and sagittal curves of the same 5 AIS cases with post-instrumentation intraoperative radiographic measurements. The comparison was also done using the position of the simulated and actual screw head using post-instrumented intraoperative radiographs as measured using Surgimap® version 2.3.2.1. A root mean square error (RMSE) approach was taken to quantify lateral (Y) and anteroposterior (X) deviations, with the distal instrumented vertebra concave screw head used as reference to calculate the relative positions of all the screw tulips. The simulated axial loads exerted on the screw elements were compared to the computational studies from Driscoll et al.(2015), Clin et al. (2019) and Tachi et al. (2021) to verify their agreement.

4.3.4.3 Quantification of model uncertainties

The simulation model uncertainties were quantified by performing a set of parameter sensitivity studies to better understand how varying key model parameters may influence measured results.

Model sensitivity for the prone position baseline simulation was characterized using a set of two positioning parameters and two patient-related parameters using the same 5 AIS cases. Changes in coronal (Cobb MT and TL/L) and sagittal (thoracic kyphosis and lumbar lordosis) angles were calculated by modifying the following: pelvic rotation, longitudinal displacement of the thoracic cushion, spinal flexibility, and effect of inter and intravertebral ligaments. Pelvic rotation was varied from 20° in extension to 40° in flexion. Thoracic pad displacement was varied by ±50 mm along the longitudinal axis. The flexibility of the spine was tested by considering 4 segments (i.e., PT, MT, TL/L, LS) and then applying a factor of 0.25 to make it more flexible up to a factor of 4 to make it more rigid, relative to the base value (1) of the elastic modulus of the intervertebral disc. Lastly, the inter and intravertebral ligaments were modeled on patient 2 only (Table 4.4). A change in coronal (Cobb MT and TL/L) and sagittal (thoracic kyphosis and lumbar lordosis) angles from the baseline prone position greater than 20% was considered significant, between 10% and 20% notable, and less than 10% small.

Model sensitivity for the instrumentation construct simulation was characterized by varying a set of three instrumentation parameters and one patient-related parameter. Coronal (Cobb MT and TL/L) and sagittal (thoracic kyphosis and lumbar lordosis) angles measurement and pedicle screws axial load magnitudes variations were calculated by modifying the following: rod material properties, rod local shape variations, screw-to-rod connection boundaries, and spine flexibility.

Rod elements material stiffness was varied from CoCr (EX = 240 GPa) to Titanium (EX = 115 GPa) for the same 5 AIS cases. Rods local shape variations were simulated on patient 2 only in a set of four independent simulation cases: a 3 mm posterior offset at T5 (case #1), T8 (case #2), and T12 (case #3), and a 3 mm lateral offset at the apical vertebra (case #4).

The sensitivity study of the screw-to-rod connection boundaries was realized on patient 2 only with two independent simulation cases: a reduction in the local adjustment translational volume of the temporary orient joint from 64 mm^3 to 8 mm^3 (case #1), and a reduction of the cylindrical joint translational boundaries from ± 3 mm to ± 1 mm (case #2).

The sensitivity of the spine flexibility was tested using the same 5 AIS cases by considering the instrumented vertebral levels only and then applying a factor of 0.8 to make it more flexible up to a factor of 1.2 to make it more rigid, relative to the base value (1) of the elastic modulus of the instrumented intervertebral disc.

4.4 Characterizing the influence of patient positioning in instrumentation surgery

To characterize the influence of patient positioning on the spine correction and screw forces resulting from instrumentation surgery, our study measured the relative changes in sagittal angles and screw elements pull-out forces between instrumented reference and instrumented 50-mm thoracic cushions raised scenarios for the 5 AIS cases. For a given case, the reference and 50-mm raised simulations used the same instrumentation; only the positioning was varied to isolate its influence. The rods sagittal profiles of each patient were modified to achieve a target thoracic kyphosis between 25º to 35º (cf. the example of Figure 4.13). These simulations did not have a validation plan, as this portion of the study leveraged the explorative potential of the numerical model.

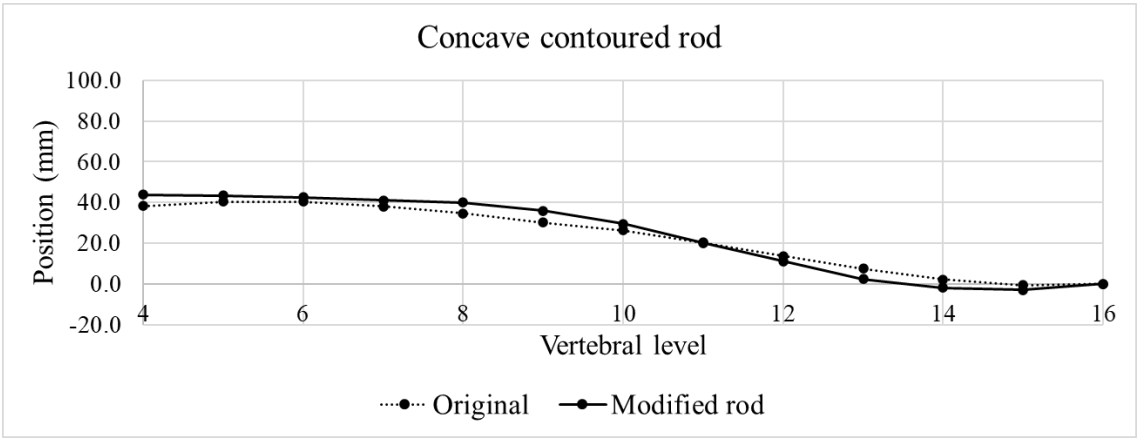

(a)

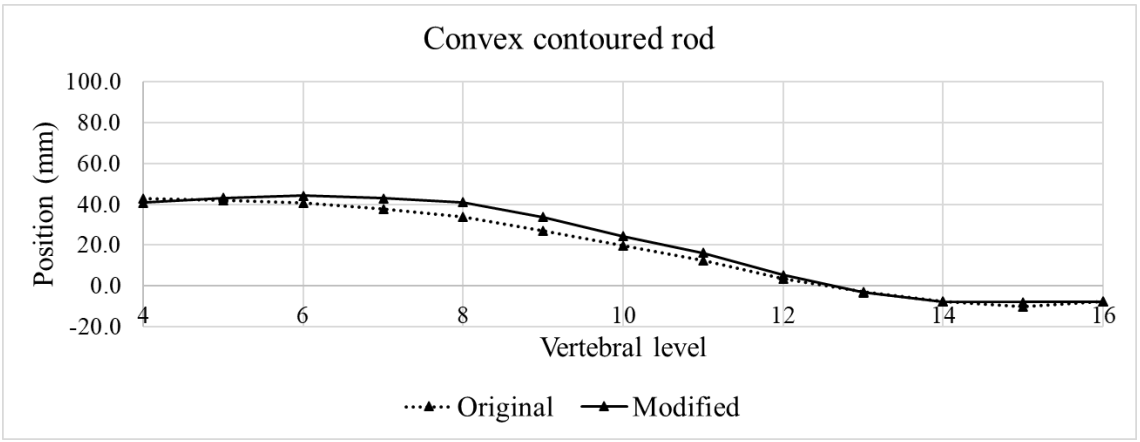

(b)

Figure 4.14 Contoured rod sagittal profiles – original (Rx) and modified for simulations (patient 5). (a) Concave rod. (b) Convex rod.

4.5 Patients

In our study, we used 5 adolescent patients with idiopathic scoliosis from the Sainte-Justine Hospital database and operated on a 4-cushion frame. The preoperative, as well as the per-operative pre- and post-instrumentation data are presented in Table 4.4 to Table 4.7

Table 4.4 Preoperative patient data (erect posture)

Case	Height (cm)	Weight (kg)	MT Cobb (end-apex-end vertebra)	TL/L Cobb (end-apex-end vertebra)	Kyphosis (T4-T12)	Lordosis (L1-L5)
1	178	60	65º T4, T8, T11	43º T11, L2, S1	16º	45º
2	156	41	56º T5, T8, T12	35º T12, L2, L4	23º	61º
3	173	62	57º T5, T8, T11	50º T11, L2, L4	15º	52º
4	160	52	56º T7, T11, L2	40º L2, L4, S1	22º	31º
5	155	43	44º T4, T7, T11	52º T11, L1, L3	21º	76º

Table 4.5 Intraoperative, pre-instrumented spine measurements (in degrees)

Case	MT Cobb	TL/L Cobb	Kyphosis	Lordosis
1	47º	34º	16 º	-*
2	40º	30º	15º	33º
3	44º	36º	7º	-*
4	33º	26º	16º	-*
5	34º	38º	17º	59º

*: Measurement not possible with the available radiographs

Table 4.6 Intraoperative, post-instrumented spine measurements (in degrees)

Case	MT Cobb	TL/L Cobb	Kyphosis	Lordosis
1	27º	-*	21º	-*
2	18º	18º	19º	-*
3	17º	11º	9º	-*
4	15º	-*	18º	24º
5	11º	9º	21º	53º

*: Measurement not possible with the available radiographs

Table 4.7 Instrumented levels

Level	Case									
	1		2		3		4		5	
	Left	Right	Left	Right	Left	Right	Left	Right	Left	Right
T1										
T2										
T3	X	X								
T4	X	X	X	X	X	X			X	X
T5	X	X	X	X	X	X	X	X	X	X
T6	X	X	X	X	X	X	X	X	X	X
T7	X	X	X	X	X	X	X	X	X	X
T8	X	X	X	X	X	X	X	X	X	X
T9	X	X	X	X	X	X	X	X	X	X
T10	X	X	X	X	X	X	X	X	X	X
T11	X	X	X	X	X	X	X	X	X	X
T12	X	X	X	X	X	X	X	X	X	X
L1	X	X	X	X	X	X	X	X	X	X
L2					X	X	X	X	X	X
L3					X	X	X	X	X	
L4									X	X
L5										
No. of Implants	22		20		24		22		25	
Instrumentation system	-*		Expedium®		CD-Horizon®		Expedium®		Expedium®	

*: Details of instrumentation type not available

CHAPTER 5 RESULTS

5.1 Validation of the simulations

5.1.1 Baseline prone position simulation results

The simulation model was able to match the clinical results with an average absolute difference of 4.6º (-4º to 7º) for MT, 1.8º (1º to 3º) for TL/L, 2.0º (-5º to 2º) for kyphosis and a difference of 2º and 5º for lordosis on the two cases for which we were able to measure it on the radiographs. The detailed results are summarized in Table 5.1.

Table 5.1 Comparison of radiographic (RX) and simulated (Sim) results for the baseline prone position

Case		Cobb Angles		Sagittal curvatures	
		MT	TL/L	Kyphosis	Lordosis
1	RX	44º	34º	17º	-
	Sim	40º	36º	19º	32º
2	RX	40º	30º	15º	33º
	Sim	46º	31º	14º	28º
3	RX	44º	36º	7º	-
	Sim	41º	38º	5º	41º
4	RX	37º	28º	18º	-
	Sim	44º	29º	18º	25º
5	RX	41º	42º	18º	51º
	Sim	44º	45º	13º	49º
Average absolute difference		4.6º	1.8º	2.0º	3.5º
Min		-4º	1º	-5º	-5º
Max		7º	3º	2º	-2º

5.1.2 Thorax raised simulation results

The thoracic cushions 50 mm raise increased the kyphosis by an average of 9.2º, reduced lordosis by an average of 5.6º, and reduced MT by an average of 5.4º (Table 5.2). Comparison with similar

experimental studies in the literature (Canet, 2008; C. Driscoll, Aubin, Canet, et al., 2010) showed a similar effect on thoracic kyphosis for a higher cushion elevation; increase in kyphosis of 14° and 11° on average for a thoracic cushion displacement of 145 and 148 mm respectively (Table 5.3).

Table 5.2 Thorax raised differences from baseline prone position

Case	Cobb Angles		Sagittal curvatures	
	MT	TL/L	Kyphosis	Lordosis
1	-7º	-4º	15º	-1º
2	-8º	2º	15º	3º
3	-8º	2º	7º	-17º
4	-3º	2º	5º	0º
5	-1º	0º	4º	-13º
Average	-5.4º	0.4º	9.2º	-5.6º

Table 5.3 Thorax raised results with comparable studies

Study	Experiment	Number and type of cases	Cushion Travel (mm)	Average Kyphosis Increase (T4-T12)
Our study	*In silico*	5 (AIS)	50	9.2º
Driscoll et al. (2010)	*In vivo*	6 (Healthy)	145*	14º
Canet (2008)	*In vivo*	4 (Healthy)	148*	11º

*Sternum lifting device angled at 15º; converted to a vertical travel value for comparison

5.1.3 Instrumentation construct simulation results

The simulated correction of the spine was quite similar to the reference actual angles with an average absolute difference of 2.2º (-2º to 3º) for MT, 2.2º (-2º to 4º) for kyphosis, a difference of 3º, 8º and 1º for TL/L, and a difference of 3º and 1º for lordosis on the cases for which we were able to measure it on the radiographs. The detailed results are summarized in Table 5.4.

The simulated rods were within 3 mm RMSE of that of the measured shape using the post-operative radiographs, except for the convex rod for patient 4 which reached a difference of 7 mm (Table 5.5). The graphical simulation results of the base and post-instrument prone position for a typical

case are shown in Figure 5.1, while Figure 5.2 illustrates the shape of the rods. Graphical results for all the patients included in the study are reported in Appendix A (Figure A.1 to Figure A.10).

The average screw pull-out force was 74 ± 17 N for the five simulated instrumentation cases, with an average maximum at 236 ± 73 N (Table 5.6). Figure 5.3 shows the pull-out forces for a typical case at each screw and for each level, allowing to appreciate how the forces are distributed within the instrumented construct for the spine correction obtained. Graphical results for all the patients included in the study are reported in Appendix A (figures Figure A.11 to Figure A.15). The simulated screw pull-out forces were in the lower range of reported values from *in silico* studies for multi-axis screws chosen for comparison. The average post-instrumented axial load magnitude was within 6% of studies from Clin et al. (2019) and Tachi et al. (2021) and showed significantly lower magnitudes as compared to results from Driscoll et al. (2015) (Table 5.7).

Table 5.4 Simulated post-instrumentation correction results (Sim) compared to reference radiographic data (RX)

Case		**Cobb Angle**		**Sagittal curvatures**	
		MT	**TL/L**	**Kyphosis**	**Lordosis**
1	RX	27º	-	21º	-
	Sim	28º	31º	23º	31º
2	RX	18º	18º	19º	-
	Sim	21º	21º	17º	30º
3	RX	17º	11º	9º	-
	Sim	20º	19º	8º	38º
4	RX	15º	-	18º	24º
	Sim	17º	14º	20º	21º
5	RX	11º	9º	21º	53º
	Sim	9º	8º	25º	52º
Average absolute difference		2.2º	4.0º	2.2º	2.0º
Min		-2º	-1º	-2º	-3º
Max		3º	8º	4º	-1º

Table 5.5 Position deviations (RMSE) between simulated and actual screw heads post-instrumentation

Case	RMSE Lateral (mm)		RMSE Anteroposterior (mm)	
	Concave side	Convex side	Concave side	Convex side
1	2	2	1	3
2	2	2	1	1
3	1	2	1	1
4	1	2	3	7
5	1	1	2	2

Table 5.6 Summary of screw pull-out forces

Case	Average Axial Load Magnitude (N)	Standard Deviation (N)	Max (N)
1	48	41	131
2	85	85	313
3	93	70	260
4	73	74	283
5	74	52	194
Summary 5 cases	74 ± 17		236 ± 73

Table 5.7 Post-instrumentation screw load magnitudes from computational studies

Study	Model Type	Patient Number (AIS)	Screw Load Results	Average Axial Load Magnitude (N)	Standard Deviation (N)	Max (N)
Our study	FEM	5	Axial	74	17	313
Driscoll et al. 2015	FEM	3	Axial	642*	290	-
Clin et al. 2019	FEM	5	Axial	70	-	-
Tachi et al. 2021	FEM	47	Axial	74	-	497

*Average across all steps of simulated instrumentation surgery

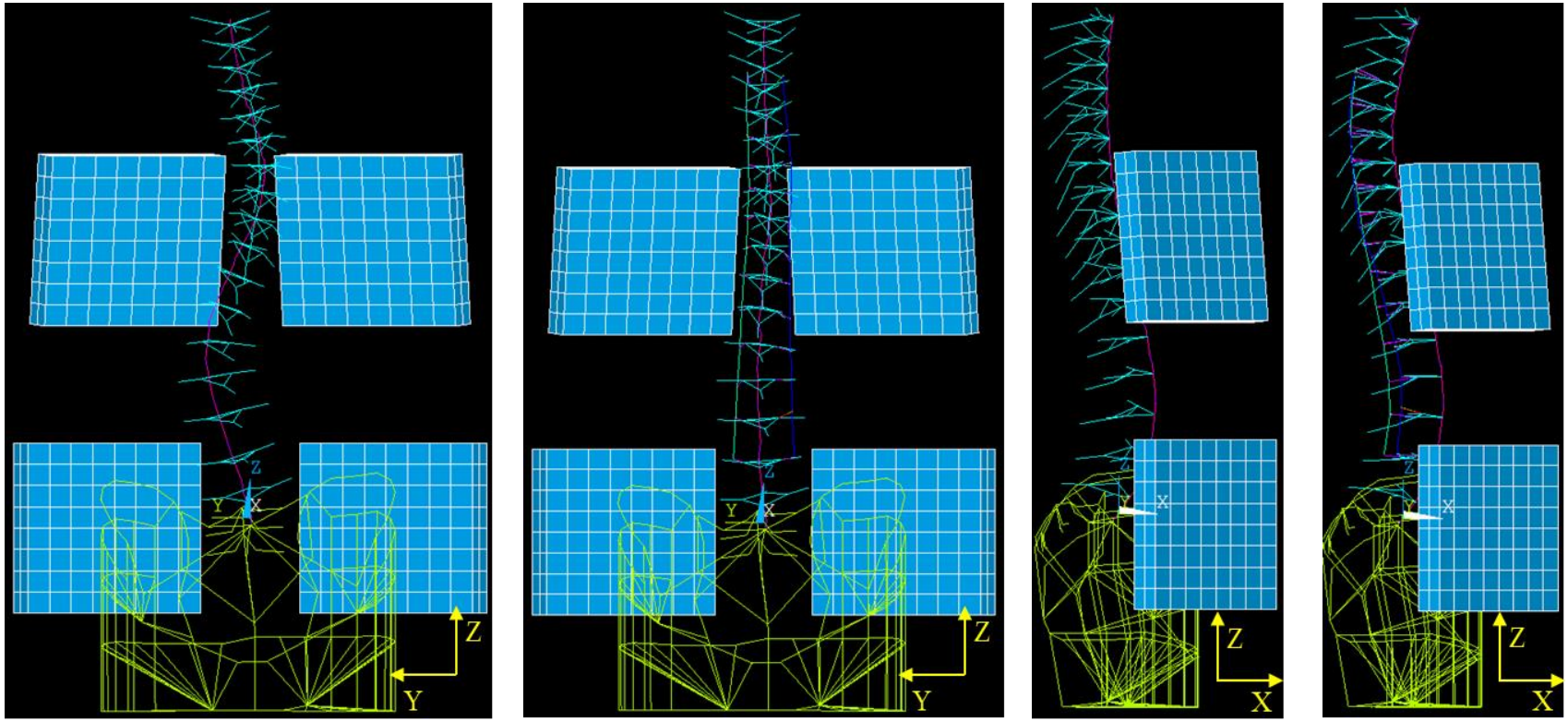

(a) (b) (c) (d)

Figure 5.1 Simulated prone position baseline (a, c) and post-instrumented intraoperative (b, d), for patient 5 (some elements removed for visual clarity) (PA (a,b) and lateral (c,d) views).

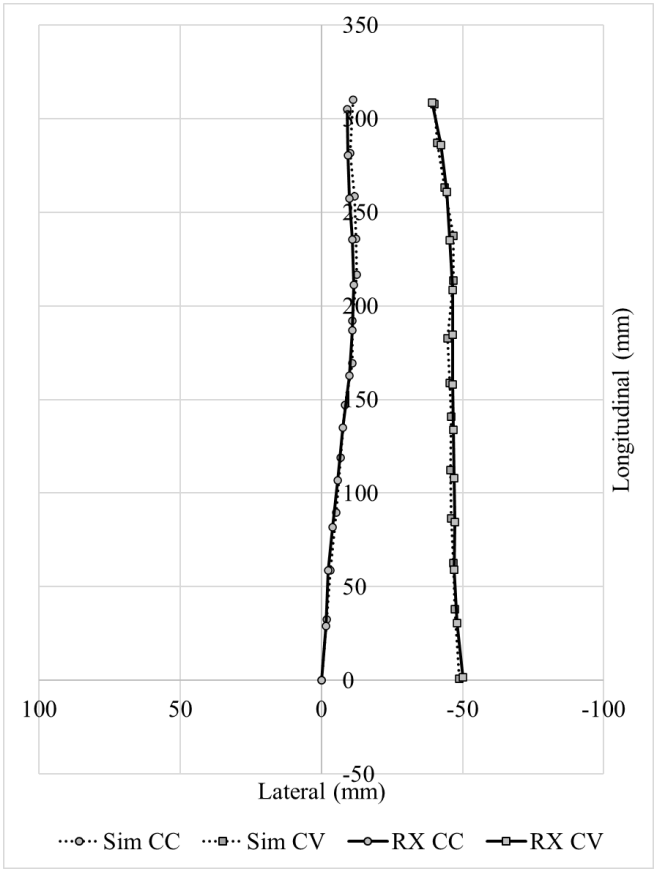

(a)

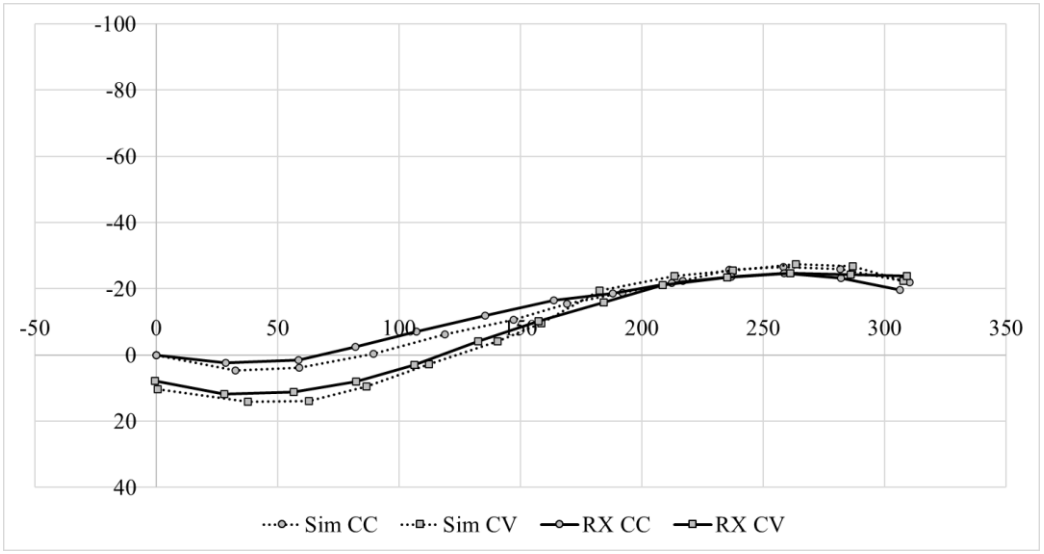

(b)

Figure 5.2 Patient 5 simulated (Sim) and actual (RX) concave (CC) and convex (CV) rods. (a) Coronal plane. (b) Sagittal plane.

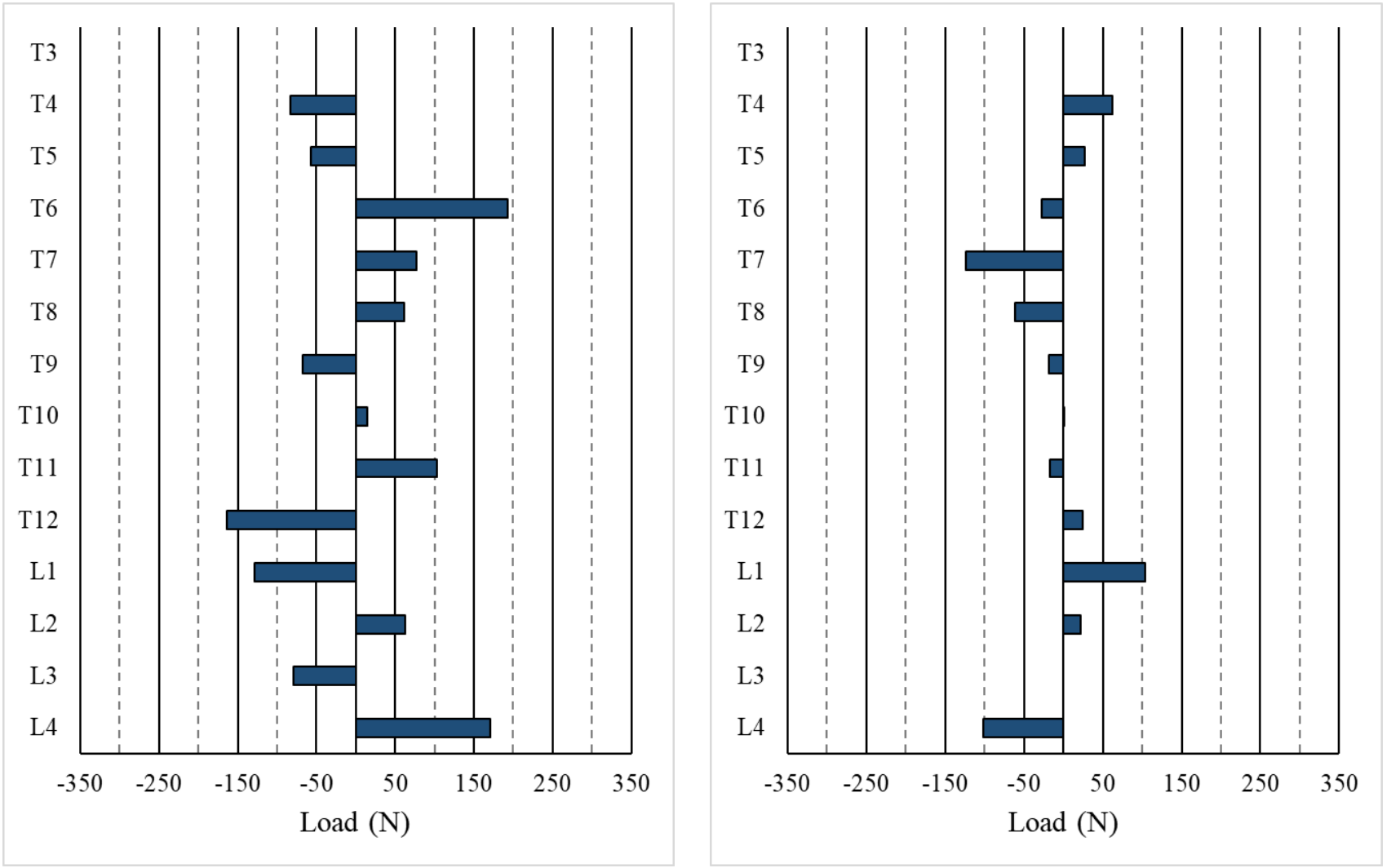

Figure 5.3 Pull-out forces exerted on the screws, per level (Patient 5). (a) Concave side. (b) Convex side.

5.1.4 Quantification of model uncertainties

5.1.4.1 Sensitivity study of the model in the prone position

Varying the pelvic rotation by 40º in flexion to 20º in extension influenced the sagittal curves with an average reduction of 32º (max flexion) to an increase of 14º (max extension) in lordosis, and an average reduction of 6º (max flexion) to a reduction of 2º (max extension) in kyphosis. For Cobb angles, measurements showed an average reduction of 1º (max flexion) to an increase of 6º (max extension) in TL/L, and only small changes equal to or less than 2º in MT.

The +50 mm cephalad displacement of the thoracic cushions induced an average 6º reduction in kyphosis, no change in lordosis, a 2º increase in MT, and no change in TL/L, whereas the -50 mm caudal displacement showed an average 4º increase in kyphosis and only small changes of 1º on all other geometric indices.

The variations in spinal flexibility influenced the sagittal curves with an average increase of 6º (most flexible) to a reduction of 7º (most rigid) in lordosis, and a reduction of 5º (most flexible) to an increase of 5º (most rigid) in kyphosis. For Cobb angles, an average reduction of 5º (most flexible) to an increase of 4º (most rigid) in both MT and TL/L were observed. Modeling of the inter and intravertebral ligaments showed only a small influence on sagittal curves and Cobb angles, with average measured variations all below 1º. Refer to Table 5.8 for tabulated results of these model sensitivity studies.

Table 5.8 Effects on the curves of the spinal model from the modulation of selected parameters within the described value ranges (mean +/- standard deviation, and % of the impact on the baseline value). Prone position simulation.

Tested Parameter	Values	Cobb Angle				Sagittal curvatures			
		MT		TL/L		Kyphosis		Lordosis	
		Deg.	%	Deg.	%	Deg.	%	Deg.	%
Pelvic rotation	40º Flexion	1º ± 4º	3%	-1º ± 4º	-3%	-6º ± 4º	-46%	-32º ± 5º	-90%
	20º Extension	2º ± 2º	5%	6º ± 4º	16%	-2º ± 1º	-12%	14º ± 4º	40%
Thoracic cushion longitudinal displacement	+50 mm (cephalad)	2º ± 2º	6%	0º ± 1º	0%	-6º ± 5º	-42%	0º ± 2º	-1%
	-50 mm (caudal)	-1º ± 2º	-2%	1 ± 2º	4%	4º ± 3º	27%	-1º ± 4º	-2%
Spinal Flexibility	Most flexible (factor = 0.25)	-5º ± 3º	-11%	-5º ± 3º	-13%	-5º ± 2º	-34%	6º ± 4º	18%
	Most rigid (factor = 4)	4º ± 1º	8%	4º ± 1º	10%	5º ± 3º	36%	-7º ± 4º	-20%
Ligaments*	Inter and intravertebral ligaments removed	< 1º	1%	< 1º	< 1%	< 1º	< 1%	< 1º	< 1%

*Patient 2 only

5.1.4.2 Model sensitivity for instrumentation simulation

For the spine curvatures, varying the rod material, screw-to-rod connection boundaries and spine flexibility showed only small changes of less than 2º on all geometric indices. The rods' 3 mm sagittal offset at T8 influenced the sagittal curves with an increase of 2.4º in kyphosis, and the 3 mm lateral offset at the apical vertebra influenced the Cobb angles with a reduction of 2.5º in MT. The offsets at T5 and T12 showed only small changes of less than 2º on all geometric indices. Refer to Table 5.9 for tabulated results of these model sensitivity studies.

For the screw pull-out forces, reducing the rod material stiffness from 240 GPa to 115 GPa resulted in an average increase of 7% in average forces and of 2% in average maximum. The rods' 3mm sagittal offsets showed an increase ranging from 2% (Apical) to 30% (T12) in average forces and 2% (Apical) to 69% (T12) in maximums. Reducing the orient joint and cylindrical joint boundaries resulted in an increase of 21% in average forces for both, and in an increase of 9% and 29% in maximum respectively. Varying the spine flexibility with a 20% more rigid spine resulted in an average increase of 8% in average forces and 10% in average maximum, while a 20% more flexible spine resulted in an average reduction of 11% in average forces and 12% in maximum. Refer to Table 5.10 for tabulated results of these model sensitivity studies.

Table 5.9 Effects on the curves of the spinal model from the modulation of selected parameters within the described value ranges (mean +/- standard deviation, and % of the impact on the baseline value). Instrumentation simulation.

Tested Parameter	Values	Cobb Angle				Sagittal curvatures			
		MT		TL/L		Kyphosis		Lordosis	
		Deg.	%	Deg.	%	Deg.	%	Deg.	%
Rod material	Titanium (EX = 115 GPa)	0.4º ± 0.6º	2%	0.5º ± 0.3º	3%	-0.5º ± 0.5º	-2%	0.0º ± 0.3º	0%
Rod local shape variations*	T5 3 mm post.	1.0º	4%	0.3º	1%	1.2º	7%	0.1º	0%
	T8 3 mm post.	-0.3º	-1%	-0.2º	-1%	2.4º	14%	0.0º	0%
	T12 3 mm post.	-0.9º	-4%	-1.0º	-5%	0.0º	0%	1.5º	5%
	Apical 3 mm lat.	-2.5º	-11%	-0.6º	-3%	0.3º	2%	0.1º	0%
Screw-to-rod connection boundaries*	Orient joint 8 mm^3 volume	-0.6º	-3%	-0.4º	-2%	0.8º	5%	1.5º	5%
	Cylindrical joint ± 1 mm translation	1.3º	6%	-0.1º	-1%	-0.8º	-5%	-0.2º	-1%
Spine Flexibility	Factor: 1.2	0.7º ± 0.5º	3%	0.7º ± 0.3º	4%	-0.5º ± 0.3º	-3%	0.1º ± 0.5º	0%
	Factor: 0.8	-0.8º ± 1.7º	-4%	-0.4º ± 0.7º	-2%	0.2º ± 0.6º	1%	0.3º ± 0.5º	1%

*Patient 2 only

Table 5.10 Effects on the screw pull-out forces of the spinal model from the modulation of selected parameters within the described value ranges (mean and % of the impact on the baseline value). Instrumentation simulation.

Tested parameter	Values	Average Axial Load Magnitude		Average Max	
		N	%	N	%
Rod material	Titanium (EX = 115 GPa)	80	7%	241	2%
Rod local shape variations*	T5 3 mm post.	98	15%	340	8%
	T8 3 mm post.	102	20%	338	8%
	T12 3 mm post.	111	30%	530	69%
	Apical 3 mm lat.	87	2%	318	2%
Screw-to-rod connection boundaries*	Orient joint 8 mm^3 volume	103	21%	342	9%
	Cylindrical joint ± 1 mm translation	103	21%	404	29%
Spine Flexibility	Factor: 1.2	81	8%	259	10%
	Factor: 0.8	66	-11%	208	-12%

*Patient 2 only

5.2 Influence of patient positioning in instrumentation surgery

Comparison of the instrumented reference and instrumented with 50-mm thoracic cushions raised scenarios resulted in an average absolute difference of 2.6º (-1º to 6º) for kyphosis and 8.4º (-15º to 5º) for lordosis. For the screw pull-out forces, raising the thorax showed a reduction of 23 N or 28% to an increase of 13 N or 17% in average forces and a reduction of 80N or 37% to an increase of 52N or 27% in maximum. Average absolute differences were 14 N for average forces and 45 N for maximum. Refer to Table 5.11 for tabulated results. Figure 5.4 shows the pull-out forces for a typical case at each screw and for each level for both scenarios. Graphical results for all the patients included in the study are reported in Appendix A (Figure A.15 to Figure A.18).

Table 5.11 Comparison of instrumented reference and instrumented with 50 mm thoracic cushions raised results for sagittal curvatures and screw pull-out forces (average and maximum).

Case		Sagittal curvatures		Average Axial Load Magnitude		Max Axial Load	
		Kyphosis	**Lordosis**	**N**	**% change**	**N**	**% change**
1	Inst. reference	26º	43º	47 ± 32	+11%	107	+21%
	Inst. 50 mm raised	29º	35º	52 ± 37		130	
2	Inst. reference	28º	34º	82 ± 56	-28%	215	-37%
	Inst. 50 mm raised	27º	36º	59 ± 41		135	
3	Inst. reference	29º	43º	67 ± 58	+16%	238	-8%
	Inst. 50 mm raised	31º	28º	78 ± 64		218	
4	Inst. reference	30º	24º	91 ± 99	-20%	423	-11%
	Inst. 50 mm raised	36º	29º	73 ± 81		375	
5	Inst. reference	28º	52º	75 ± 61	+17%	194	+27%
	Inst. 50 mm raised	29º	40º	88 ± 66		246	
Average absolute difference		2.6º	8.4º	14	-	45	-
Min		-1º	-15º	-23		-80	
Max		6º	5º	13		52	

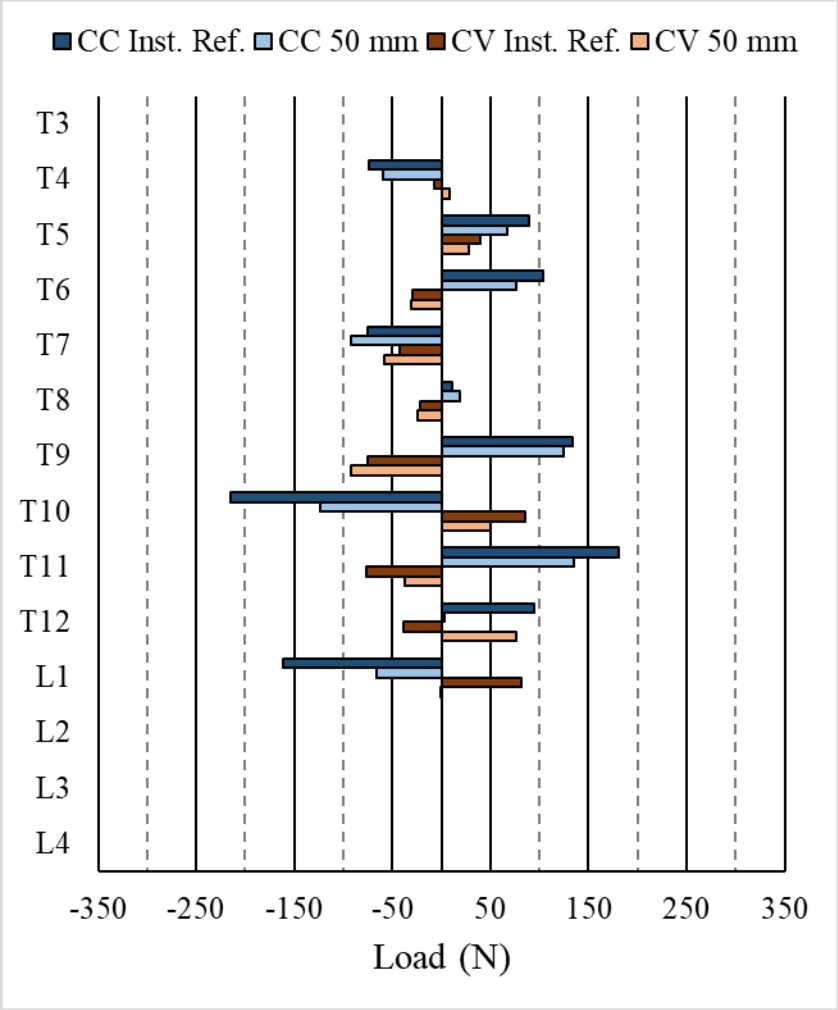

Figure 5.4 Pull-out forces exerted on the screws at each level on the concave (CC) and convex (CV) sides for the simulated instrumented reference spine (Inst. Ref.) and instrumented with 50-mm thoracic cushions raised spine (50 mm). Patient 2.

CHAPTER 6 GENERAL DISCUSSION

6.1 Validation of the simulations

6.1.1 Baseline prone position simulation

The use of a simplified pFEM automatically generated from the 3D reconstructed patient's trunk and adapted to our context was successful in representing how spine curvature is influenced by positioning on a surgical frame. The cushion model and point-to-surface contact elements between rib nodes and thoracic cushion surfaces, combined with prone position gravitational forces allowed to stabilize the thorax as expected. During simulations, it was observed that the defined point-to-surface contact elements on the rib cage had to stay clear of the cushion's surface edges to allow for model convergence. The proposed series of three steps with associated boundary conditions to simulate the prone position resulted in a match with radiographic data within clinical significance ($\leq 5^{o}$) without requiring a personalization of the spine flexibility of each patient. Pelvic flexion in the 0^{o} to 20^{o} range allowed to facilitate the match in spine curvatures while ensuring satisfactory concordance in measured lordosis angles for the two patients with available clinical data.

6.1.2 Thorax raised simulation

Posteriorly raising the thorax via a 50-mm vertical displacement of the thoracic cushions significantly increased thoracic kyphosis. Positioning the proximal edge of the thoracic cushions at T7 promoted movement in the unsupported T1-T7 segment. Gravitational forces acting on this segment as the cushions were raised increased thoracic kyphosis as expected. When compared to the experimental studies from Driscoll et al. (2010) and Canet (2008), our model agreed with their findings. Their studies showed that during the travel of the sternum vertical displacer (SVD) the head was displaced suggesting an influence of the upper limbs at T1, which supported our boundary condition strategy for T1. The selected cushion dimensions and inclination angles in the model caused a posterior raise of the T7-T12 segment by supporting the lower rib cage, as compared to the slender SVD which interfaced with the patient just below the sternoclavical joint and did not contact the lower rib cage. Based on the above findings, our proposed thorax raised simulation methodology was considered suitable for providing a realistic positioning induced thoracic kyphosis increase for characterizing the influence of patient positioning on instrumented surgery.

6.1.3 Instrumentation construct simulation

The intraoperative and post-operative radiographs provided the reference information to model the screw heads positions and extract the rods' contours to guide the simulated instrumentation procedure. Our instrumentation modeling allowed to match the intraoperative radiographs within clinical significance for spine curvatures. Measured screw heads position deviations using RMSE were satisfactory, with only patient 4 showing a larger deviation on the convex side. For this patient, the simulated post-instrumented position showed a transverse plane rotation of the thorax (Figure 6.1) not apparent in the radiograph. The simulated instrumentation induced a rib cage deformation which resulted in this intraoperative thorax rotation. The measured position deviations in the sagittal plane showed a convex rod anterior translation relative to the concave rod, which explained the larger deviations measured when compared to radiographs.

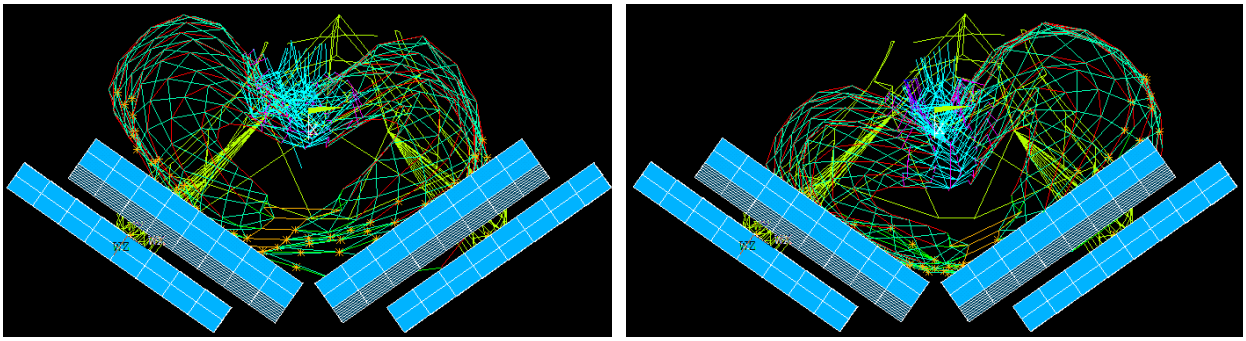

(a) (b)

Figure 6.1 Patient 4 simulated thorax position (top view). (a) Baseline prone position. (b) Post-instrumentation showing a transverse plane rotation of the thorax.

Comparison of our simulated screw pull-out forces with selected *in silico* studies for the multi-axis screw showed comparable results, expect when compared to Driscoll et al. (2015). They reported an average value across all steps of the simulated instrumentation surgery and did not isolate the post-instrumented state. In our study, our simplified representation of the 5 DoF kinematic chain of the multi-axis screw used a single 2 DoF cylindrical joint, which is more consistent with a single-axis screw. Normally, this would have resulted in higher forces than those usually reported for multi-axis screws, but our modeling included a temporary joint model which allowed us to mitigate the forces to the levels expected for multi-axis screws. In the simulation procedure the translation maneuver initially forced the implants to be aligned with the rod, which imposed extra strain on

the IVD typical of single-axis screws (Wang et al., 2011a). The additional 3 DoF in translation from the temporary joint model allowed to find an optimized position of the screw head within a prescribed volume which improved inter-vertebral alignment and thus reduced the strain on the IVDs. Another implant load alleviating strategy came from the locking of the screw-rod joint which did not consider any screw head saddle orientation, hence with no extra loads associated with the seating of the rigid rod into the saddle typical of monoaxial screws (Wang et al., 2011a). These modelling strategies allowed to obtain comparable load levels to previous studies while using simplified representations of the multi-axis screw kinematics and its screw-to-rod connection.

6.1.4 Model uncertainty

6.1.4.1 Baseline prone position

The orientation of the V-shaped surgical frame cushions in the transverse plane stabilized the trunk laterally. The model sensitivity study showed significant effects only in the sagittal curves. Pelvic rotation was confirmed as an important parameter to influence sagittal curves, which is possible with modern operating table devices such as the Axis Jackson System® showcased in the *in vivo* study from Sebastian et al. (2018) or the MFPF reported in the work by Driscoll et al. (2011, 2012). The thoracic cushions' longitudinal displacement showed how a variation of the contact position with the rib cage can significantly influences the thoracic kyphosis. In our simulations, moving the cushion in the cephalad direction promoted on average a loss of kyphosis due to the increase in continuous vertebral levels not directly supported between the pelvic and thoracic cushions (Figure 6.2). Inversely, a caudal displacement of the cushions on average increased kyphosis as compared to baseline. Our model did not capture any changes in lordosis from these variations in thoracic cushions position, which may be linked to the fixed position boundary conditions imposed on the pelvis. From this finding, the recommendation would be to favor, when possible, a more caudal thoracic cushion position to minimize further position induced loss in kyphosis, which agrees with the recommendation from the experimental study of Delorme et al. (2000).

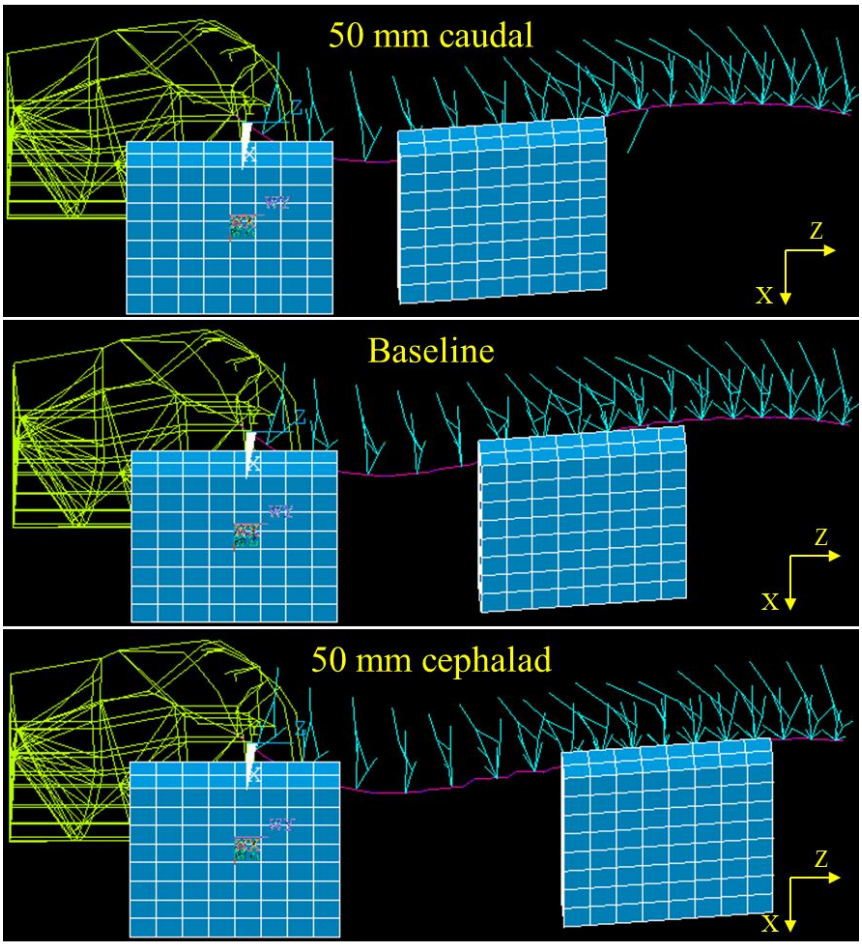

Figure 6.2 Spine sagittal curves visualization from thoracic cushions longitudinal displacement. 50 mm caudal, baseline and 50 mm cephalad for patient 5 (some elements removed for visual clarity).

Our model showed how the spine flexibility can have a significant influence on the simulated sagittal curvatures during the prone positioning, also noting a concomitant variation of the coronal curves. With a more supple spine, the lordosis was increased during the positioning and paired with an increased loss in kyphosis. A more rigid spine was less susceptible to position induced loss in kyphosis and paired with a loss in lordosis. Patient variability in spine flexibility should therefore be considered in the intraoperative positioning strategy with the potential to leverage lower limb positioning to induce pelvic rotations capable of manipulating lordosis and thoracic cushions placement (i.e., longitudinal and vertical) to manipulate kyphosis.

6.1.4.2 Instrumentation construct

Uncertainties related to changes in rod material, rod connection, and spine flexibility had little influence on the model's instrumented spine geometrical indices. This is realistic considering that the selected patients all had high screw density patterns (screws per vertebra ranging from 1.92 to 2), which combined with a simulated rod diameter of 6.35 mm made the instrumented constructs particularly rigid. Introducing rod local shape variations similar to the measured RMSE deviations in screw head positions also showed little influence on spine curvatures. Based on these observations, the contoured rod's general shape was the mean to manipulate the spine curvatures with minimal influence from local screw-to-rod modelling uncertainties.

The instrumented constructs allowed to maintain the rod's general shape for the two rod materials evaluated and maintain similar screw axial load magnitudes. Rod local shape variations had a significant influence on screw pull-out forces with a higher increase for the distal vertebra level case (30% at T12) compared to the proximal level case (15% at T5). Pull-out forces were also very sensitive to screw-to-rod modelling. By reducing the allowable local travel at the screw-to-rod connection, the improvement in inter-vertebral alignment associated with our load mitigation strategy to model multi-axis screws was inhibited (cf. section 6.1.3). This resulted in a less optimized position of the screw head when locked to the rod and thus higher pull-out forces. These findings were in line with the studies from Wang et al. (2011a, 2012) and Clin et al. (2019) characterizing how variations in degrees of freedom at screw-to-rod connection had a significant impact on forces sustained in implants. Our findings exemplified how millimetre level adjustments in the instrumentation play a significant role in measured load levels, noting that the measured variations remained within safe load levels for utilisation of pedicle screws.

For spine flexibility, a variation of ± 20% from the baseline elastic modulus resulted in about a ±10% variation on average screw pull-out forces. Initial selection of a baseline IVD elastic modulus will therefore have a significant influence on the measured screw pull-out forces, which agrees with the IVD sensitivity findings reported by Driscoll et al. (2015) with his numerical model and is of interest for evaluating the risk of screw pull-out for patients.

6.2 Influence of patient positioning in instrumentation surgery

By following the VVUQ workflow (section 4.3), our proposed model proved credible in matching the intraoperative prone and post-instrumented prone positions within clinical significance, as well as providing screw pull-out forces that are comparable to reported *in silico* studies. These validation activities were combined with the quantification of model uncertainties to confirm the model as credible for our COU. This allowed to confidently proceed with our comparative analysis targeting the influence of patient positioning on the instrumentation correction and screw pull-out forces.

When first looking at sagittal curves for the instrumented reference and instrumented with 50 mm thoracic cushions raised cases, the defined rod contours for each patient provided similar correction in the instrumented segment. The larger kyphosis variation in patient 4 was attributed to spine mobility in the T1-T4 non-instrumented segment. Lordosis variations were expected between reference and raised positions, considering that patients had varying spine mobility in the lumbar segment and that the pre-instrumented thorax raised simulations had shown an influence on lordosis.

The screw pull-out forces were significantly affected by raising the thoracic cushions, but results were not consistent across the patients. Patient 2, who had the least number of instrumented levels (T4-L1) showed a significant reduction in average (-28%) and maximum (-37%) axial loads. Patient 5, with the highest number of instrumented levels (T4-L4), showed the highest increase in average (17%) and maximum (27%) axial loads. From this observation, it is deduced that depending on the patient's instrumentation strategy, the contoured rod's sagittal shape may work in combination with or against the positioned induced spine shape. This finding highlights the need to plan the rod contouring strategy in conjunction with the positioning strategy to take full advantage of position induced spine corrections. The third hypothesis of this project was therefore not fully tested in our study as we have not fully leveraged the changes induced by the positioning to further adapt the rod contouring. However, intraoperative positioning induced corrections disappear when the patient returns to an erect posture, and it can be assumed that the forces will then be distributed between the different anchor points to the rod. In a future study, we could retrieve the results of the positioning simulation to deduce the shape of the rods that would minimize the resulting forces.

6.3 Limitations

Our numerical study has some limitations. Conservatism in the findings is of order considering that no direct *in vivo* experiment was conducted and that a cohort of 5 patients remains quite small for statistical significance. Analysis of a larger patient cohort would strengthen the confidence in the findings obtained by providing statistical power to our results. The FEM was built using linear elastic and isotropic material properties, which do not approximate non-linear behaviors like the spine's soft tissues known for exhibiting creep behavior or the potential for plastic deformation of the rods during the corrective surgery. Our reported screw pull-out forces may differ from *in vivo* results, which is why our study focused on a comparative analysis to neglect the influence of non-linear effects. For its validation activities, our study calibrated the simulation parameters using the intra-operative radiographs to match the spine curvatures and instrumentation placement, thus preventing a direct validation of the model via a prospective methodology. Direct intraoperative measurements of the operating table configuration as well as true pelvic rotation of the patients were not possible, hence the proposed thoracic cushion position and pelvic flexion used in the model calibration may slightly differ from reality.

The presented methodology did not capture bone-screw loads at intermediate stages of the instrumentation surgery, which have been shown to increase peak loads as compared to the post-instrumentation state and was an initial component of this project's research question. Studies from Le Navéaux et al. (2016) and Driscoll et al. (2015) reported how rod-to-screw reduction followed by concave rod derotation showed significant increases in peak bone-screw loads as compared to the post-instrumentation state. Vertebra level distraction and compression maneuvers were not implemented in the simulation and should be considered in the sequence of corrective maneuvers. Modeling of the 5 DoF kinematic chain of the multi-axis screw using a single 2 DoF cylindrical joint combined with load mitigation strategies was a numerical modeling abstraction to obtain comparable pull-out forces and would benefit from the incorporation of the full 5 DoF kinematic chain in the model to eliminate the need for load mitigation strategies. Further work is required to introduce these capabilities in the current model and assess whether patient positioning can significantly influence bone-screw loads at intermediate stages of surgery for various corrective maneuvers and screw types.

The clinical applicability of a thorax raised position should be evaluated with consideration for the patient's morphology, spine deformity severity and correction strategy. The selected cohort had standing thoracic kyphosis clinical measurements in the 15º to 23º range, hence more likely to benefit from a kyphosis increase via intraoperative positioning. For example, hyperkyphotic patients would not benefit from a thorax raise, since the intent would be to reduce their thoracic kyphosis. For our study, the thoracic cushion design, contact area and raising action was not optimized to provide the highest targeted spine curvature manipulation for each patient. For patient 5 the simulation boundary conditions inhibited upper body rotation in the thoracic cushion raised position, resulting in a less realistic upper body position for this patient's morphology (Figure 6.3). Calibrating our model with dedicated *in vivo* experiments would aid in defining a pelvic flexion to thorax raise relationship. A slightly slanted trajectory of the cushions, as opposed to vertical (C. Driscoll, Aubin, Canet, et al., 2010) could also promote upper body rotation. Lastly, our simulation of the instrumentation procedure with the 50 mm thoracic cushions raised position did not consider cushion contact pressures which could lead to a possible time limitation in the clinical context (C. Driscoll, Aubin, Canet, et al., 2010).

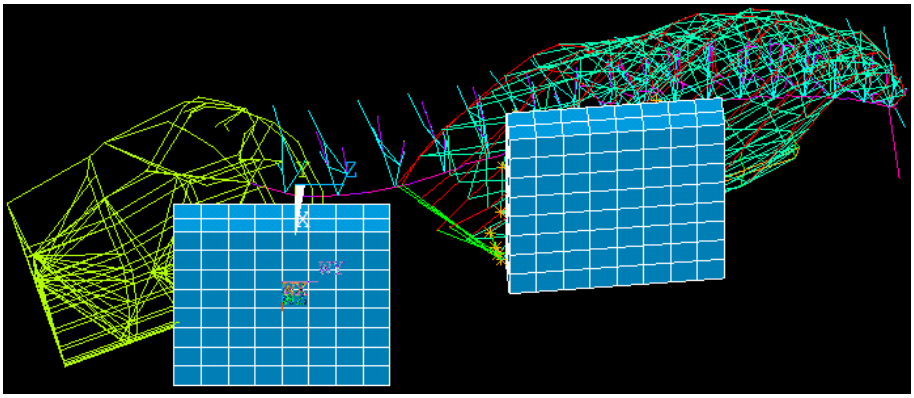

Figure 6.3 50-mm thoracic cushions raised position, pre-instrumentation (Patient 5). Lateral view.

CHAPTER 7 CONCLUSIONS AND PERSPECTIVES

7.1 Conclusions

This project sought to characterize whether intraoperative sagittal manipulations of the spine could further improve and facilitate the correction of spinal deformities, as well as reduce the forces required to perform intraoperative corrective maneuvers when compared to the current practice. Numerical tools combined with a simulation methodology were developed to study this question. A personalized biomechanical finite-element model of the human spine was developed incorporating the spine, thoracic cage, pelvis, abdominal soft tissues, spine correction instrumentation and a simplified adjustable 4-post positioning system. The model allowed for the simulation of intraoperative prone patient positioning in posterior instrumentation surgeries with rods and pedicle screws, with the ability to measure spine curvatures and axial forces at the bone-screw interface.

The model credibility for positioning and spinal instrumentation was established using a verification and validation plan based on the ASME V&V40 guidelines. The Ansys® off-the-shelf software was used to generate the pFEM and its adaptations, and the simulations were performed using a cohort of 5 AIS patients from the Sainte-Justine University Hospital patient database. Simulation results were validated using a combination of intraoperative radiographs from the studied patients, *in vivo* experimental results and *in silico* results from comparable studies. Model uncertainty was quantified via a series of parameter sensitivity studies with a varied set of positioning, patient-related and instrumentation parameters. Lastly, the model was used to characterize the influence of patient positioning in instrumented surgery by measuring the influence of a 50-mm thoracic cushions raise on the resulting axial loads at the screws. All three specific objectives were therefore achieved on this project.

The developed model allowed to reproduce the intraoperative pre-instrumented prone position with resulting spine geometrical indices within clinical significance ($\leq 5^{o}$) on average, confirming our first hypothesis. Raising the thorax via a 50-mm vertical displacement of the thoracic cushions proved effective at increasing thoracic kyphosis as previously exemplified by the work of Driscoll et al. (2010) and Canet (2008).

The developed model allowed to reproduce the intraoperative post-instrumented prone position with resulting spine geometrical indices within clinical significance ($\leq 5^{o}$) on average and within the measured range of comparable *in silico* studies for forces, confirming our second hypothesis. Average measured deviations between simulated and actual screw heads positions showed satisfactory accuracy, but for one patient highlighted how modeling of the rib cage deformation after instrumentation can result in a rotation of the thorax. Our instrumentation construct modeling and simulation methodology allowed for the incorporation of simplified pedicle screw and screw-to-rod connection models with comparable axial load levels as the multi-axis screw.

The parameter sensitivity studies showed how the standard 4-post surgical frame favored spine mobility in the sagittal plane, where pelvic rotation and thoracic cushions longitudinal placement played a significant role in manipulating the spine. For the instrumented construct, measured load levels at the screw elements were significantly influenced by the choice of screw-to-rod modeling assumptions and local rod shape variations.

The developed model allowed to demonstrate a significant change in screw axial loads resulting from a thoracic kyphosis manipulation using patient positioning. However, this effect was different for each case, sometimes having the effect of increasing the loads, sometimes decreasing them. This shows that the positioning parameters have to be adjusted in order to achieve the desired effect in terms of correction but also forces on the implants. This significant difference found for the positioning of the thorax allows us to verify our third hypothesis. It should be noted that the measured screw axial loads were obtained for the post-instrumented position only and did not capture bone-screw loads at intermediate stages of the instrumentation surgery which have been shown to exhibit the highest peak loads.

7.2 Project perspectives

This project is an incremental step in the development of a credible patient positioning and surgical planning numerical toolset and provides the following recommendations for future projects:

- The development of a FEM based modeling and simulation methodology which incorporates a higher fidelity screw-to-rod kinematic chain with a finer geometrical representation of the contoured rods curvatures. The model should allow for bone-screw load monitoring at intermediate stages of the instrumentation procedure. With surgical

planning in mind and similar to the methodology developed by Wang et al. (2011a, 2011b, 2017) and Le Navéaux et al. (2016) using MBM, the model should also allow to start with pre-instrumented rod shapes as opposed to post-instrumented shapes obtained from intraoperative radiographs.

- The evaluation of the potential of position induced intraoperative spine manipulations to improve and facilitate the correction of spinal deformities on other spine deformities like spondylolisthesis and on different instrumented levels, densities, and corrective maneuvers. The subject of improvement and facilitation in the correction of spinal deformities could be expanded to include other surgical steps like screw insertion and osteotomy, similar to the work of Vedantam et al (2020).
- The modeling of an existing specialized operating frame with positioning modalities capable of spine manipulations like the Axis Jackson System® with central hinge to calibrate the model to *in vivo* tests and refine the simulation methodology.
- The modeling of patient soft tissues like skin, muscles, and adipose tissues at the patient to table cushion interface using surface-to-surface contact elements, enabling the characterization of positioning and instrumented surgery induced contact pressures. This recommendation is inline with the recommendations from Driscoll (2010).

This project's findings supported the importance and potential of patient positioning in improving and facilitating the correction of spinal deformities and to the author's knowledge is the first to link position-induced spine manipulations with bone-screw forces from instrumentation surgery. Our proposed numerical model could allow for the rapid development and first evaluation of novel designs in specialized operating frames and their intraoperative influence on the spine prior to prototyping and *in vivo* testing. These numerical tools, in combination with *in vivo* testing, have the potential to be paired with existing and future articulated operating tables to complement surgical planning and the development of new positioning modalities.

REFERENCES

Abelin-Genevois, K. (2021). Sagittal balance of the spine. *Orthopaedics and Traumatology: Surgery and Research*, *107*(1), 102769. https://doi.org/10.1016/j.otsr.2020.102769

Acaroglu, E., Doany, M., Cetin, E., & Castelein, R. (2019). Correction of rotational deformity and restoration of thoracic kyphosis are inversely related in posterior surgery for adolescent idiopathic scoliosis. *Medical Hypotheses*, *133*(August), 109396. https://doi.org/10.1016/j.mehy.2019.109396

Anderton, J. M. (1991). The prone position for the surgical patient: A historical review of the principles and hazards. *British Journal of Anaesthesia*, *67*(4), 452–463. https://doi.org/10.1093/bja/67.4.452

Andriacchi, T., Schultz, A., Belytschko, T., & Galante, J. (1974). A model for studies of mechanical interactions between the human spine and rib cage. *Journal of Biomechanics*, *7*(6), 497–507. https://doi.org/https://doi.org/10.1016/0021-9290(74)90084-0

Asiedu, G. B., Lowndes, B. R., Huddleston, P. M., & Hallbeck, S. (2018). " The Jackson table is a pain in the …": a qualitative study of providers ' perception toward a spinal surgery table. *Journal of Patient Safety*, *14*(1), 21–26.

Benfanti, P. L., & Geissele, A. E. (1997). The effect of intraoperative hip position on maintenance of lumbar lordosis. *Spine*, *22*(19), 2299–2303. https://doi.org/10.1097/00007632-199710010-00021

Bertrand, S., Laporte, S., Parent, S., Skalli, W., & Mitton, D. (2008). Three-dimensional reconstruction of the rib cage from biplanar radiography. *Irbm*, *29*(4), 278–286. https://doi.org/10.1016/j.rbmret.2008.03.005

Bianco, R. J., Arnoux, P. J., Mac-Thiong, J. M., & Aubin, C. E. (2019). Thoracic pedicle screw fixation under axial and perpendicular loadings: A comprehensive numerical analysis. *Clinical Biomechanics*, *68*(September 2018), 190–196. https://doi.org/10.1016/j.clinbiomech.2019.06.010

Borkowski, S. L., Tamrazian, E., Bowen, R. E., Scaduto, A. A., Ebramzadeh, E., & Sangiorgio, S. N. (2016). Challenging the conventional standard for thoracic spine range of motion: a

systematic review. *JBJS Reviews*, *4*(4), e51–e511. https://doi.org/10.2106/JBJS.RVW.O.00048

Boyer, L. (2017). *Analyse biomécanique de techniques de dérotation vertébrale pour la correction 3D de la scoliose lors de la chirurgie d'instrumentation postérieure du rachis*. Doctorate thesis, École Polytechnique de Montréal.

Bruna-Rosso, C., Arnoux, P. J., Bianco, R. J., Godio-Raboutet, Y., Fradet, L., & Aubin, C. É. (2015). Finite element analysis of sacroiliac joint fixation under compression loads. *International Journal of Spine Surgery*, *10*, 1–11. https://doi.org/10.14444/3016

Bydon, M., Moinuddin, F. M., Yolcu, Y. U., Wahood, W., Dudakovic, A., Nassr, A., Larson, A. N., & Wijnen, A. J. Van. (2020). Lumbar intervertebral disc mRNA sequencing identifies the regulatory pathway in patients with disc herniation and spondylolisthesis. *Gene*, *750*(March), 144634. https://doi.org/10.1016/j.gene.2020.144634

Canet, F. (2008). *Conception et évaluation d'un système de positionnement dynamique pour les chirurgies du rachis*. Masters thesis, École Polytechnique de Montréal.

Cheung, J. P. Y. (2020). The importance of sagittal balance in adult scoliosis surgery. *Annals of Translational Medicine*, *8*(2), 35–35. https://doi.org/10.21037/atm.2019.10.19

Clin, J., Aubin, C. É., Lalonde, N., Parent, S., & Labelle, H. (2011). A new method to include the gravitational forces in a finite element model of the scoliotic spine. *Medical and Biological Engineering and Computing*, *49*(8), 967–977. https://doi.org/10.1007/s11517-011-0793-4

Clin, J., Le Navéaux, F., Driscoll, M., Mac-Thiong, J. M., Labelle, H., Parent, S., Shah, S. A., Lonner, B. S., Newton, P. O., & Serhan, H. (2019). Biomechanical comparison of the load-sharing capacity of high and low implant density constructs with three types of pedicle screws for the instrumentation of adolescent idiopathic scoliosis. *Spine Deformity*, *7*(1), 2–10. https://doi.org/10.1016/j.jspd.2018.06.007

Cobetto, N. (2017). *Planification chirurgicale pour la correction 3D de la scoliose pédiatrique proressive à l'aide d'un dispositif sans fusion flexible*. Doctorate thesis, École Polytechnique de Montréal.

Cobetto, N., Aubin, C.-É., Clin, J., Le May, S., Desbiens-Blais, F., Labelle, H., & Parent, S. (2014). Braces optimized with computer-assisted design and simulations are lighter, more

comfortable, and more efficient than plaster-cast braces for the treatment of adolescent idiopathic scoliosis. *Spine Deformity*, *2*(4), 276–284. https://doi.org/10.1016/j.jspd.2014.03.005

Cobetto, N., Aubin, C.-É., & Parent, S. (2018). Surgical planning and follow-up of anterior vertebral body growth modulation in pediatric idiopathic scoliosis using a patient-specific finite element model integrating growth modulation. *Spine Deformity*, *6*(4), 344–350. https://doi.org/10.1016/j.jspd.2017.11.006

Cobetto, N., Aubin, C.-É., Parent, S., Clin, J., Barchi, S., Turgeon, I., & Labelle, H. (2016). Effectiveness of braces designed using computer-aided design and manufacturing (CAD/CAM) and finite element simulation compared to CAD/CAM only for the conservative treatment of adolescent idiopathic scoliosis: a prospective randomized controlled trial. *European Spine Journal*, *25*(10), 3056–3064. https://doi.org/10.1007/s00586-016-4434-3

Cobetto, N., Aubin, C. É., Parent, S., Barchi, S., Turgeon, I., & Labelle, H. (2017). 3D correction of AIS in braces designed using CAD/CAM and FEM: A randomized controlled trial. *Scoliosis and Spinal Disorders*, *12*(1), 1–8. https://doi.org/10.1186/s13013-017-0128-9

Davies, M. K., Mackintosh, P., Cayton, R. M., Page, A. J., Shiu, M. F., & Littler, W. A. (1980). The straight back syndrome. *The Quarterly Journal of Medicine*, *49*(196), 443–460.

De Leva, P. (1996). Adjustments to Zatsiorsky-Seluyanov's Segement Inertia Parameters. *Journal of Biomechanics*, *29*(9), 1223–1230.

Delikaris, A., Wang, X., Boyer, L., Larson, A. N., Ledonio, C. G. T., & Aubin, C.-E. (2018). Implant density at the apex is more important than overall implant density for 3D correction in thoracic adolescent idiopathic scoliosis using rod derotation and en bloc vertebral derotation technique. *Spine*, *43*(11), E639–E647. https://doi.org/10.1097/BRS.0000000000002465

Delorme, S., Labelle, H., Poitras, B., Rivard, C. H., Coillard, C., & Dansereau, J. (2000). Pre-, intra-, and postoperative three-dimensional evaluation of adolescent idiopathic scoliosis. *Journal of Spinal Disorders*, *13*(2), 93–101. https://doi.org/10.1097/00002517-200004000-00001

DePasse, J. M., Palumbo, M. A., Haque, M., Eberson, C. P., & Daniels, A. H. (2015). Complications associated with prone positioning in elective spinal surgery. *World Journal of*

Orthopaedics, *6*(3), 351–359. https://doi.org/10.5312/wjo.v6.i3.351

Deschênes, S., Charron, G., Beaudoin, G., Labelle, H., Dubois, J., Miron, M.-C., & Parent, S. (2010). Diagnostic imaging of spinal deformities: reducing patients radiation dose with a new slot-scanning X-ray imager. *Spine*, *35*(9), 989–994. https://doi.org/10.1097/BRS.0b013e3181bdcaa4

Driscoll, C. (2010). *Patient positioning for surgeries of the spine: how does it impact spinal geometry and how can it be exploited to improve surgical procedures*. Doctorate thesis, École Polytechnique de Montréal.

Driscoll, C., Aubin, C.-É., Canet, F., Dansereau, J., & Labelle, H. (2010). The impact of intra-operative sternum vertical displacement on the sagittal curves of the spine. *European Spine Journal*, *19*(3), 421–426. https://doi.org/10.1007/s00586-009-1199-y

Driscoll, C., Aubin, C.-É., Canet, F., Labelle, H., & Dansereau, J. (2012). Impact of prone surgical positioning on the scoliotic spine. *Journal of Spinal Disorders and Techniques*, *25*(3), 173–181. https://doi.org/10.1097/BSD.0b013e318211ffa6

Driscoll, C., Aubin, C.-É., Canet, F., Labelle, H., Horton, W., & Dansereau, J. (2012). Biomechanical study of patient positioning: Influence of lower limb positioning on spinal geometry. *Journal of Spinal Disorders and Techniques*, *25*(2), 69–76. https://doi.org/10.1097/BSD.0b013e31820d5804

Driscoll, C., Aubin, C.-E., Labelle, H., & Dansereau, J. (2010). Optimized use of multi-functional positioning frame features for scoliosis surgeries. *Studies in Health Technology and Informatics*, *158*, 83–88.

Driscoll, C., Aubin, C. E., Labelle, H., & Dansereau, J. (2011). Assessment of two novel surgical positions for the reduction of scoliotic deformities: Lateral leg displacement and hip torsion. *European Spine Journal*, *20*(10), 1711–1719. https://doi.org/10.1007/s00586-011-1801-y

Driscoll, M., Mac-Thiong, J. M., Labelle, H., & Parent, S. (2013). Development of a detailed volumetric finite element model of the spine to simulate surgical correction of spinal deformities. *BioMed Research International*, *2013*. https://doi.org/10.1155/2013/931741

Driscoll, M., Mac-Thiong, J. M., Labelle, H., Stad, S., Serhan, H., & Parent, S. (2015). Biomechanical comparison of 2 different pedicle screw systems during the surgical correction

of adult spinal deformities. *Spine Deformity*, *3*(2), 114–121. https://doi.org/10.1016/j.jspd.2014.07.004

Duke, K. (2005). *The design and biomechanical analysis of a dynamic positioning frame for scoliosis surgery*. Doctorate thesis, École Polytechnique de Montréal.

Duke, K., Aubin, C.-E., Dansereau, J., & Labelle, H. (2005). Biomechanical simulations of scoliotic spine correction due to prone position and anaesthesia prior to surgical instrumentation. *Clinical Biomechanics (Bristol, Avon)*, *20*(9), 923–931. https://doi.org/10.1016/j.clinbiomech.2005.05.006

Duke, K., Dansereau, J., Labelle, H., Koller, A., Joncas, J., & Aubin, C.-E. (2002). Study of patient positioning on a dynamic frame for scoliosis surgery. *Studies in Health Technology and Informatics*, *91*, 144–148.

Dupuis, S., Fortin, C., Caouette, C., Leclair, I., & Aubin, C. É. (2018). Global postural re-education in pediatric idiopathic scoliosis: a biomechanical modeling and analysis of curve reduction during active and assisted self-correction. *BMC Musculoskeletal Disorders*, *19*(1), 1–9. https://doi.org/10.1186/s12891-018-2112-9

Dvorak, J., Panjabi, M. M., Chang, D. G., Theiler, R., & Grob, D. (1991). Functional radiographic diagnosis of the lumbar spine. *Spine*, *16*(5), 562–571. https://doi.org/10.1097/00007632-199105000-00014

Egea-Gámez, R. M., Galán-Olleros, M., Rodríguez del Real, T., González-Menocal, A., & González-Díaz, R. (2021). Variations in the position of the aorta and vertebral safe zones in supine, prone, and lateral decubitus for adolescent idiopathic scoliosis. *European Spine Journal*, *0123456789*. https://doi.org/10.1007/s00586-021-06813-4

El Bojairami, I., El-Monajjed, K., & Driscoll, M. (2020). Development and validation of a timely and representative finite element human spine model for biomechanical simulations. *Scientific Reports*, *10*(1), 1–15. https://doi.org/10.1038/s41598-020-77469-1

Fradet, L., Wang, X., Lenke, L. G., & Aubin, C. E. (2016). Biomechanical analysis of proximal junctional failure following adult spinal instrumentation using a comprehensive hybrid modeling approach. *Clinical Biomechanics*, *39*, 122–128. https://doi.org/10.1016/j.clinbiomech.2016.10.008

Gardner-Morse, M. G., Laible, J. P., & Stokes, I. A. F. (1990). Incorporation of spinal flexibility measurements into finite element analysis. *Journal of Biomechanical Engineering*, *112*(4), 481–483. https://doi.org/10.1115/1.2891216

Ghezelbash, F., Eskandari, A. H., Shirazi-Adl, A., Arjmand, N., El-Ouaaid, Z., & Plamondon, A. (2018). Effects of motion segment simulation and joint positioning on spinal loads in trunk musculoskeletal models. *Journal of Biomechanics*, *70*, 149–156. https://doi.org/10.1016/j.jbiomech.2017.07.014

Gignac, D. (1998). *Optimisation du traitement de la scoliose par corsets*. Masters thesis, École Polytechnique de Montréal.

Glaser, D. A., Doan, J., & Newton, P. O. (2012). Comparison of 3-dimensional spinal reconstruction accuracy: Biplanar radiographs with eos versus computed tomography. *Spine*, *37*(16), 1391–1397. https://doi.org/10.1097/BRS.0b013e3182518a15

Glassman, S. D., Bridwell, K., Dimar, J. R., Horton, W., Berven, S., & Schwab, F. (2005). The impact of positive sagittal balance in adult spinal deformity. *Spine*, *30*(18), 2024–2029. https://doi.org/10.1097/01.brs.0000179086.30449.96

Gracovetsky SA. (1997). Linking the spinal engine with the legs: a theory of human gait. *Movement, Stability & Low Back Pain. The Essential Role of the Pelvis*, *January 1997*, 243–251.

Guanciale, A. F., Dinsay, J. M., & Watkins, R. G. (1996). Lumbar lordosis in spinal fusion: a comparison of intraoperative results of patient positioning on two different operative table frame types. In *Spine* (Vol. 21, Issue 8, pp. 964–969). https://doi.org/10.1097/00007632-199604150-00012

Harimaya, K., Lenke, L. G., Mishiro, T., Bridwell, K. H., Koester, L. A., & Sides, B. A. (2009). Increasing lumbar lordosis of adult spinal deformity patients via intraoperative prone positioning. *Spine*, *34*(22), 2406–2412. https://doi.org/10.1097/BRS.0b013e3181bab13b

Hicks, J. M., Singla, A., Shen, F. H., & Arlet, V. (2010). Complications of pedicle screw fixation in scoliosis surgery: a systematic review. *Spine*, *35*(11), 465–470. https://doi.org/10.1097/BRS.0b013e3181d1021a

Hongo, M., Ilharreborde, B., Gay, R. E., Zhao, C., Zhao, K. D., Berglund, L. J., Zobitz, M., & An,

K. N. (2009). Biomechanical evaluation of a new fixation device for the thoracic spine. *European Spine Journal*, *18*(8), 1213–1219. https://doi.org/10.1007/s00586-009-0999-4

Humbert, L., De Guise, J. A., Aubert, B., Godbout, B., & Skalli, W. (2009). 3D reconstruction of the spine from biplanar X-rays using parametric models based on transversal and longitudinal inferences. *Medical Engineering and Physics*, *31*(6), 681–687. https://doi.org/10.1016/j.medengphy.2009.01.003

Imperial Surgical. (n.d.). *Relton-Hall scoliosis operating frame product brochure*. Imperial Surgical. https://www.surgmed.com/product/curtain-cubicle-tracks/

Jackson, R. P. (1992). *Spinal Surgery Table* (Patent No. US5131106A). U.S. Patent and Trademark Office. https://patents.google.com/patent/US5131106A/en

Jackson, R. P. (2020). *Modular multi-articulated patient support system* (Patent No. US10835438B2). U.S. Patent and Trademark Office. https://patents.google.com/patent/US10835438B2/en

Johnston, C. E., Stephens Richards, B., Sucato, D. J., Bridwell, K. H., Lenke, L. G., & Erickson, M. (2011). Correlation of preoperative deformity magnitude and pulmonary function tests in adolescent idiopathic scoliosis. *Spine*, *36*(14), 1096–1102. https://doi.org/10.1097/BRS.0b013e3181f8c931

Kadoury, S., Cheriet, F., Beauséjour, M., Stokes, I. A., Parent, S., & Labelle, H. (2009). A three-dimensional retrospective analysis of the evolution of spinal instrumentation for the correction of adolescent idiopathic scoliosis. *European Spine Journal*, *18*(1), 23–37. https://doi.org/10.1007/s00586-008-0817-4

Kassebaum, N. J., Arora, M., Barber, R. M., Brown, J., Carter, A., Casey, D. C., Charlson, F. J., Coates, M. M., Coggeshall, M., Cornaby, L., Dandona, L., Dicker, D. J., Erskine, H. E., Ferrari, A. J., Fitzmaurice, C., Foreman, K., Forouzanfar, M. H., Fullman, N., Goldberg, E. M., … Zuhlke, L. J. (2016). Global, regional, and national disability-adjusted life-years (DALYs) for 315 diseases and injuries and healthy life expectancy (HALE), 1990–2015: a systematic analysis for the Global Burden of Disease Study 2015. *The Lancet*, *388*(10053), 1603–1658. https://doi.org/10.1016/S0140-6736(16)31460-X

Katzman, W. B., Wanek, L., Shepherd, J. A., & Sellmeyer, D. E. (2010). Age-related

hyperkyphosis: its causes, consequences, and management. *Journal of Orthopaedic & Sports Physical Therapy*, *40*(6), 352–360. https://doi.org/10.2519/jospt.2010.3099

Kwee, M. M., Ho, Y. H., & Rozen, W. M. (2015). The prone position during surgery and its complications: a systematic review and evidence-based guidelines. *International Surgery*, *100*(2), 292–303. https://doi.org/10.9738/INTSURG-D-13-00256.1

Labelle, H., Aubin, C. E., Jackson, R., Lenke, L., Newton, P., & Parent, S. (2011). Seeing the spine in 3D: how will it change what we do? *Journal of Pediatric Orthopaedics*, *31*(1 SUPPL.), 37–45. https://doi.org/10.1097/BPO.0b013e3181fd8801

Le Naveaux, F. (2016). *Biomécanique des configurations d'instrumentation chirurgicale de la scoliose idiopathique de l'adolescence*. Doctorate thesis, École Polytechnique de Montréal.

Le Navéaux, F., Larson, A. N., Labelle, H., Wang, X., & Aubin, C. É. (2016). How does implant distribution affect 3D correction and bone-screw forces in thoracic adolescent idiopathic scoliosis spinal instrumentation? *Clinical Biomechanics*, *39*, 25–31. https://doi.org/10.1016/j.clinbiomech.2016.09.002

Lee, S. M., Suk, S. Il, & Chung, E. R. (2004). Direct vertebral rotation: a new technique of three-dimensional deformity correction with segmental pedicle screw fixation in adolescent idiopathic scoliosis. *Spine*, *29*(3), 343–349. https://doi.org/10.1097/01.BRS.0000109991.88149.19

Lim, R. K., Morrison, M. M., McGahan, T. V., & Hynes, R. A. (2020). *Surgical frame including torso-sling and method for use thereof* (Patent No. US10849809B2). U.S. Patent and Trademark Office. https://patents.google.com/patent/US10849809B2/en

Lim, R., Morrison, M., & Hynes, R. (2017). *Surgical frame facilitating articulatable support for a patient during surgery* (Patent No. US20170049651A1). U.S. Patent and Trademark Office. https://patents.google.com/patent/US20170049651A1/en

Mac-Thiong, J. M., Labelle, H., Petit, Y., & Aubin, C. E. (2002). The effect of the Relton-Hall operative frame on trunk deformity in adolescent idiopathic scoliosis. *European Spine Journal*, *11*(6), 556–560. https://doi.org/10.1007/s00586-002-0419-5

Madigan, L., Vaccaro, A. R., Spector, L. R., & Milam, R. A. (2009). Management of symptomatic lumbar degenerative disk disease. *Journal of the American Academy of Orthopaedic*

Surgeons, *17*(2), 102–111. https://doi.org/10.5435/00124635-200902000-00006

Mills, M. J., & Sarigul-Klijn, N. (2019). Validation of an in vivo medical image-based young human lumbar spine finite element model. *Journal of Biomechanical Engineering*, *141*(3), 1–12. https://doi.org/10.1115/1.4042183

Miyazaki, M., Ishihara, T., Abe, T., Kanezaki, S., Notani, N., Kataoka, M., & Tsumura, H. (2019). Effect of intraoperative position in single-level transforaminal lumbar interbody fusion at the L4/5 level on segmental and overall lumbar lordosis in patients with lumbar degenerative disease. *Medicine (United States)*, *98*(39), 1–7. https://doi.org/10.1097/MD.0000000000017316

Noorian, S., Sorensen, K., & Cho, W. (2018). A systematic review of clinical outcomes in surgical treatment of adult isthmic spondylolisthesis. *Spine Journal*, *18*(8), 1441–1454. https://doi.org/10.1016/j.spinee.2018.04.022

Ochia, R. S., Inoue, N., Renner, S. M., Lorenz, E. P., Lim, T. H., Andersson, G. B. J., & An, H. S. (2006). Three-dimensional in vivo measurement of lumbar spine segmental motion. *Spine*, *31*(18), 2073–2078. https://doi.org/10.1097/01.brs.0000231435.55842.9e

Ouellet, J. (n.d.). *AO Surgery Reference: Clinical evaluation*. Retrieved April 30, 2021, from https://surgeryreference.aofoundation.org/spine/deformities/spondylolisthesis/further-reading/clinical-evaluation

Ovadia, D. (2013). Classification of adolescent idiopathic scoliosis (AIS). *Journal of Children's Orthopaedics*, *7*(1), 25–28. https://doi.org/10.1007/s11832-012-0459-2

Oxland, T. R. (2016). Fundamental biomechanics of the spine-What we have learned in the past 25 years and future directions. *Journal of Biomechanics*, *49*(6), 817–832. https://doi.org/10.1016/j.jbiomech.2015.10.035

Panjabi, M. M., Brand, R. A., & White, A. A. (1976). Three-dimensional flexibility and stiffness properties of the human thoracic spine. *Journal of Biomechanics*, *9*(4), 185–192. https://doi.org/https://doi.org/10.1016/0021-9290(76)90003-8

Pea, R., Dansereau, J., Caouette, C., Cobetto, N., & Aubin, C. É. (2018). Computer-assisted design and finite element simulation of braces for the treatment of adolescent idiopathic scoliosis using a coronal plane radiograph and surface topography. *Clinical Biomechanics*, *54*(July

2017), 86–91. https://doi.org/10.1016/j.clinbiomech.2018.03.005

Pearsall, D. J., Reid, J. G., & Livingston, L. A. (1996). Segmental inertial parameters of the human trunk as determined from computed tomography. *Annals of Biomedical Engineering*, *24*(2), 198–210. https://doi.org/10.1007/BF02667349

Périé, D., Aubin, C. E., Lacroix, M., Lafon, Y., & Labelle, H. (2004). Biomechanical modelling of orthotic treatment of the scoliotic spine including a detailed representation of the brace-torso interface. *Medical and Biological Engineering and Computing*, *42*(3), 339–344. https://doi.org/10.1007/BF02344709

Peterson, M. D., Nelson, L. M., McManus, A. C., & Jackson, R. P. (1995). The effect of operative position on lumbar lordosis. A radiographic study of patients under anesthesia in the prone and 90-90 positions. *Spine*, *20*(12), 1419–1424.

Pintar, F. A. (1986). The biomechanics of spinal elements [Doctorate thesis, Marquette University]. In *ProQuest Dissertations and Theses*. https://www.proquest.com/dissertations-theses/biomechanics-spinal-elements-ligaments-vertebral/docview/303435301/se-2?accountid=40695

Prophete, B. (2012). *Développement et évaluation d'un système multipositions pour les chirurgies du rachis*. Masters thesis, École Polytechnique de Montréal.

Rajaee, M. A., Arjmand, N., & Shirazi-Adl, A. (2021). A novel coupled musculoskeletal finite element model of the spine – Critical evaluation of trunk models in some tasks. *Journal of Biomechanics*, *119*, 110331. https://doi.org/10.1016/j.jbiomech.2021.110331

Relton, J. E. S., & Hall, J. E. (1967). An operation frame for spinal fusion. A new apparatus designed to reduce haemorrhage during operation. *The Journal of Bone and Joint Surgery. British Volume*, *49 2*, 327–332.

Schonauer, C., Bocchetti, A., Barbagallo, G., Albanese, V., & Moraci, A. (2004). Positioning on surgical table. *European Spine Journal*, *13*(SUPPL. 1), 50–55. https://doi.org/10.1007/s00586-004-0728-y

Schwab, F., Patel, A., Ungar, B., Farcy, J. P., & Lafage, V. (2010). Adult spinal deformity-postoperative standing imbalance: How much can you tolerate? An overview of key parameters in assessing alignment and planning corrective surgery. *Spine*, *35*(25), 2224–2231.

https://doi.org/10.1097/BRS.0b013e3181ee6bd4

Sebastian, A. S., Ahmed, A., Vernon, B., Nguyen, E. C., Aleem, I., Clarke, M. J., Currier, B. L., Anderson, P., Bydon, M., & Nassr, A. (2018). Effect of an adjustable hinged operating table on lumbar lordosis during lumbar surgery. *Spine*, *43*(4), 302–306. https://doi.org/10.1097/BRS.0000000000002345

Shirazi-Adl, A., Ahmed, A. M., & Shrivastava, S. C. (1986). A finite element study of a lumbar motion segment subjected to pure sagittal plane moments. *Journal of Biomechanics*, *19*(4), 331–350. https://doi.org/https://doi.org/10.1016/0021-9290(86)90009-6

Shriver, M. F., Zeer, V., Alentado, V. J., Mroz, T. E., Benzel, E. C., & Steinmetz, M. P. (2015). Lumbar spine surgery positioning complications: A systematic review. *Neurosurgical Focus*, *39*(4), 1–9. https://doi.org/10.3171/2015.7.FOCUS15268

Stephens, G. C., Yoo, J. U., & Wilbur, G. (1996). Comparison of Lumbar Sagittal Alignment Produced by Different Operative Positions. *Spine*, *21*(15). https://journals.lww.com/spinejournal/Fulltext/1996/08010/Comparison_of_Lumbar_Sagittal_Alignment_Produced.16.aspx

Sterba, M., Aubin, C. É., Wagnac, E., Fradet, L., & Arnoux, P. J. (2019). Effect of impact velocity and ligament mechanical properties on lumbar spine injuries in posterior-anterior impact loading conditions: a finite element study. *Medical and Biological Engineering and Computing*, *57*(6), 1381–1392. https://doi.org/10.1007/s11517-019-01964-5

Stokes, I., Sangole, A., & Aubin, C.-E. (2009). Classification of scoliosis deformity 3-D spinal shape by cluster analysis. *Spine*, *34*(6), 584–590. https://doi.org/10.1097/BRS.0b013e318190b914.CLASSIFICATION

Strickland, B. A., Sayama, C., Briceño, V., Lam, S. K., Luerssen, T. G., & Jea, A. (2016). Use of sub-transverse process polyester bands in pediatric spine surgery: A case series of 4 patients with a minimum of 12 months' follow-up. *Journal of Neurosurgery: Pediatrics*, *17*(2), 208–214. https://doi.org/10.3171/2015.6.PEDS15255

Stull, J. D., Mangan, J. J., Vaccaro, A. R., & Schroeder, G. D. (2019). Robotic guidance in minimally invasive spine surgery: a review of recent literature and commentary on a developing technology. *Current Reviews in Musculoskeletal Medicine*, *12*(2), 245–251.

https://doi.org/10.1007/s12178-019-09558-2

Suk, S.-I., Kim, W.-J., Lee, S.-M., Kim, J.-H., & Chung, E.-R. (2001). Thoracic pedicle screw fixation in spinal deformities. *Spine*, *26*(18), 2049–2057.

Tachi, H., Kato, K., Abe, Y., Kokabu, T., Yamada, K., Iwasaki, N., & Sudo, H. (2021). Surgical outcome prediction using a four-dimensional planning simulation system with finite element analysis incorporating pre-bent rods in adolescent idiopathic scoliosis: simulation for spatiotemporal anatomical correction technique. *Frontiers in Bioengineering and Biotechnology*, *9*(October), 1–12. https://doi.org/10.3389/fbioe.2021.746902

Tohmeh, A., Isaacs, R. E., Dooley, Z. A., & Turner, A. W. (2014). Long construct pedicle screw reduction and residual forces are decreased using a computer-assisted spinal rod bending system. *The Spine Journal*, *14*(11), S143–S144. https://doi.org/10.1016/j.spinee.2014.08.348

V&V40, A. S. M. E. (2018). *Assessing credibility of computational modeling through verification and validation: application to medical devices*. The American Society of Mechanical Engineers.

Vedantam, A., Verla, T., Mayer, R. R., Raber, M. R., & Ropper, A. E. (2020). Use of an open-frame hinged surgical table to restore segmental lumbar lordosis after posterior column osteotomy. *International Journal of Spine Surgery*, *14*(3), 316–320. https://doi.org/10.14444/7042

Wang, X., Aubin, C. E., Crandall, D., & Labelle, H. (2011a). Biomechanical comparison of force levels in spinal instrumentation using monoaxial versus multi degree of freedom postloading pedicle screws. *Spine*, *36*(2), 95–104. https://doi.org/10.1097/BRS.0b013e3181f07cca

Wang, X., Aubin, C. E., Crandall, D., & Labelle, H. (2011b). Biomechanical modeling and analysis of a direct incremental segmental translation system for the instrumentation of scoliotic deformities. *Clinical Biomechanics*, *26*(6), 548–555. https://doi.org/10.1016/j.clinbiomech.2011.01.011

Wang, X., Aubin, C., Labelle, H., Parent, S., & Crandall, D. (2012). Biomechanical analysis of corrective forces in spinal instrumentation for scoliosis treatment. *Spine*, *37*(24), E1479–E1487. https://doi.org/10.1097/BRS.0b013e3182706745

Wang, X., Boyer, L., Le Naveaux, F., Schwend, R. M., & Aubin, C. E. (2016). How does

differential rod contouring contribute to 3-dimensional correction and affect the bone-screw forces in adolescent idiopathic scoliosis instrumentation? *Clinical Biomechanics*, *39*, 115–121. https://doi.org/10.1016/j.clinbiomech.2016.10.002

Wang, X., Larson, A. N., Crandall, D. G., Parent, S., Labelle, H., Ledonio, C. G. T., & Aubin, C.-E. (2017). Biomechanical effect of pedicle screw distribution in AIS instrumentation using a segmental translation technique: computer modeling and simulation. *Scoliosis and Spinal Disorders*, *12*(1), 1–10. https://doi.org/10.1186/s13013-017-0120-4

Weinstein, S. L., Dolan, L. A., Cheng, J. C. Y., Danielsson, A., & Morcuende, J. A. (2008). Adolescent idiopathic scoliosis. *The Lancet*, *371*, 1527–1537.

Wybier, M., & Bossard, P. (2013). Musculoskeletal imaging in progress: The EOS imaging system. *Joint Bone Spine*, *80*(3), 238–243. https://doi.org/10.1016/j.jbspin.2012.09.018

APPENDIX A SUPPLEMENTARY RESULTS

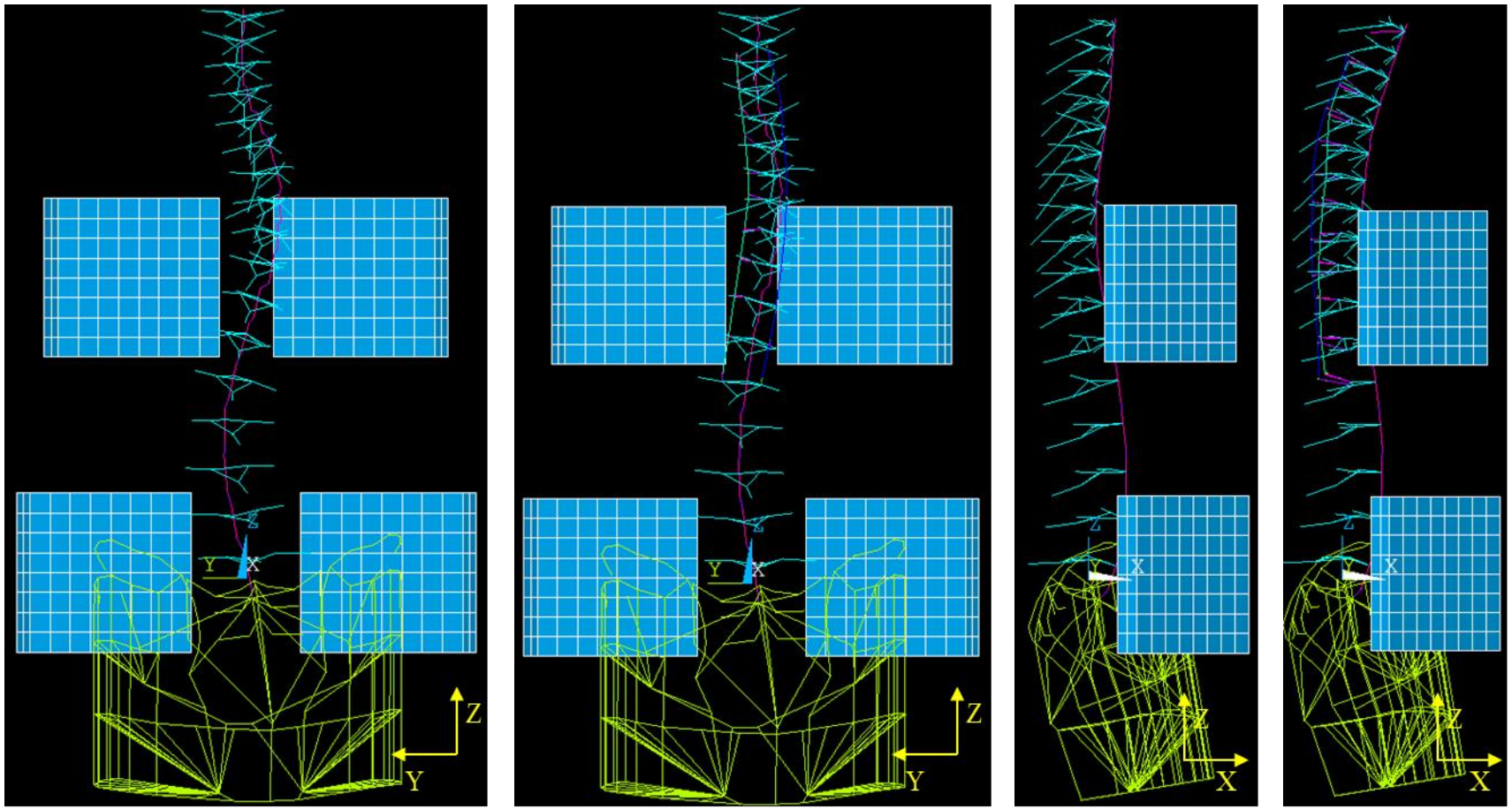

(a) (b) (c) (d)

Figure A.1 Simulated prone position baseline (a, c) and post-instrumented intraoperative (b, d), for patient 1 (some elements removed for visual clarity) (PA (a,b) and lateral (c,d) views).

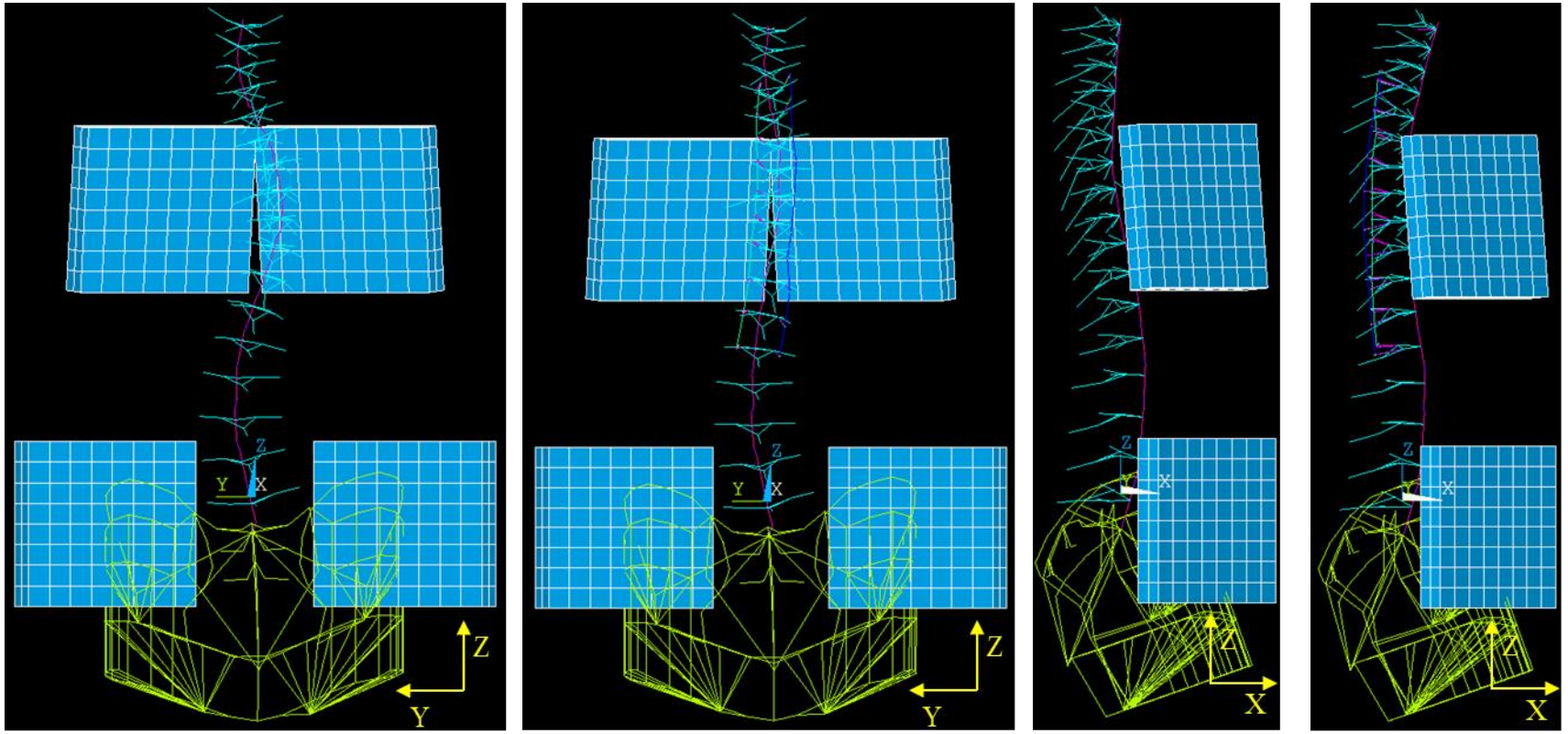

(a) (b) (c) (d)

Figure A.2 Simulated prone position baseline (a, c) and post-instrumented intraoperative (b, d), for patient 2 (some elements removed for visual clarity) (PA (a,b) and lateral (c,d) views).

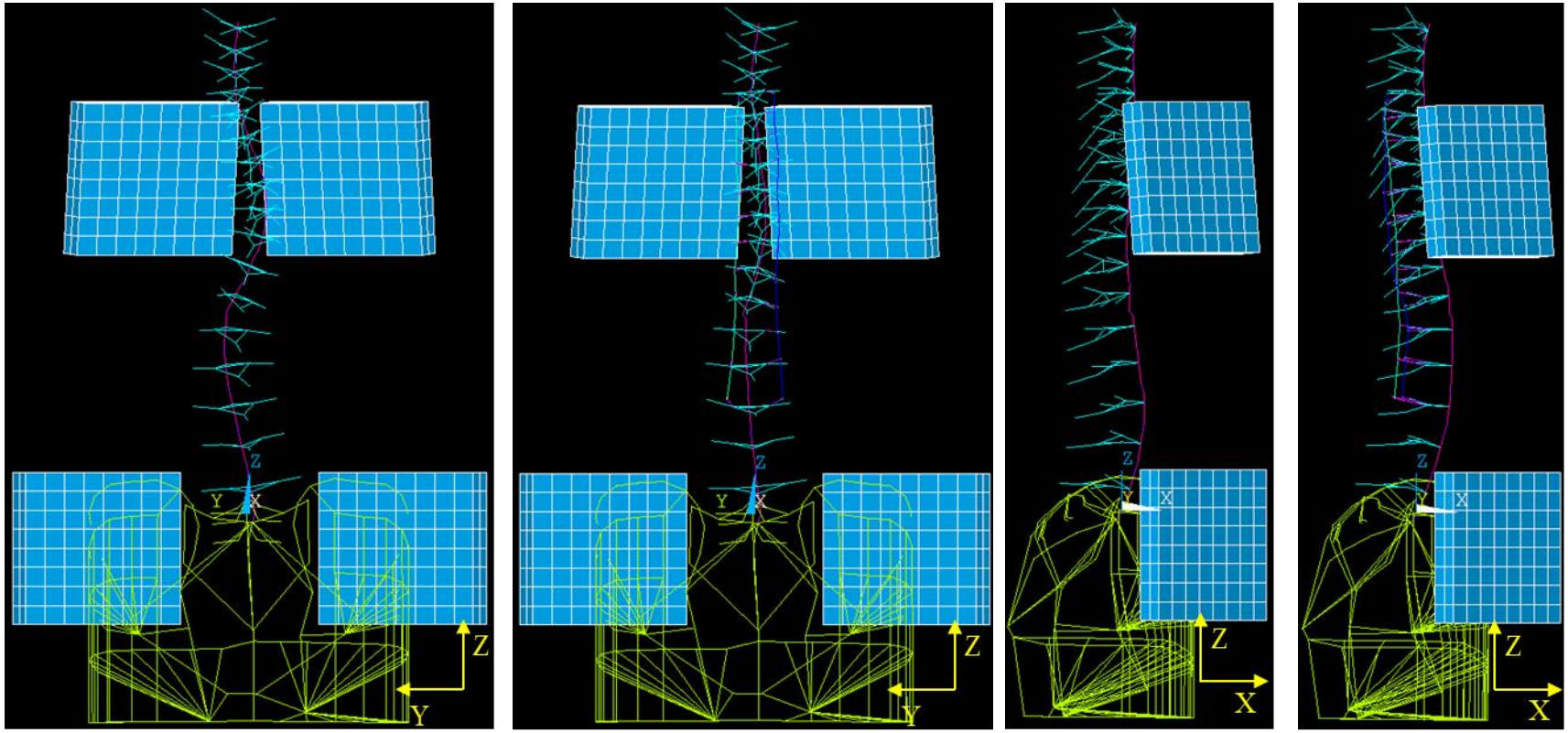

(a) (b) (c) (d)

Figure A.3 Simulated prone position baseline (a, c) and post-instrumented intraoperative (b, d), for patient 3 (some elements removed for visual clarity) (PA (a,b) and lateral (c,d) views).

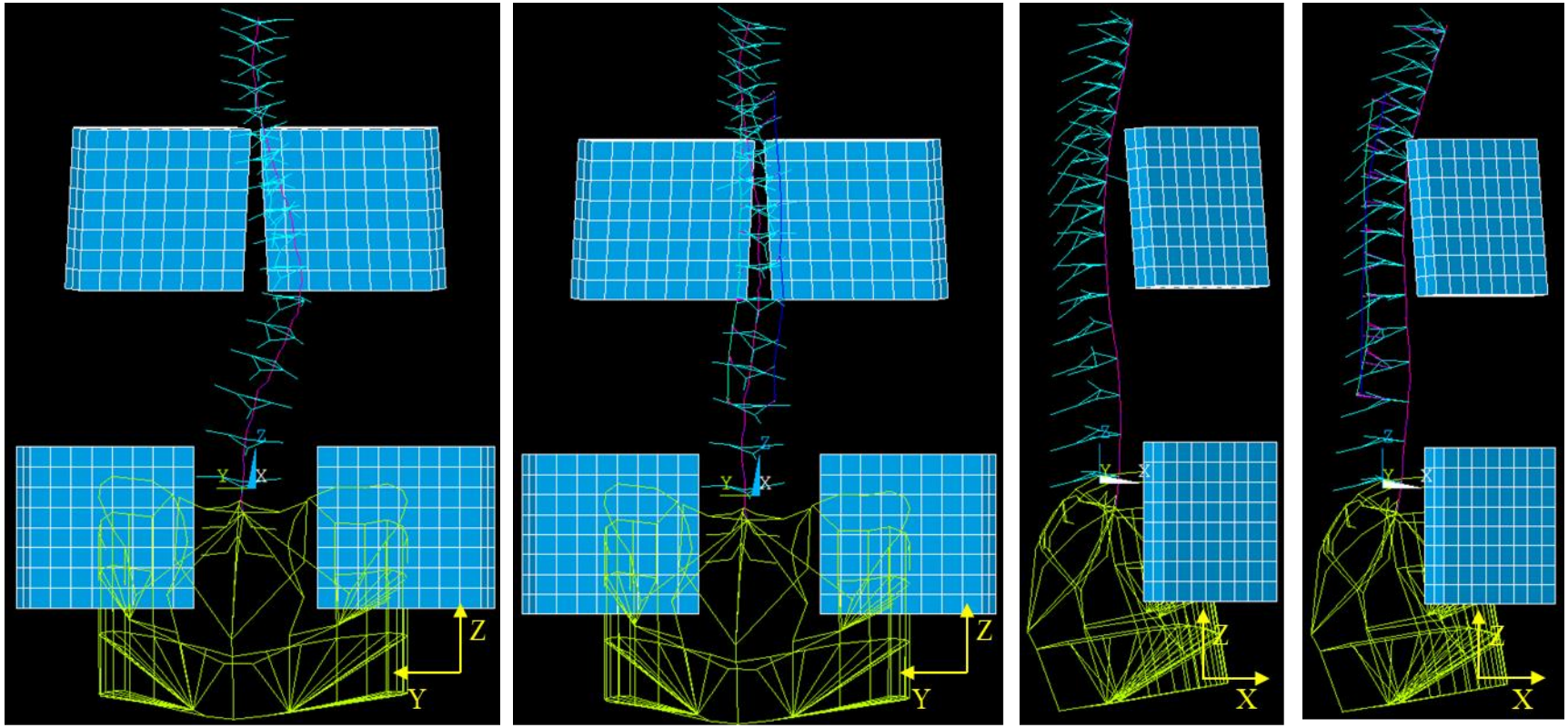

(a) (b) (c) (d)

Figure A.4 Simulated prone position baseline (a, c) and post-instrumented intraoperative (b, d), for patient 4 (some elements removed for visual clarity) (PA (a,b) and lateral (c,d) views).

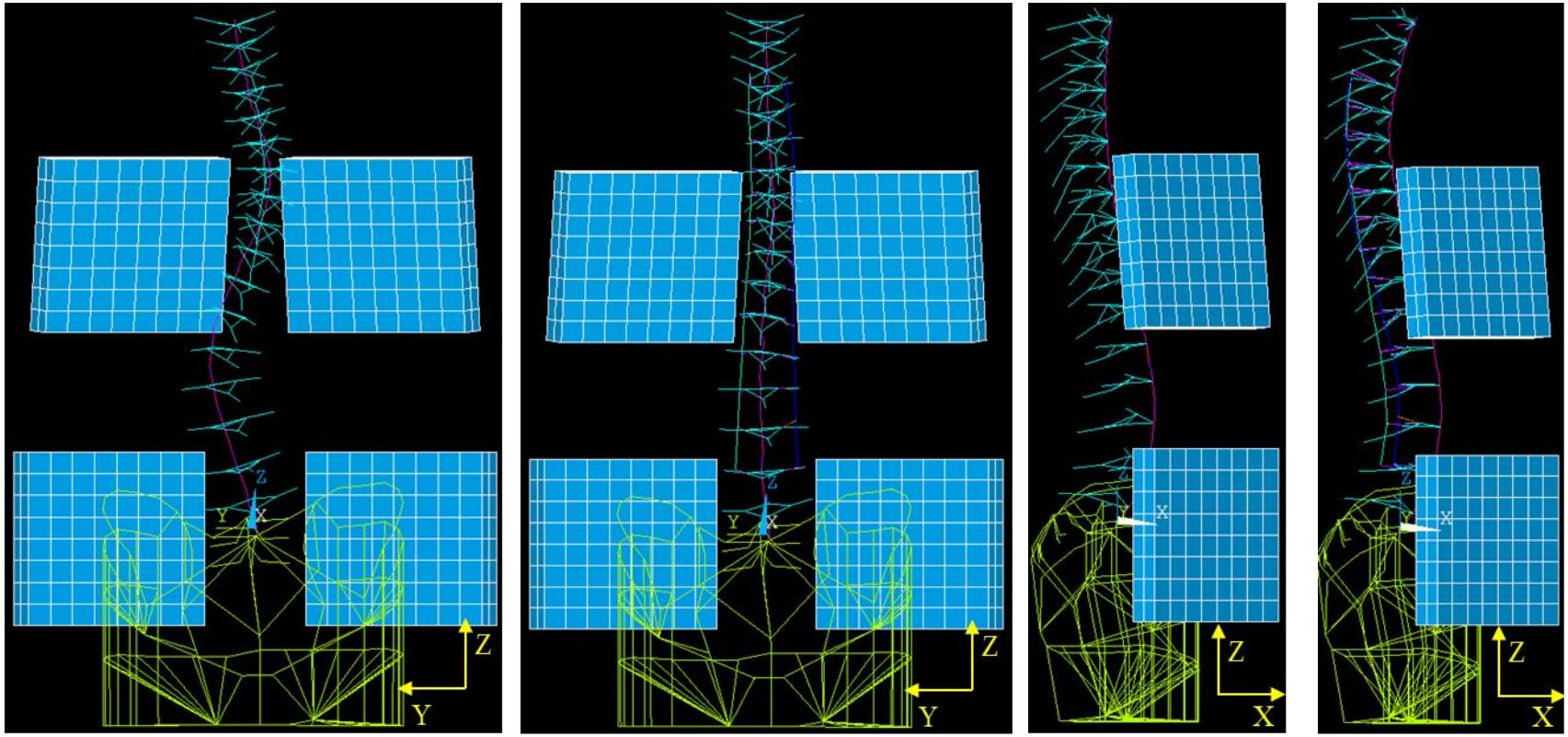

(a) (b) (c) (d)

Figure A.5 Simulated prone position baseline (a, c) and post-instrumented intraoperative (b, d), for patient 5 (some elements removed for visual clarity) (PA (a,b) and lateral (c,d) views).

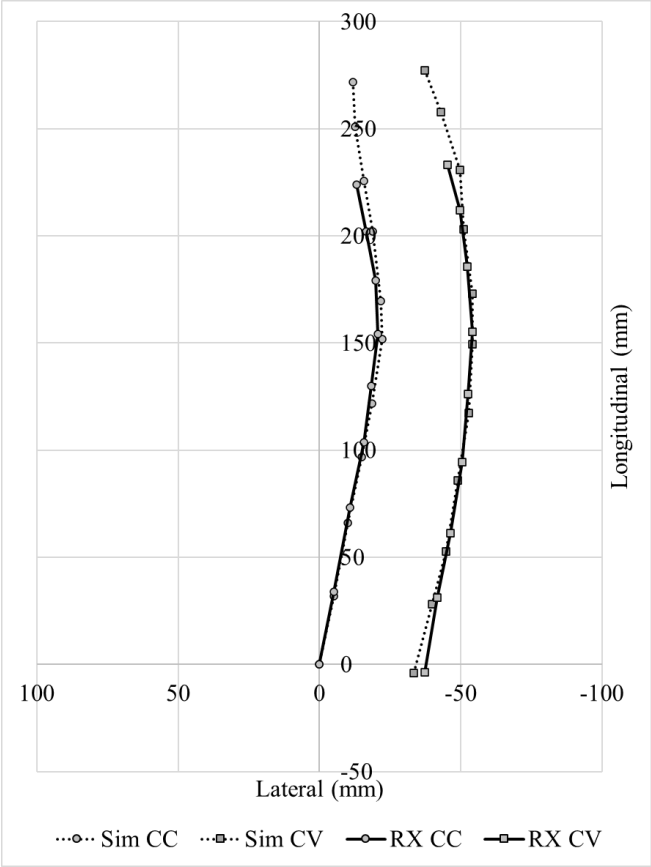

(a)

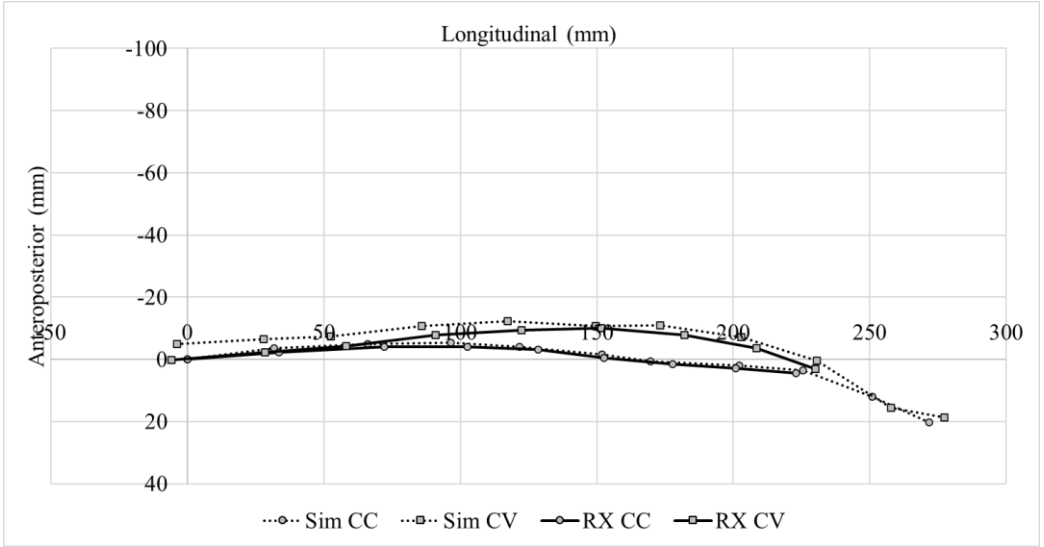

(b)

Figure A.6 Patient 1 simulated (Sim) and actual (RX) concave (CC) and convex (CV) rods. (a) Coronal plane. (b) Sagittal plane.

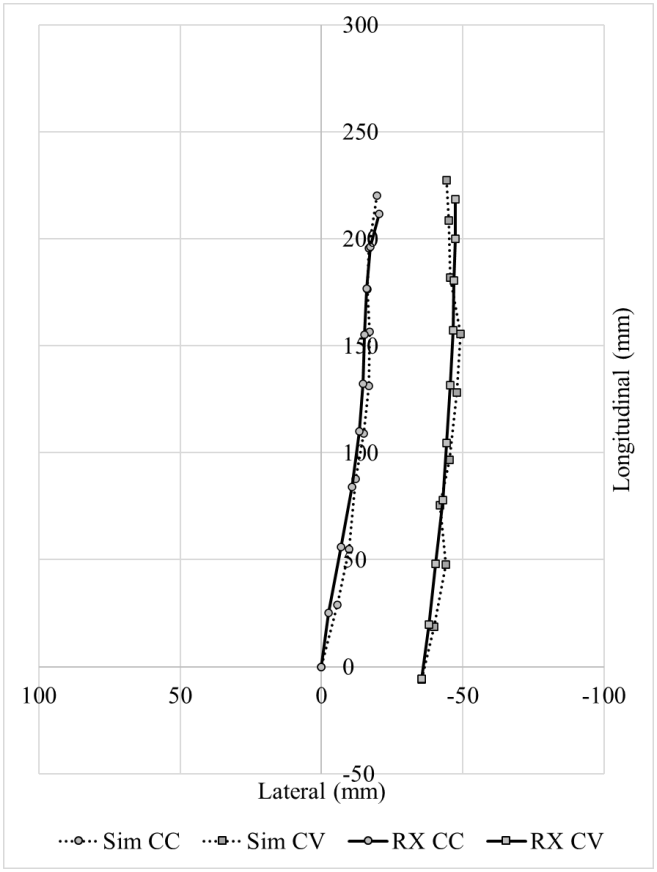

(a)

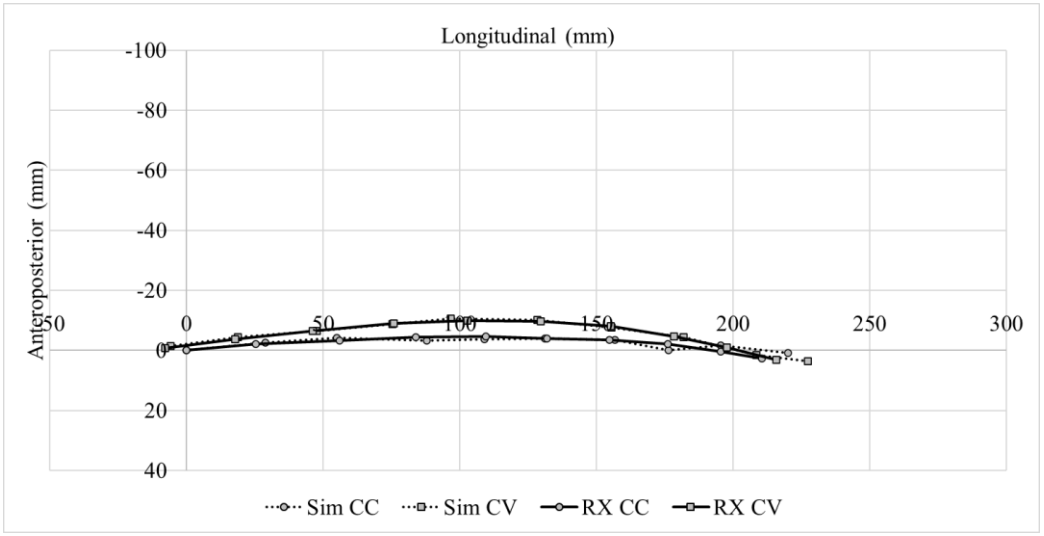

(b)

Figure A.7 Patient 2 simulated (Sim) and actual (RX) concave (CC) and convex (CV) rods. (a) Coronal plane. (b) Sagittal plane.

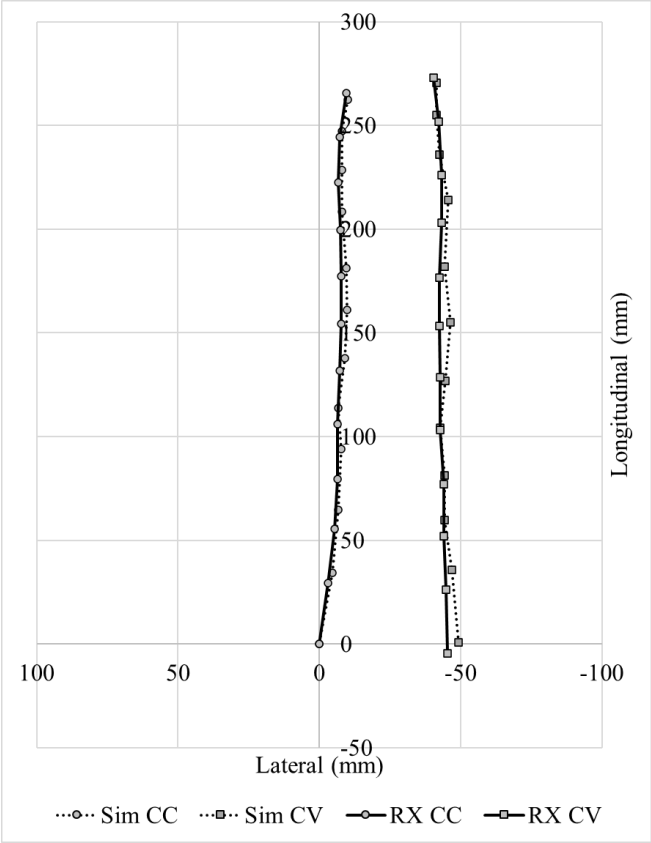

(a)

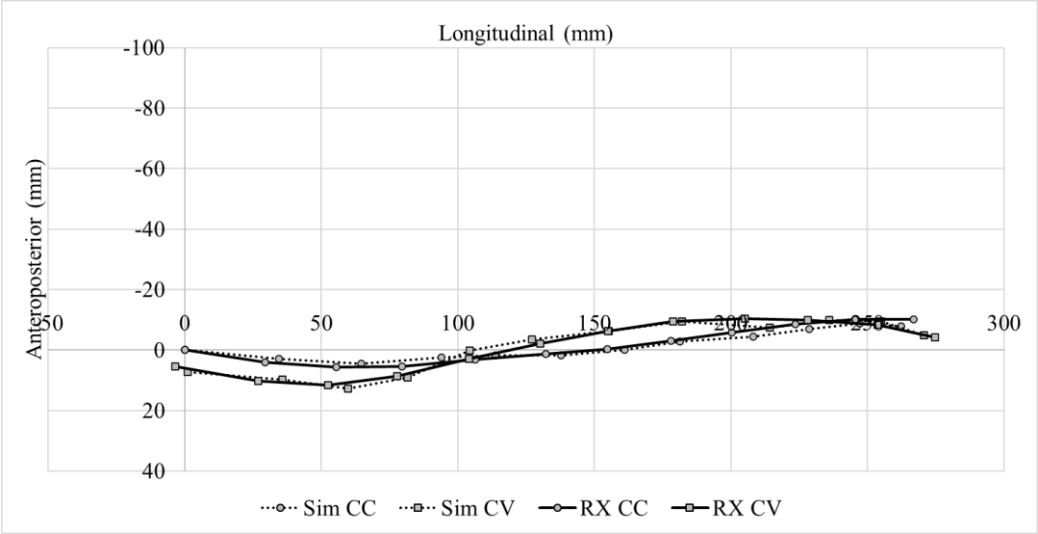

(b)

Figure A.8 Patient 3 simulated (Sim) and actual (RX) concave (CC) and convex (CV) rods. (a) Coronal plane. (b) Sagittal plane.

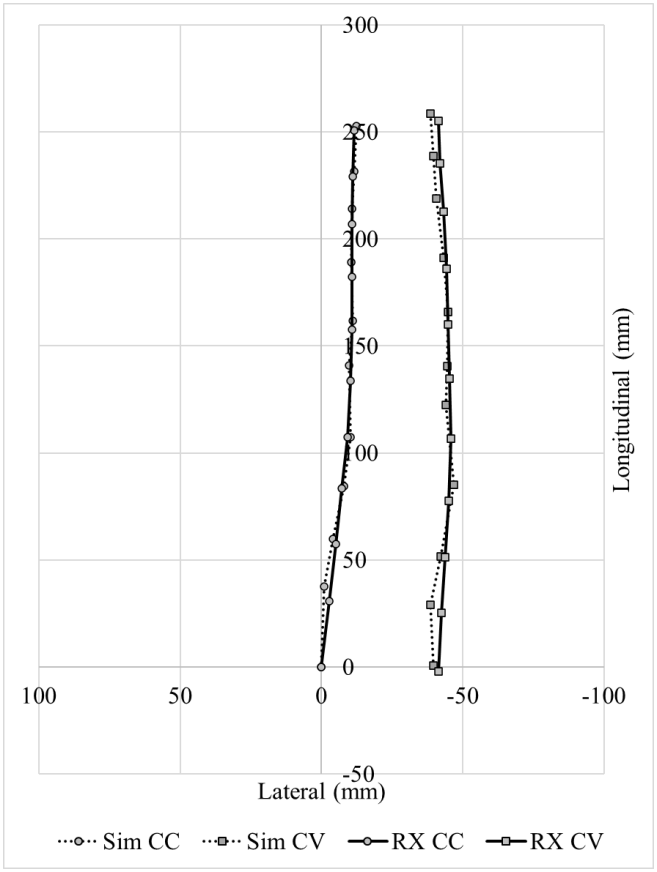

(a)

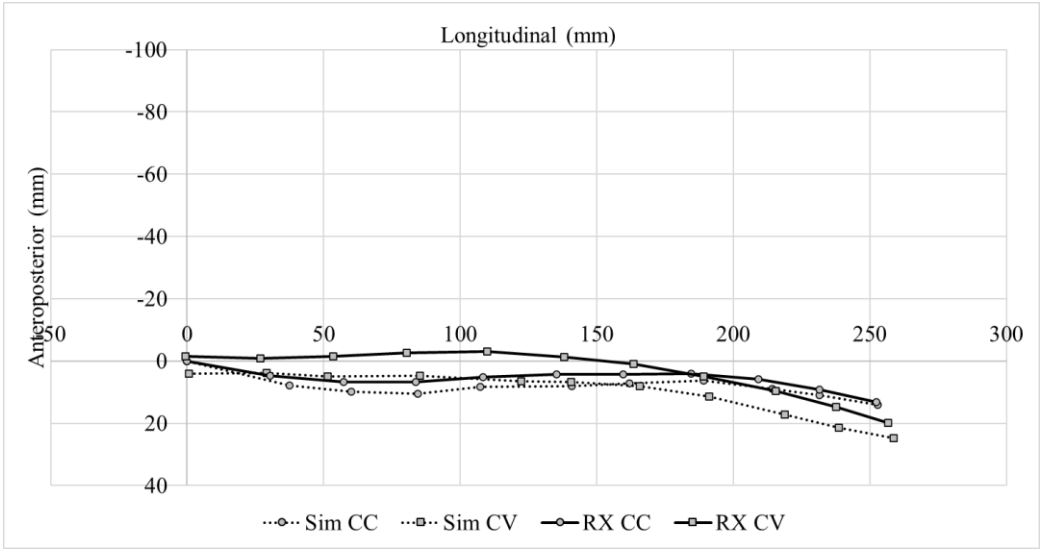

(b)

Figure A.9 Patient 4 simulated (Sim) and actual (RX) concave (CC) and convex (CV) rods. (a) Coronal plane. (b) Sagittal plane.

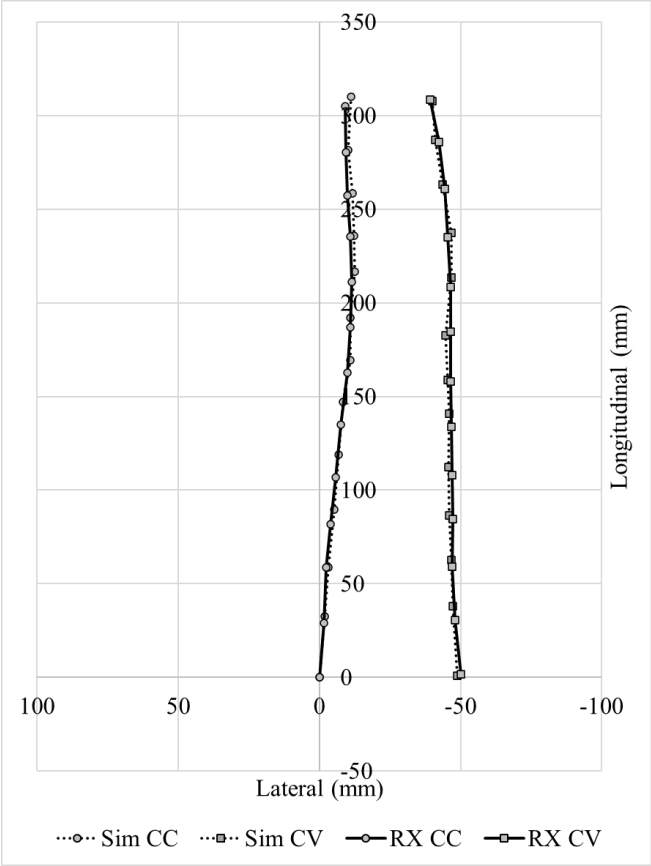

(a)

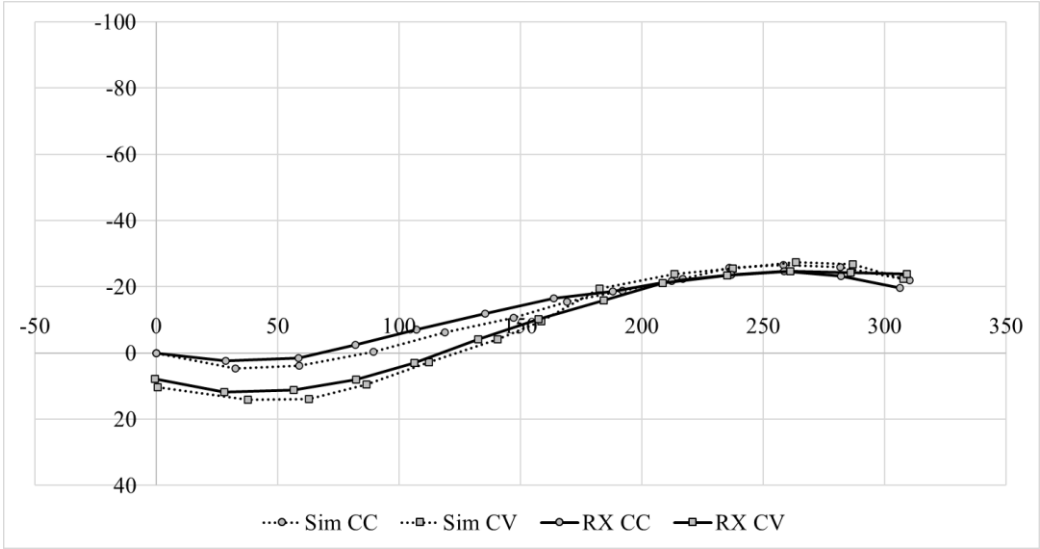

(b)

Figure A.10 Patient 5 simulated (Sim) and actual (RX) concave (CC) and convex (CV) rods. (a) Coronal plane. (b) Sagittal plane.

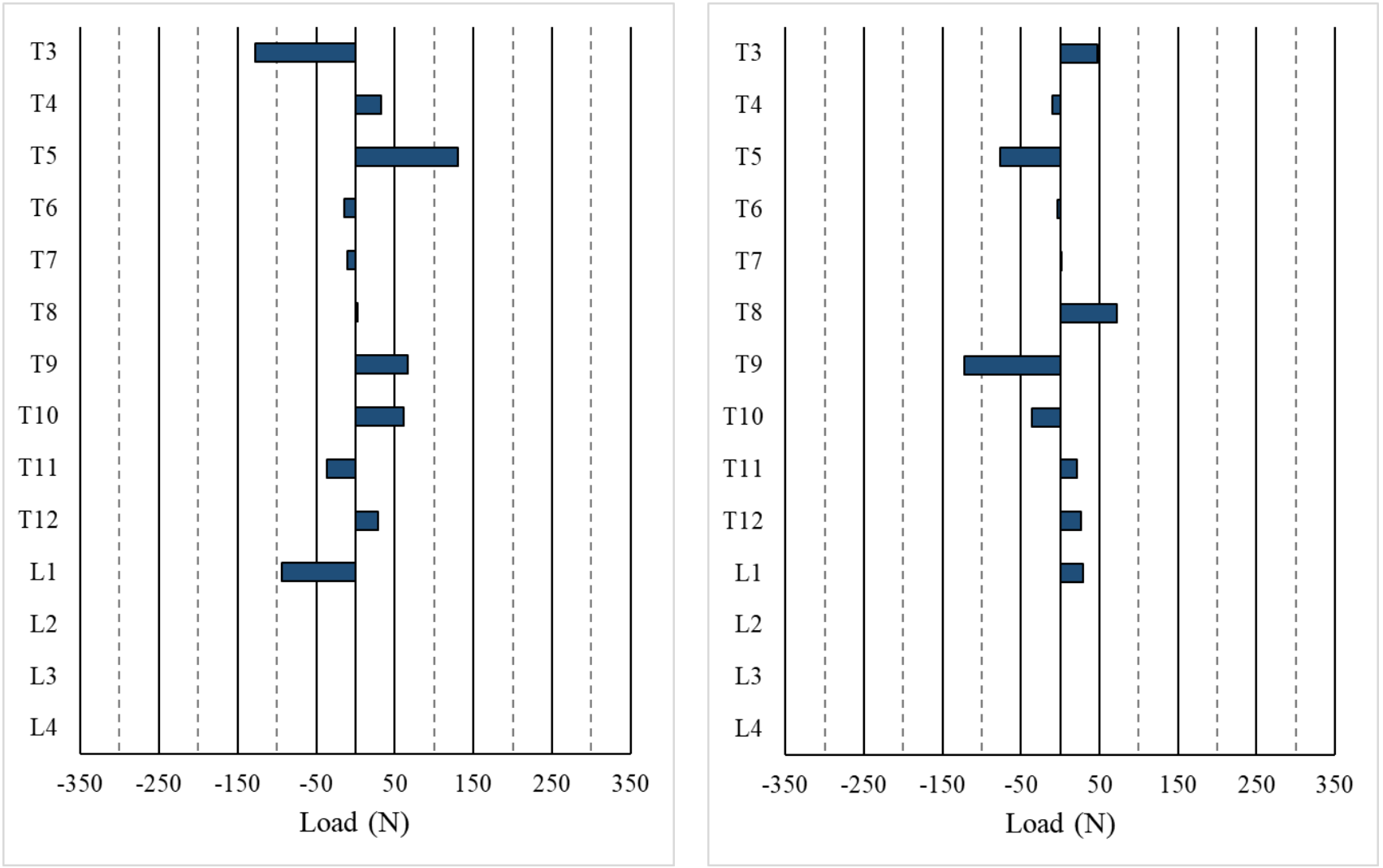

Figure A.11 Pull-out forces exerted on the screws, per level (Patient 1). (a) Concave side. (b) Convex side.

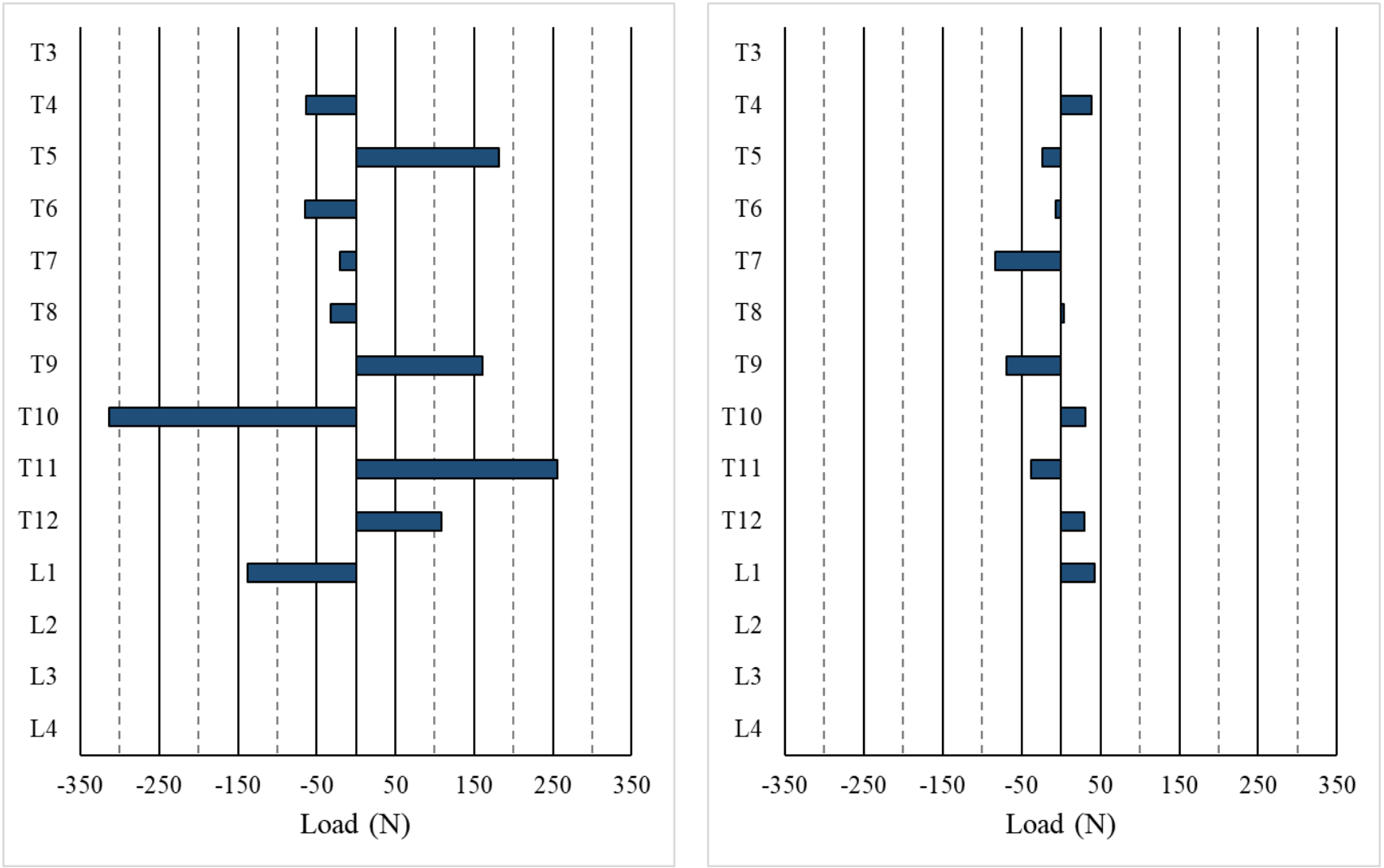

Figure A.12 Pull-out forces exerted on the screws, per level (Patient 2). (a) Concave side. (b) Convex side.

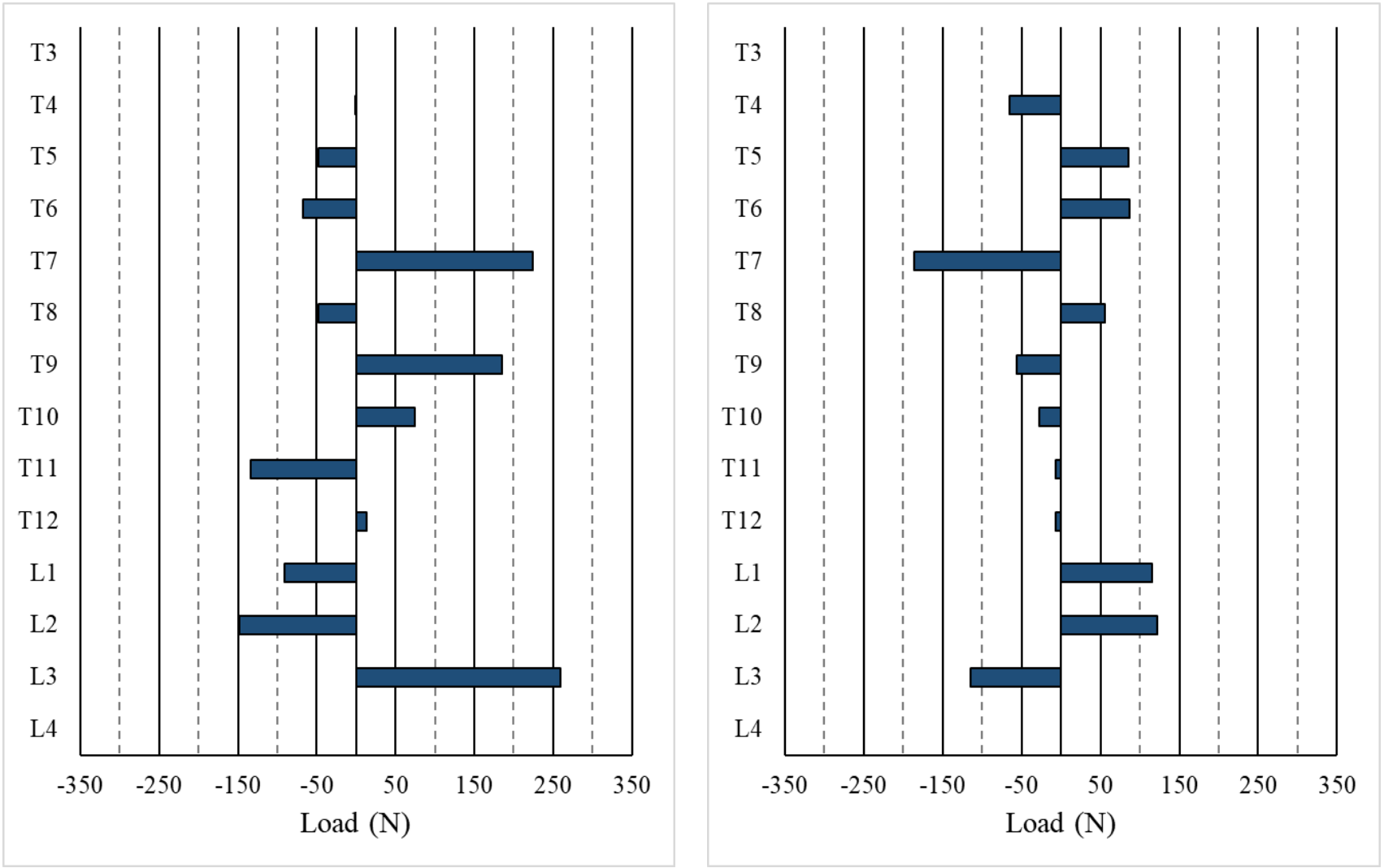

Figure A.13 Pull-out forces exerted on the screws, per level (Patient 3). (a) Concave side. (b) Convex side.

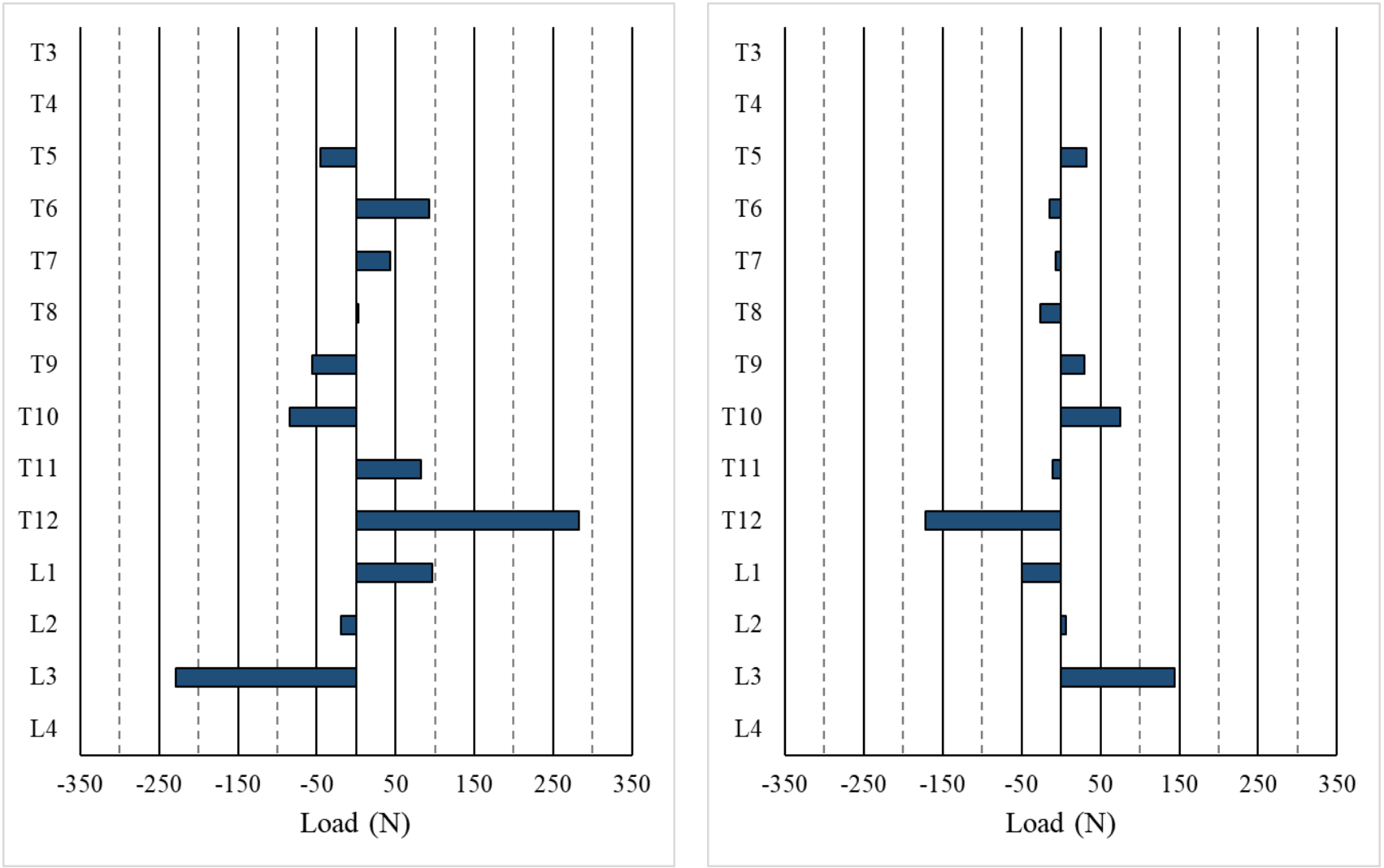

(a) (b)

Figure A.14 Pull-out forces exerted on the screws, per level (Patient 4). (a) Concave side. (b) Convex side.

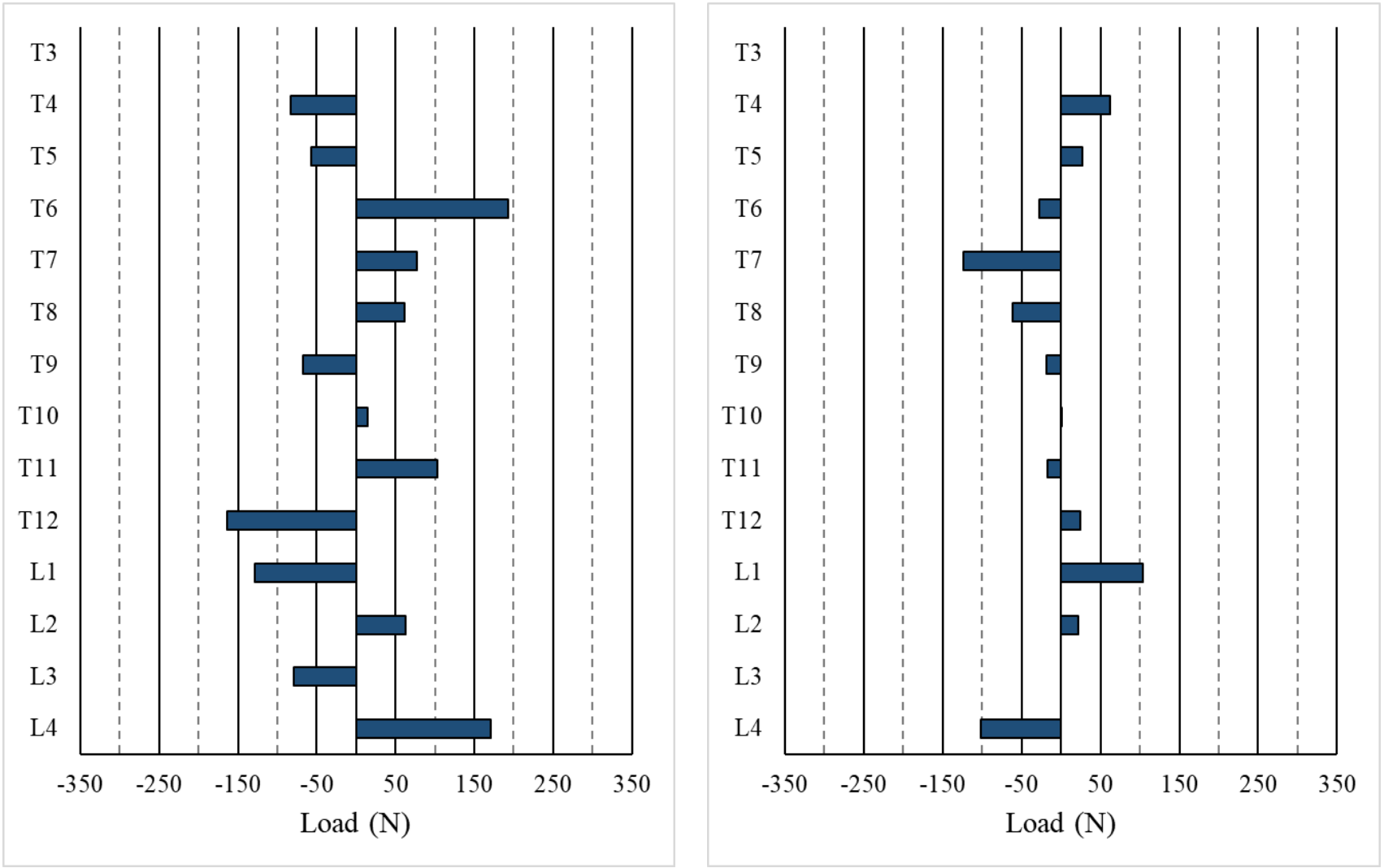

Figure A.15 Pull-out forces exerted on the screws, per level (Patient 5). (a) Concave side. (b) Convex side.

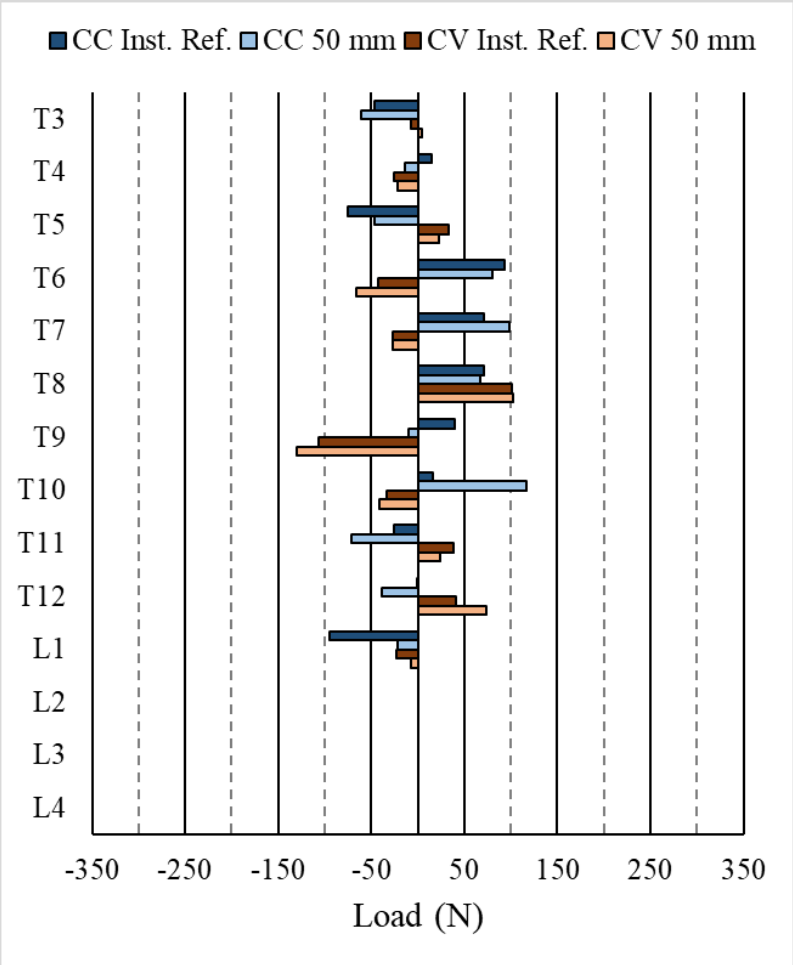

(a)

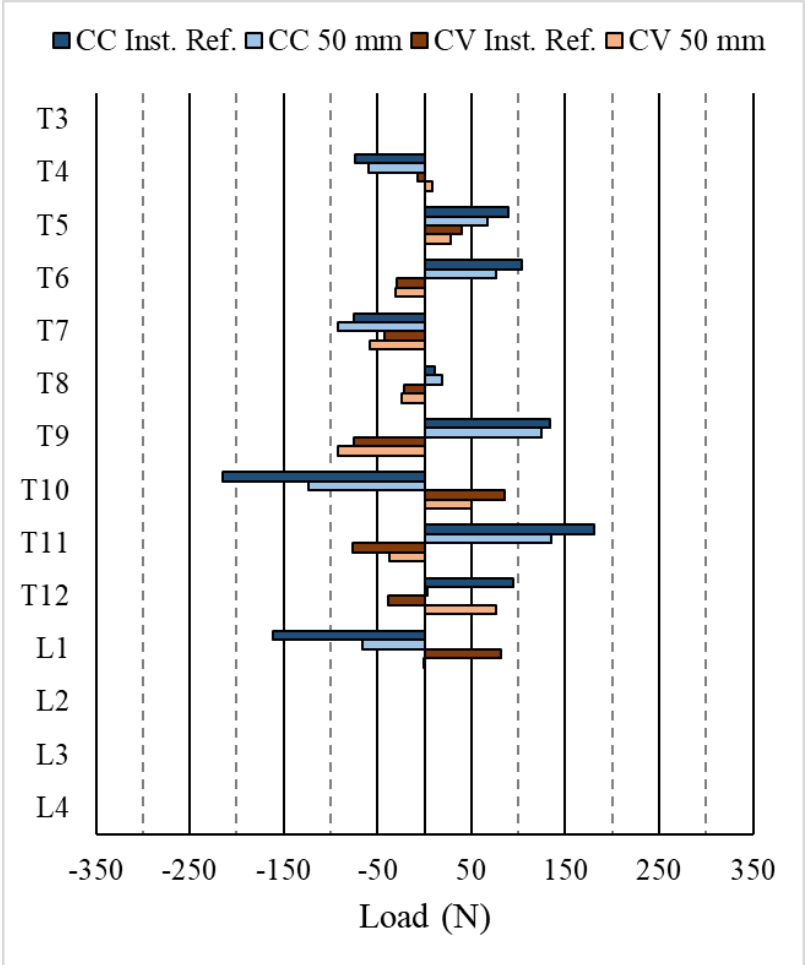

(b)

Figure A.16 Pull-out forces exerted on the screws at each level on the concave (CC) and convex (CV) sides for the simulated instrumented reference spine (Inst. Ref.) and instrumented with 50-mm thoracic cushions raised spine (50 mm). (a) Patient 1. (b) Patient 2.

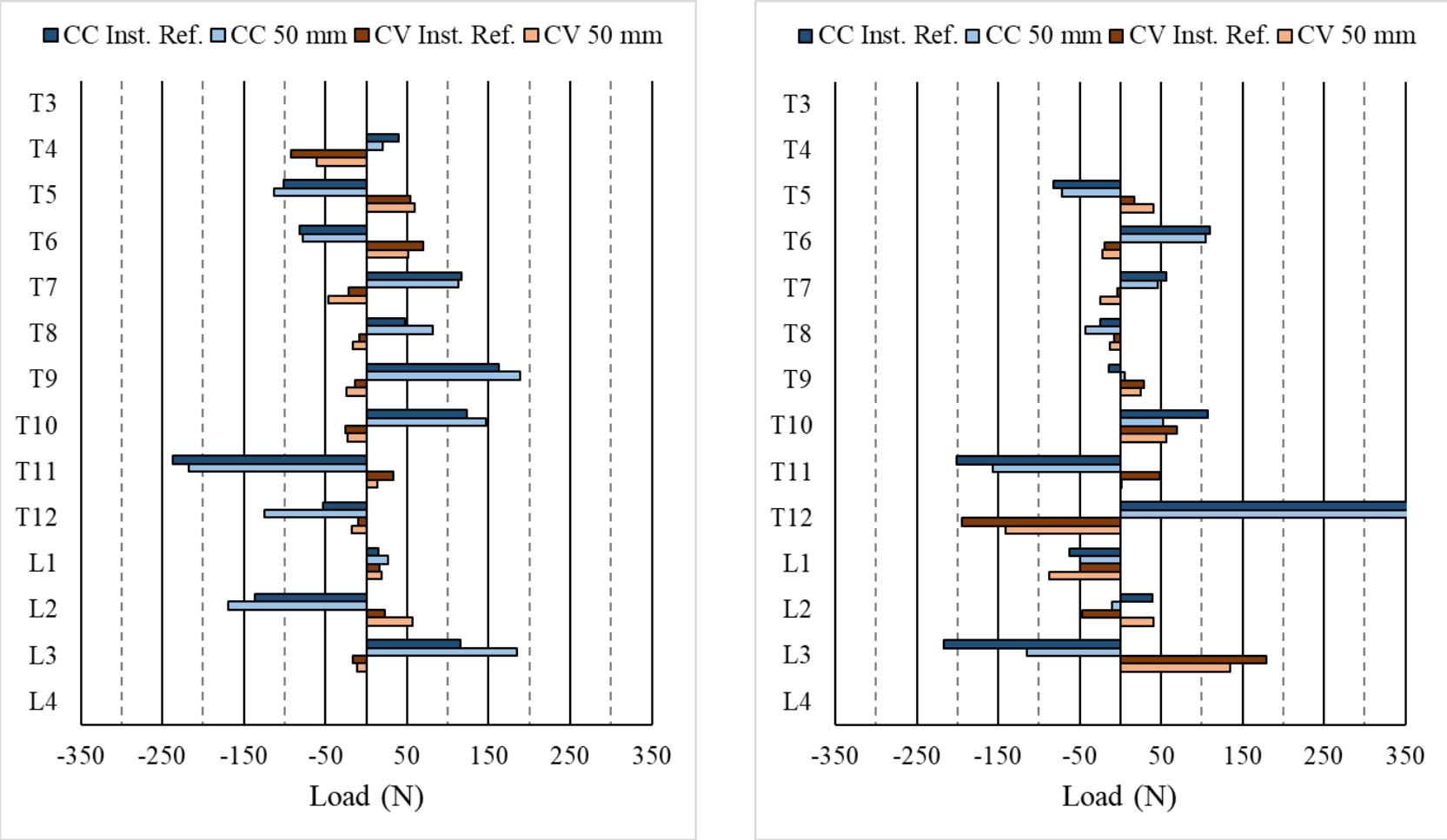

Figure A.17 Pull-out forces exerted on the screws at each level on the concave (CC) and convex (CV) sides for the simulated instrumented reference spine (Inst. Ref.) and instrumented with 50-mm thoracic cushions raised spine (50 mm). (a) Patient 3. (b) Patient 4.

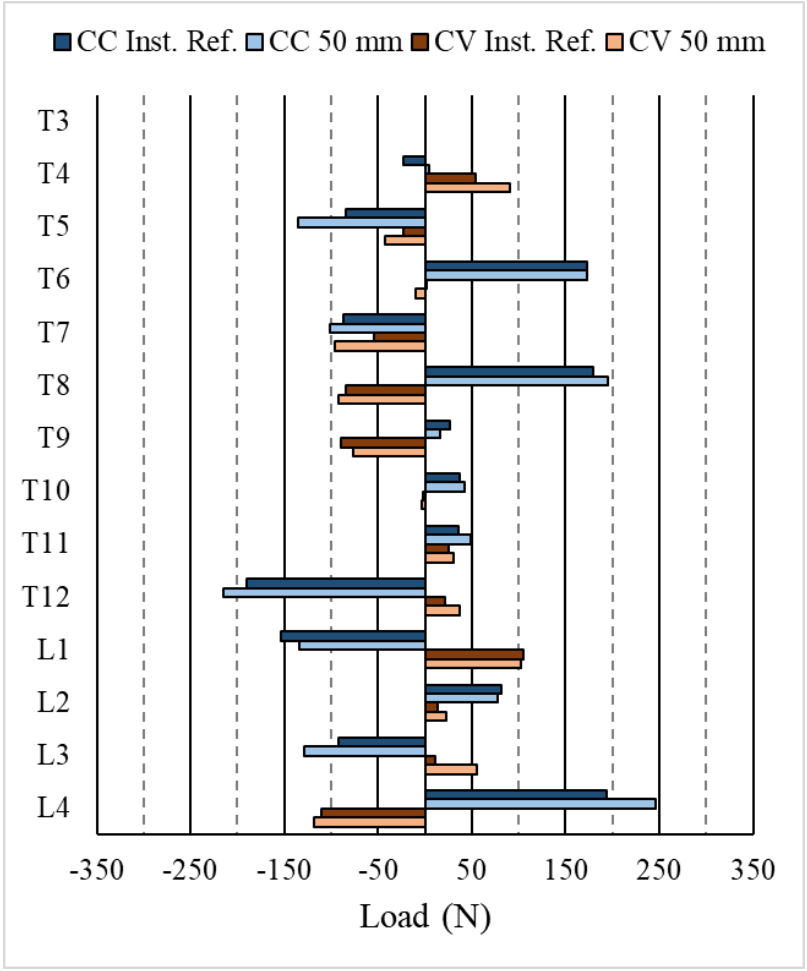

Figure A.18 Pull-out forces exerted on the screws at each level on the concave (CC) and convex (CV) sides for the simulated instrumented reference spine (Inst. Ref.) and instrumented with 50-mm thoracic cushions raised spine (50 mm). Patient 5.